PERFORMANCE ANALYSIS OF THREE NANOFLUIDS IN LIQUID TO GAS AND LIQUID TO LIQUID HEAT EXCHANGERS

By

Dustin R. Ray

RECOMMENDED:

Dr. Chuen-Sen Lin
Advisory Committee Member

Dr. Sun Woo Kim
Advisory Committee Member

Dr. Debendra Das
Advisory Committee Chair

Dr. Rorik Peterson
Chair, Department of Mechanical Engineering

APPROVED:

Dr. Douglas Goering
Dean, College of Engineering and Mines

Dr. John Eichelberger
Dean of the Graduate School

Date

PERFORMANCE ANALYSIS OF THREE NANOFLUIDS IN LIQUID TO GAS AND LIQUID TO LIQUID HEAT EXCHANGERS

A

THESIS

Presented to Faculty

of the University of Alaska Fairbanks

in Partial Fulfillment of the Requirements

for the Degree of

MASTER OF SCIENCE

By

Dustin R. Ray

Fairbanks, Alaska

December 2013

Abstract

One purpose of this research was to analyze the thermal and fluid dynamic performance of nanofluids in an automotive radiator (liquid to gas). Detailed computations were performed on an automotive radiator using three different nanofluids containing aluminum oxide, copper oxide and silicon dioxide nanoparticles dispersed in the base fluid, 60:40 ethylene glycol and water (EG/W) by mass. The computational scheme adopted was the effectiveness-Number of Transfer Unit $(\varepsilon - NTU)$ method encoded in Matlab. The computational scheme was validated by comparing the predicted results with that of the base fluid reported by other researchers. Then, the scheme was adapted to compute the performance of nanofluids. Results show that a dilute 1% volumetric concentration of nanoparticles can have substantial savings in the pumping power or surface area of the heat exchanger, while transferring the same amount of heat as the base fluid.

The second purpose of this research was to carry out experimental and theoretical studies for a plate heat exchanger (PHE). A benchmark test was performed with the minichannel PHE to validate the test apparatus with water. Next, using a 0.5% aluminum oxide nanoparticle concentration dispersed in EG/W preliminary correlations for the Nusselt number and the friction factor for nanofluid flow in a PHE were derived. Then, a theoretical study was conducted to compare the performance of three nanofluids comprised of aluminum oxide, copper oxide and silicon dioxide nanoparticles in EG/W. This theoretical analysis was conducted using the $\varepsilon - NTU$ method. The operational parameters were set by the active thermal control system currently under design by NASA. The analysis showed that for a dilute particle volumetric concentration of 1%, all the nanofluids showed improvements in their performance over the base fluid by reducing the pumping power and surface area of the PHE.

Table of Contents

Page

List of Figures

Page

List of Tables

Page

Acknowledgements

I would like to give my thanks to my committee chair, Dr. Debendra K. Das, for his continued advice, inspiration and support. I would also like to give my thanks to my committee members Dr. Chuen-Sen Lin and Dr. Sun Woo Kim for their time and guidance in completing my thesis.

My thanks also go to my family and friends for their encouragement through the years.

The financial supports from the Alaska NASA and NSF EPSCoR and the Department of Mechanical Engineering at University of Alaska Fairbanks are gratefully acknowledged.

Chapter 1: Introduction

1.1 Nanofluids

Nanotechnology has become a hot research topic to explore with applications in almost every field. A few applications of nanotechnology are: platinum particles used in catalytic converters, carbon black particles (30 nanometers (nm)) making rubber tires wear-resistant, nanofibers used to reinforce polymers (FRP), iron oxide used in magnetic material in disk drives and audio/video tapes, zinc and titanium oxide particles used in sunblock lotion, calcium carbonate used in dentistry, and high concentrations of particles used to create ballistic vest [1, 2]. Figure 1.1 illustrates the size comparison of nanoparticles to biological systems. However, the research presented in this paper is focused on one particular application of nanotechnology, nanofluid. "Nanofluids" [3] are a new generation of engineered fluids prepared by dispersing nanometer size solid particles like aluminum oxide (Al_2O_3) (less than 100 nm) into a liquid denoted as the base fluid.

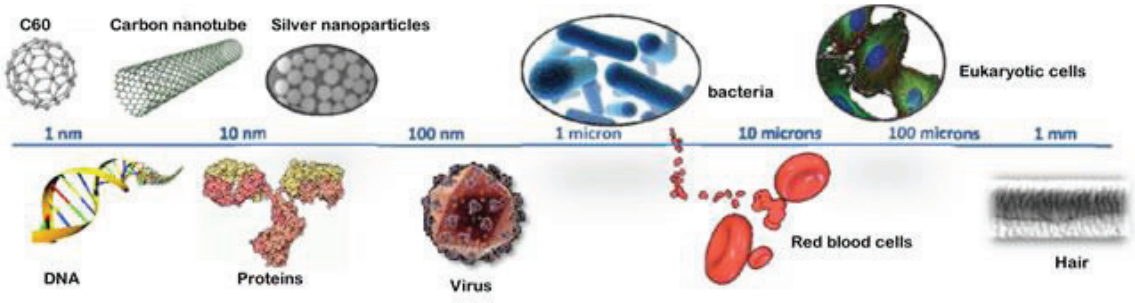

Figure 1.1: Size comparison of nanoparticles and biological systems [4]

Heat exchangers have undergone iterations of designs to improve surface area (fins, microchannels), turbulent/mixing flow (louvered, corrugated, chevron angle) and materials, but limited research has gone into improving the heat transfer fluid. Most heat transfer fluids have a low thermal conductivity compared to metals. A traditional coolant, ethylene glycol and water (EG/W) mixture with proportional mass of 60:40, has a thermal conductivity of 0.36 W/m K at 27°C (300K), whereas aluminum oxide has a thermal conductivity 100 times greater at 36.0 W/m K. However, the specific heat of metals is much lower than that of liquids. This is illustrated in Figure 1.2 with other thermophyscial properties. Thus, mixing these two can bridge the gap between fluids and solids. In recent years, researchers have shown that by dispersing small volume of nanoparticles in conventional heat transfer fluids, the base fluid's thermal

conductivity (Table 1.1) and convective heat transfer coefficient [5-7] can be significantly enhanced by as much as 45% for a constant Reynolds number with Al_2O_3 at a concentration of 1.34% dispersed in distilled water [6].

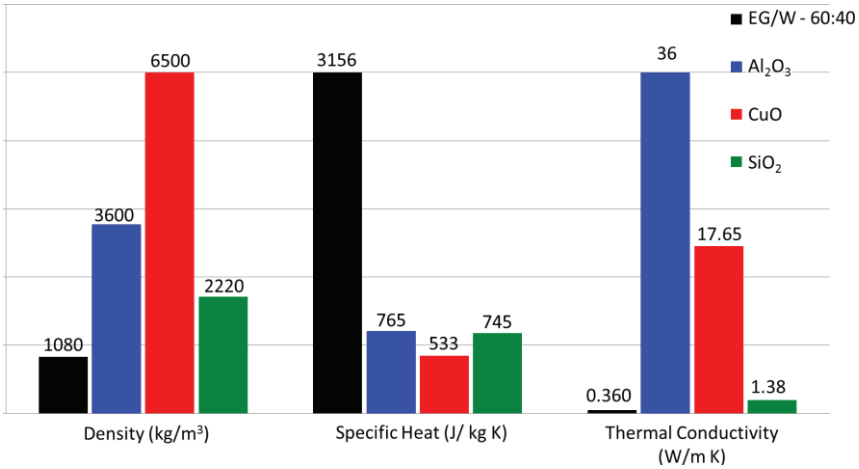

Figure 1.2: Comparison of nanoparticles (Al_2O_3, CuO, SiO_2) [8] and 60:40 EG/W [9] properties at room temperature (300K).

Table 1.1: Experimental improvement of thermal conductivity

Base Fluid	Nanoparticle			Nanofluid
	Material	Diameter (nm)	Volumetric Concentration	Thermal Conductivity
EG[10]	Cu	10	0.3%	40%
EG[11]	CuO	30.8-39.2	5%	22.4%
Oil[12]	MWCT*	25	1%	150%
EG/W(60:40)** [7]	Al_2O_3	53	6%	47%
	CuO	29	6%	60%
	ZnO	29-77	7%	48.5%

* Multiwall carbon nanotubes (L=50 μm) **T=363K

Due to the complex nature of a two-phase fluid (solid and liquid), at the present time most researchers have been developing properties correlations for nanofluids with various nanoparticles in several different base fluids. Most of the properties correlations for nanoparticles dispersed in EG/W were developed by the University of Alaska Fairbanks Nanofluids Group, which is summarized in Section 1.4. The limited literature on the application of nanofluids that correspond to the research conducted in this thesis is summarized in the respective chapters. Most of the earlier research that examined the performance of nanofluids used theoretical correlations for the thermophysical properties of nanofluids, instead of

experimental correlations. Most of the theoretical correlations (viscosity and thermal conductivity) either grossly over or under estimate the performance of nanofluids. This deficiency led to the objective of this thesis to accurately analyze the performance of nanofluids in liquid to gas (automotive radiator) and liquid to liquid (plate heat exchanger) heat exchangers using proper experimental correlations for the thermophyscial properties of nanofluids.

1.2 Nanoparticle Synthesis Techniques

Nanoparticles are being synthesized by using one or a combination of three techniques: solid-state, precipitation, or vapor-phase processing. The solid-state technique normally produces nanoparticles in the range of 100nm, but with some new development (Netzsch LMZ-25 ZETA II system and Dyno-Mill ECM) may allow nanoparticles in the range of 30 nm. The particles are created using a mechanical process by using a media mill after heating the precursor material to achieve a specific crystal structure. The solid-state technique has some draw backs, such as, limited particle size, impurity pick up from the media mill and inability to tailor precisely the shape and size of particles as well as the surface characteristics, which makes this technique best suited for creating microparticles [13]. The precipitation technique uses a chemical process to precipitate inorganic nanoparticle compounds. It has been an attractive technique to researchers when a nanocrystalline powder is the goal, instead of a dispersible nanoparticle powder [13]. The vapor-phase technique, which has been used since the early days of nanoparticles development, involves vaporizing the precursor material and cooling the vapor to create nanoparticles. This is the primary technique major companies are using for creating nanoparticles. The commonly used processes for vapor-phase techniques are described in the section below.

1.2.1 Vapor-Phase Processes

The nanofluids used in this research project are mostly produced by Alfa Aesar [14], which uses two processes following the vapor-phase technique, one or two-step process. The two-step process (“Kool-Aid” method [15]) synthesizes nanoparticles by using arc energy to vaporize precursor materials with the addition of a reactant gas to cool the vapor at a controlled rate and condense the vapor to form nanoparticles as shown in Figure 1.3a. The nanoparticle powder is

mixed into a base fluid creating nanofluids. The two-step process can yield nanoparticles with an average size ranging from 35-75nm [16, 17].

The one-step process also uses arc energy and vaporizes the precursor material. Then, the vapor condenses into nanoparticles by direct contact with a flowing cooled fluid, as shown in Figure 1.3b [15]. Using the one-step process allows for a wide range of precursor materials, such as pure metals (e.g. copper) and can produce nanoparticles with average size in the range of 20-60 nm.

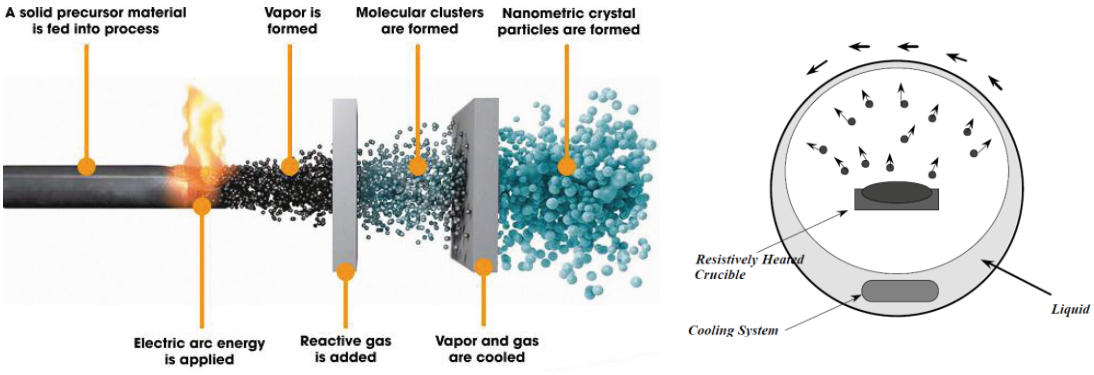

(a) (b)

Figure 1.3: Nanoparticle synthesis techniques a) Two-step process [16] b) One-step process [15]

1.3 Agglomeration Prevention

One of the challenges with nanofluids is to achieve a stable dispersion, meaning no agglomeration (clumping) of the particles. This is achieved by using surfactants or dispersants, which is the medium interface between the nanoparticle and the base fluid. The surfactants aid in the prevention of agglomeration by increasing the zeta-potential of the nanoparticles.

1.3.1 Zeta-Potential

The zeta-potential is a measurement of the particle's charge. The larger the absolute value of the zeta-potential the larger amount of charge is on the particle's surface. The zeta-potential in a sense could be viewed as an index for the stability of nanofluids. A physically stable nanosuspension solely stabilized by electrostatic repulsion will have a minimum zeta-potential of ±30mV [18].

Along with the use of surfactants, zeta-potential can also be affected by the pH of the fluid. Wamkam et al. [19] performed a study examining how the pH factors into nanofluids thermal and fluid dynamic performance with different average particle sizes. Figure 1.4 illustrates their

results. The average stable nanoparticle size is dependent on the zeta-potential, which is a function of pH. At either the high (≈ 15 mV) or low (≈ -25 mV) zeta-potential, the average particle size is the smallest around 100 nm.

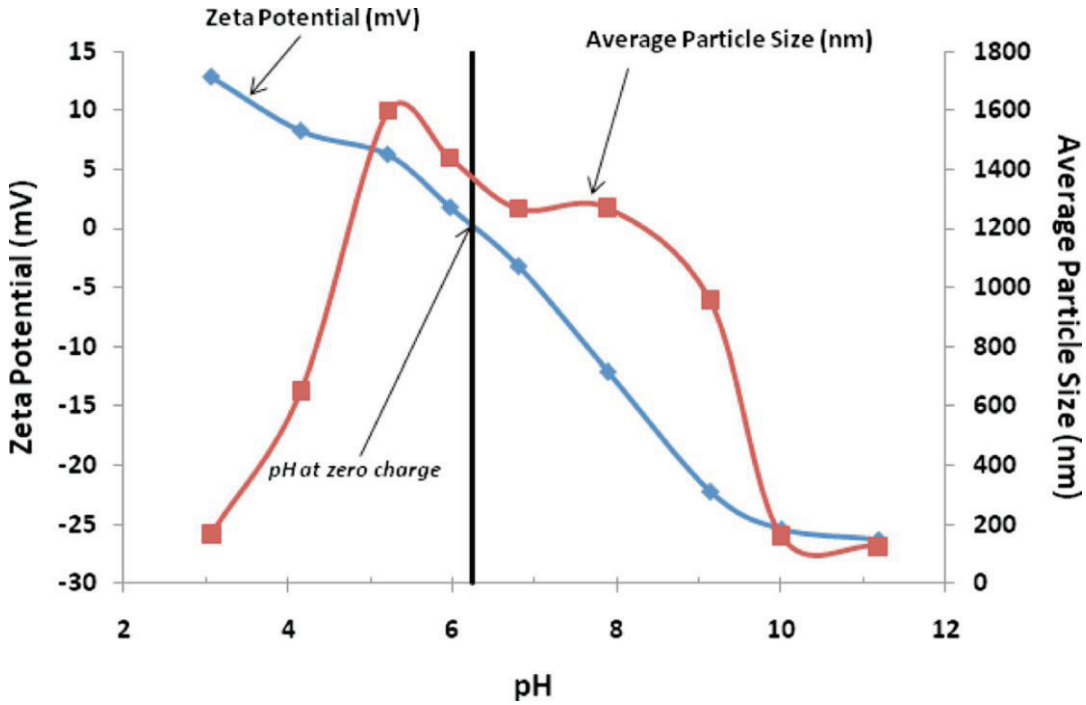

Figure 1.4: [19] Zirconium oxide zeta-potentials and average particle size versus different pH values

1.3.2 Ultrasonication

Once agglomeration has occurred, the nanoparticles can be separated by ultrasonication. Previous researchers[7, 20, 21] have found using a sonicator under a frequency of 40 kHz and a power of 185W for three sessions each of two hours duration is sufficient to break down the particles that have agglomerated, which is usually due to long term storage.

1.4 Nanofluids Thermophysical Properties

In sections 1.4.1-1.4.4, a brief outline of present correlations for the thermophysical properties of nanofluids dispersed in EG/W 60:40 by mass is given.

1.4.1 Density

Vajjha et al. [22] compared the theoretical density equation Eq. (1.1) presented by Pak and Cho[6] to the experimentally determined density of three different nanofluids: aluminum oxide,

antimony-tin oxide, and zinc oxide using Anton Paar density meter. They found the theoretical equation to be in good agreement with their data. Therefore this theoretical density equation was adopted for future computations to determine the density of the nanofluids.

$$\rho_{nf} = \phi\rho_p + (1-\phi)\rho_{bf} \tag{1.1}$$

Using Eq. (1.1), Figure 1.5 was created to illustrate the effects of nanoparticles and temperature on the density of the nanofluid. As expected, increasing the volumteric concentration of nanoparticles increases the density of the nanofluid and temperature variation shows a very mild effect.

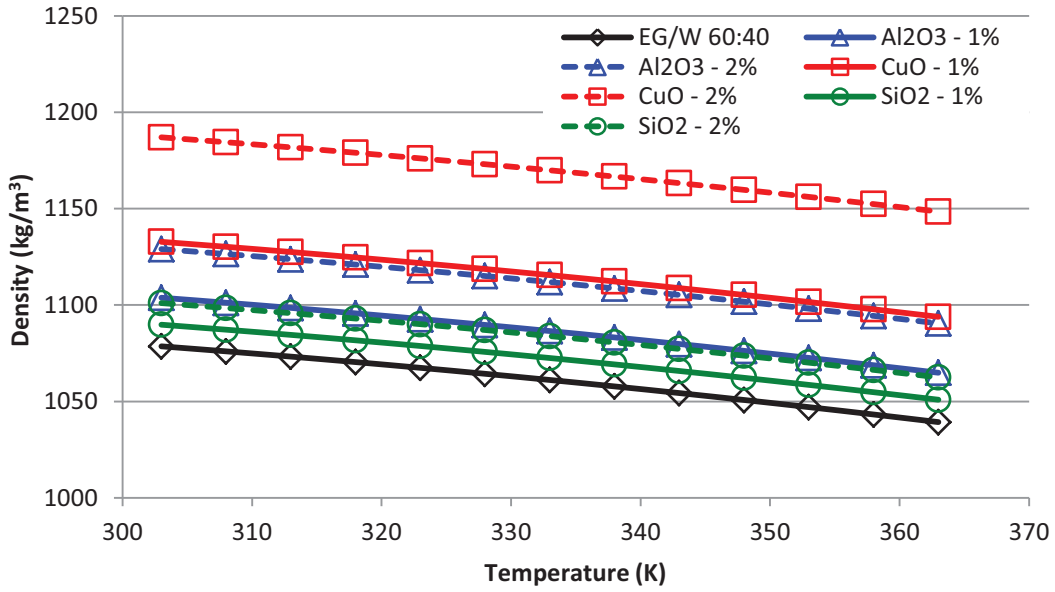

Figure 1.5: The variation of density with increasing temperature for the base fluid (EG/W) and three nanofluids (Al_2O_3, CuO, SiO_2) with concentrations 1-2%

1.4.2 Specific Heat

Vajjha and Das [20] conducted specific heat measurements on three nanofluids (Al_2O_3, ZnO, SiO_2) and developed a correlation given by Eq.(1.2), where A, B and C are curve-fit coefficients for each nanoparticle.

$$\frac{c_{p,nf}}{c_{p,bf}} = \frac{(A(T/T_0) + B(c_{p,p}/c_{p,bf}))}{(C+\phi)} \tag{1.2}$$

The Al_2O_3 and ZnO nanoparticles were dispersed in 60:40 EG/W, while the SiO_2 was dispersed in deionized water, due to gelling in EG/W. Therefore, the Eq. (1.3) presented by Xuan and Roetzel [23] was used to determine the specific heat for copper oxide and silicon dioxide dispersed in EG/W.

$$c_{p,nf} = \frac{\phi \rho_p c_{p,p} + (1-\phi)\rho_{bf} c_{p,bf}}{\rho_{nf}} \tag{1.3}$$

The effects of the concentration and temperature on specific heat are shown in Figure 1.6 using Eq. (1.2) and (1.3). Figure 1.6 illustrates that increasing the concentration decreases the specific heat, which diminishes the amount of thermal energy the fluid can carry for a given mass. However, if we look at volumetric heat capacity $(\rho \cdot c_p)$ shown in Figure 1.7, it can be seen that increasing the concentration has very little effect especially for 1% concentration for Al_2O_3 and CuO, which overlaps the values of the base fluid, EG/W.

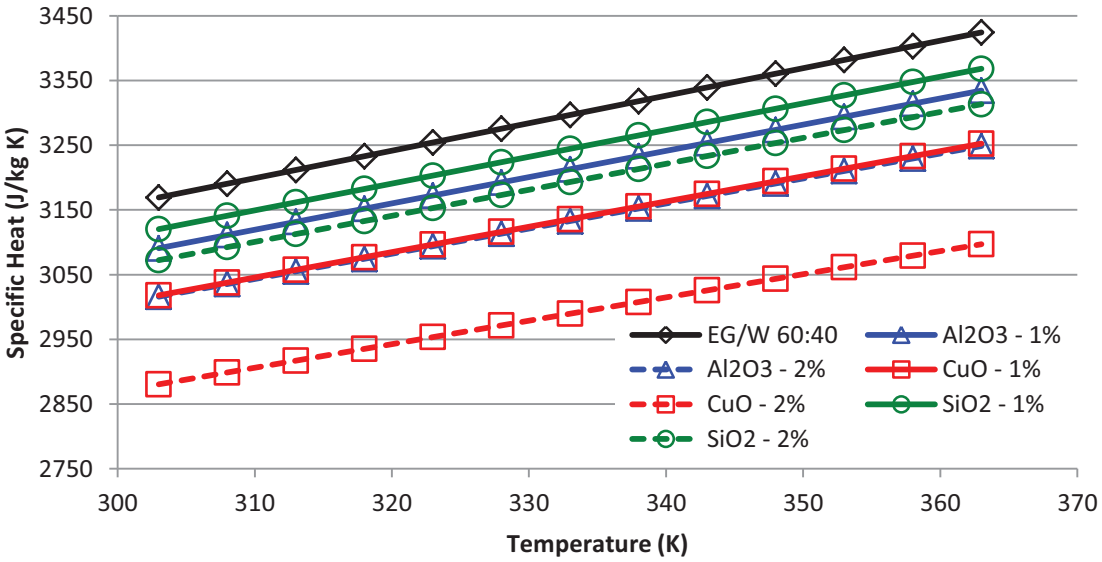

Figure 1.6: The variation of specific heat with increasing temperature for the base fluid (EG/W) and three nanofluids (Al_2O_3, CuO, SiO_2) with concentrations 1-2%

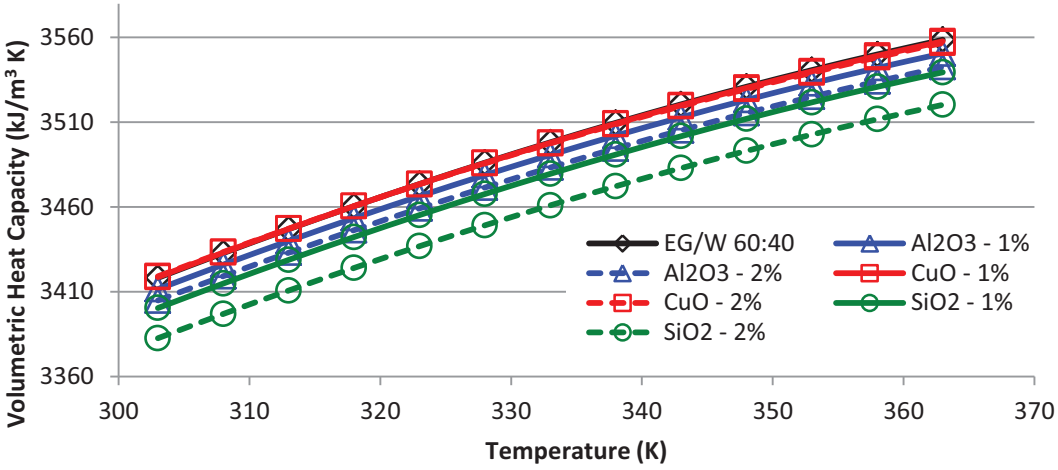

Figure 1.7: The variation of volumetric heat capacity with increasing temperature for the base fluid (EG/W) and three nanofluids (Al_2O_3, CuO, SiO_2) with concentrations 1-2%

1.4.3 Viscosity

Vajjha et al.[24] combined the experimental viscosity data from several researchers (Namburu et al. [25, 26] and Sahoo et al.[27]) to develop a nondimensional correlation Eq. (1.4) for three nanofluids (Al_2O_3, CuO, SiO_2) dispersed in EG/W 60:40 for the temperature range of 0˚C to 90˚C, where A and B are curve-fit constants for each nanoparticle. The previous researchers [25-27] measured the viscosity of nanofluids using a Brookfield viscometer equipped with a computer controlled temperature bath.

$$\frac{\mu_{nf}}{\mu_{bf}} = A\exp(B\phi) \tag{1.4}$$

The weakness of nanofluids from pumping power consideration is the increase in viscosity over the base fluid as clarified in Figure 1.8 using Eq. (1.4). However, at high temperatures the increase in viscosity becomes marginal.

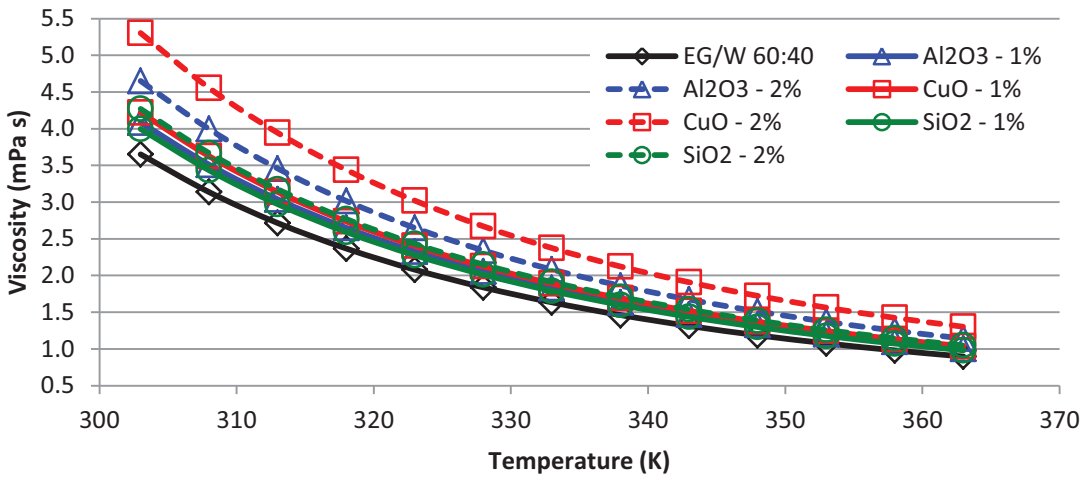

Figure 1.8: The variation of viscosity with increasing temperature for the base fluid (EG/W) and three nanofluids (Al_2O_3, CuO, SiO_2) with concentrations 1-2%

1.4.4 Thermal Conductivity

Koo and Kleinstreuer [5] expanded upon the Maxwell model which was suitable for determining the thermal conductivity of particles down to micrometer size dispersed in a fluid. They added the Brownian motion[1] term for nanoparticles shown in Eq. (1.5a). Using Koo and Kleinstreuer model, Vajjha and Das [7] and Sahoo [28] have developed correlations for nanoparticles dispersed in 60:40 EG/W mixture. They experimentally determined the thermal conductivity of aluminum oxide, copper oxide [7], and silicon dioxide [28] nanofluids using an apparatus by P.A. Hilton that uses the steady state measurement technique. The Eq. (1.5a) presented by them has an average deviation of 0.23%, 5.74% and 1.97%, with the experimental data for Al_2O_3, CuO and SiO_2, respectively. The parameter β is a curve-fit function of ϕ for each nanoparticle.

$$k_{nf} = \underbrace{\frac{k_p + 2k_{bf} - 2(k_{bf} - k_p)\phi}{k_p + 2k_{bf} + (k_{bf} - k_p)\phi} k_{bf}}_{\text{Maxwell}} + \underbrace{5\times10^4 \beta\phi\rho_{bf} c_{pbf} \times \sqrt{\frac{\kappa T}{\rho_p d_p}} f(T,\phi)}_{\text{Brownian Motion}} \tag{1.5a}$$

$$f(T,\phi) = (2.8217\times10^{-2}\phi + 3.917\times10^{-3})\left(\frac{T}{T_0}\right) + (-3.0669\times10^{-2}\phi - 3.91123\times10^{-3}) \tag{1.5b}$$

[1] Brownian motion is the random movement of particles suspended in a fluid resulting from colliding with the fast-moving atoms or molecules in the fluid.

Figure 1.9 indicates increasing the concentration and temperature increases thermal conductivity over the base fluid. At 363 K (90˚C) CuO at 2% concentration shows an enhancement of 51% over that of the base fluid.

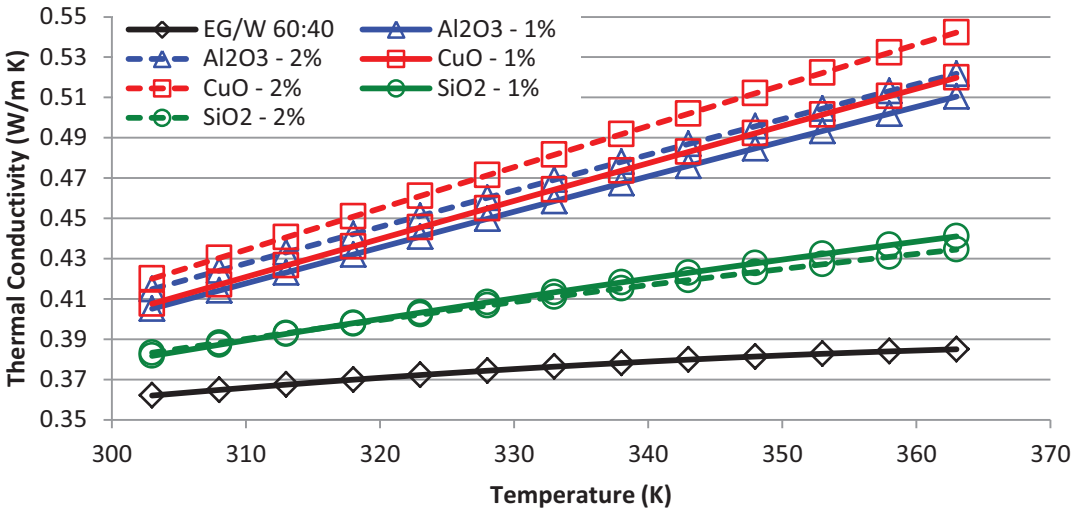

Figure 1.9: The variation of thermal conductivity with increasing temperature for the base fluid (EG/W) and three nanofluids (Al_2O3, CuO, SiO_2) with concentrations 1-2%

1.5 Nanofluids' Nusselt Number and Friction Factor Correlations

The Nusselt number and friction factor correlations for nanoparticles (Al_2O_3, CuO, SiO_2) dispersed in EG/W were developed by Vajjha et al. [24] expressed in Eq. (1.6a) and (1.7a), respectively. They found the nanofluid correlation yields a 30% increase in Nusselt Number for Al_2O_3 at 1% concentration at a Reynolds Number of 4500 over the Gnielinski correlation [29] for the base fluid expressed in Eq. (1.6b). The friction factor correlation was modeled after the Blasius correlation [30] shown in Eq. (1.7b).

$$Nu_{nf} = 0.0222(Re_{nf}^{0.8} - 60)Pr_{nf}^{0.4}(1 + 0.32178\phi^{0.64788}) \qquad 3000 \le Re \le 16000 \qquad (1.6a)$$

$$Nu = 0.012(Re^{0.87} - 280)Pr^{0.4} \qquad 3\times10^3 \le Re \le 10^6,\ 1.5 \le Pr \le 500 \qquad (1.6b)$$

$$f_{nf} = 0.3164Re_{nf}^{-0.25}\left(\frac{\rho_{nf}}{\rho_{bf}}\right)^{0.797}\left(\frac{\mu_{nf}}{\mu_{bf}}\right)^{0.108} \qquad 4000 < Re < 16000,\ 0\% < \phi < 6\% \qquad (1.7a)$$

$$f = 0.3164 Re^{-0.25} \qquad 4000 < Re < 10^5 \qquad (1.7b)$$

1.6 Summary of Subsequent Chapters

This thesis has been written in the manuscript format. As the chapters were completed, they were submitted to journals for review towards publications. Therefore, the manuscripts are expressed as chapters in this thesis, which is an accepted practice.

Chapter two compares the performance of three nanoparticles (Al_2O_3, CuO, SiO_2) dispersed in EG/W 60:40 by mass in an automotive radiator. The computational scheme adopted is the effectiveness-Number of Transfer Unit $(\varepsilon - NTU)$ method encoded in Matlab. The computational scheme has been validated by comparing the results on pumping power, convective heat transfer coefficients on the air, overall heat transfer coefficient, effectiveness and NTU, reported by other researchers. The scheme was then modified for nanofluids with two performance analyses. The first (pumping power analysis) was on the basis of equal surface area and heat dissipation, which determined the maximum reduction in pumping power. The second (surface area analysis) was conducted on the basis of equal pumping power and heat dissipation, which determined the maximum reduction for surface area/size/weight of the radiator. In each of these comparisons, nanofluid performed better than the base fluid.

Chapter three describes the experimental and theoretical studies carried out for a plate heat exchanger (PHE). Experimental data were measured from a minichannel PHE in a test loop employing water to validate the test apparatus by comparing with single phase fluid correlations. Using a 0.5% aluminum oxide nanoparticle concentration dispersed in EG/W, preliminary correlations for the Nusselt number and the friction factor for nanofluid flow in a PHE were derived. In the theoretical study, a comparison of three nanofluids comprised of aluminum oxide, copper oxide and silicon dioxide nanoparticles in ethylene glycol and water mixture was conducted using the $\varepsilon - NTU$ method for the operational parameters set by NASA's active thermal control system. The study showed that for a dilute particle volumetric concentration of 1%, all the nanofluids showed improvements in their performance over the base fluid. The results showed reduction in weight and pumping power for the heat exchanger, which will be beneficial to the NASA thermal control project.

1.7 Nomenclature

$A, B, C, \ldots$	Dimensionless curve-fit constants	**Greek Letters**	
c_p	Specific heat, $J / kg{\cdot}K$	κ	Boltzmann constant, $1.38\times10^{-23}\ J / K$
d_p	Particle diameter, m	μ	Viscosity, $Pa{\cdot}s$
f	Friction factor	ρ	Density, kg / m^3
k	Thermal conductivity, $W / m{\cdot}K$	ϕ	Volumetric concentration
Nu	Nusselt number	**Subscripts**	
Pr	Prandtl number	bf	Base fluid
Re	Reynolds number	nf	Nanofluid
T	Temperature, K	p	Nanoparticle

1.8 References

[1] "Tooth Builder Nanoparticles," http://www.homesteadmarket.com/product/347/articles.

[2] Yury, G., 2006, Nanomaterials Handbook, CRC Press, Boca Raton, FL.

[3] Choi, S. U. S., and Eastman, J. A., 1995, "Enhancing thermal conductivity of fluids with nanoparticles," p. Medium: ED; Size: 8 p.

[4] Contera, S., 2013, "Physics in Nanomedicine: Interfaces and Mechanical Properties of Nanomaterials and Biological Systems with AFM," http://www.azonano.com/article.aspx?ArticleID=3012.

[5] Koo, J., and Kleinstreuer, C., 2005, "A new thermal conductivity model for nanofluids," Journal of Nanoparticle Research, 7(2-3), pp. 324-324.

[6] Pak, B. C., and Cho, Y. I., 1998, "Hydrodynamic and heat transfer study of dispersed fluids with submicron metallic oxide particles," Exp Heat Transfer, 11(2), pp. 151-170.

[7] Vajjha, R. S., and Das, D. K., 2009, "Experimental determination of thermal conductivity of three nanofluids and development of new correlations," International Journal of Heat and Mass Transfer, 52(21-22), pp. 4675-4682.

[8] Çengel, Y. A., 2007, Heat and Mass Transfer: A Practical Approach, McGraw-Hill, New York, NY.

[9] ASHRAE, 2005, ASHRAE Handbook: Fundamentals, American Society of Heating, Refrigerating and Air-Conditioning Engineers, Atlanta, GA.

[10] Eastman, J. A., Choi, S. U. S., Li, S., Yu, W., and Thompson, L. J., 2001, "Anomalously increased effective thermal conductivities of ethylene glycol-based nanofluids containing copper nanoparticles," Applied Physics Letters, 78(6), p. 718.

[11] Liu, M. S., Lin, M. C. C., Huang, I. T., and Wang, C. C., 2006, "Enhancement of Thermal Conductivity with CuO for Nanofluids," Chemical Engineering & Technology, 29(1), pp. 72-77.

[12] Choi, S. U. S., Zhang, Z. G., Yu, W., Lockwood, F. E., and Grulke, E. A., 2001, "Anomalous thermal conductivity enhancement in nanotube suspensions," Applied Physics Letters, 79(14), p. 2252.

[13] Ganesh, S., and Amit, S., 2006, "Perspectives on the Science and Technology of Nanoparticle Synthesis," Nanomaterials Handbook, CRC Press, Boca Raton, FL.

[14] "Alfa Aesar," http://www.alfaaesar.com/.

[15] Kostic, M.,2003, "Nanofluids Advanced flow and heat transfer fluids", Northern Illinois University

[16] 2013, "Nanoparticle and Dispersions," A. Aesar, ed.

[17] Nanophase, 2013, "Dispersion, Surface, Production."

[18] Meredith, L. H., and Anthony, M. L., 2006, "Nanoparticles for Drug Delivery," Nanomaterials Handbook, CRC Press, Boca Raton, FL.

[19] Wamkam, C. T., Opoku, M. K., Hong, H., and Smith, P., 2011, "Effects of pH on heat transfer nanofluids containing ZrO2 and TiO2 nanoparticles," Journal of Applied Physics, 109(2), p. 024305.

[20] Vajjha, R. S., and Das, D. K., 2009, "Specific heat measurement of three nanofluids and development of new correlations," Journal of Heat Transfer, 131(7), pp. 1-10.

[21] Vajjha, R. S., and Das, D. K., 2012, "A review and analysis on influence of temperature and concentration of nanofluids on thermophysical properties, heat transfer and pumping power," International Journal of Heat and Mass Transfer, 55(15–16), pp. 4063-4078.

[22] Vajjha, R. S., Das, D. K., and Mahagaonkar, B. M., 2009, "Density measurement of different nanofluids and their comparison with theory," Petroleum Science & Technology, 27(6), pp. 612-624.

[23] Xuan, Y., and Roetzel, W., 2000, "Conceptions for heat transfer correlation of nanofluids," International Journal of Heat and Mass Transfer, 43(19), pp. 3701-3707.

[24] Vajjha, R. S., Das, D. K., and Kulkarni, D. P., 2010, "Development of new correlations for convective heat transfer and friction factor in turbulent regime for nanofluids," International Journal of Heat and Mass Transfer, 53(21-22), pp. 4607-4618.

[25] Namburu, P. K., Kulkarni, D. P., Dandekar, A., and Das, D. K., 2007, "Experimental investigation of viscosity and specific heat of silicon dioxide nanofluids," Micro & Nano Letters, 2(3), p. 67.

[26] Namburu, P. K., Kulkarni, D. P., Misra, D., and Das, D. K., 2007, "Viscosity of copper oxide nanoparticles dispersed in ethylene glycol and water mixture," Experimental Thermal and Fluid Science, 32(2), pp. 397-402.

[27] Sahoo, B. C., Vajjha, R. S., Ganguli, R., Chukwu, G. A., and Das, D. K., 2009, "Determination of rheological behavior of aluminum oxide nanofluid and development of new viscosity correlations," Petroleum Science and Technology, 27(15), pp. 1757-1770.

[28] Sahoo, B. C., Das, D. K., Vajjha, R. S., and Satti, J. R., 2013, "Measurement of the thermal conductivity of silicon dioxide nanofluid and development of correlations," Journal of Nanotechnology in Engineering and Medicine, 3(4), pp. 041006-041006.

[29] Bejan, A., 1993, Heat Transfer, John Wiley & Sons, Inc., New York.

[30] White, F. M., 2003, Fluid Mechanics, McGraw-Hill, New York, NY.

Chapter 2: Superior Performance of Nanofluids in an Automotive Radiator[2]

ABSTRACT: This study compares the performance of three different nanofluids containing aluminum oxide, copper oxide, and silicon dioxide nanoparticles dispersed in the same base fluid, 60:40 ethylene glycol and water by mass, as coolant for automobile radiators. The computational scheme adopted here is the effectiveness-Number of Transfer Unit $(\varepsilon - NTU)$ method encoded in Matlab. Appropriate correlations of thermophysical properties for these nanofluids developed from measurements are summarized in this paper. The computational scheme has been validated by comparing the results of pumping power, convective heat transfer coefficients on the air and coolant side, overall heat transfer coefficient, effectiveness and NTU, reported by other researchers. Then, the scheme was adopted to compute the performance of nanofluids. Results show that a dilute 1% volumetric concentration of nanoparticles performs better than higher concentration. It is proven that at optimal conditions of operation of the radiator, under the same heat transfer basis, a reduction of 35.3% in pumping power or 7.4% of the surface area can be achieved by using the Al_2O_3 nanofluid. The CuO nanofluid showed slightly lower magnitudes than the Al_2O_3 nanofluid, with 33.1% and 7.2% reduction for pumping power or surface area, respectively. The SiO_2 nanofluid showed the least performance gain of the three nanofluids, but still could reduce the pumping power or area by 26.2% or 5.2%. The analysis presented in this paper was used for an automotive radiator but can be extended to any liquid to gas heat exchanger.

KEY WORDS: Compact heat exchanger, Convective heat transfer, Friction factor, Nanofluids, Nusselt number, Radiator, Prandtl number, Reynolds number, Thermophysical properties, louvered fins

[2]Ray, Dustin R. and Debendra K. Das. 2013. Superior Performance of Nanofluids in an Automotive Radiator. Prepared for submission to ASME Journal of Thermal Science and Engineering Applications

2.1 Introduction

With increasing demands for greater engine output, air conditioning (AC) capacity, smaller hood space and more stringent emission standards, the heat dissipation requirements for automobiles have increased significantly over the past decades. Automobiles use several heat exchangers to get rid of the heat: radiators, condensers and evaporators for the AC, and oil coolers. Over the years steady improvements have been made to increase the performance of these heat exchangers, such as, different style of fin designs, increasing the number of fins and use of different fin and tube materials. However, these improvements were made only to the heat exchanger body, while the heat transfer fluid has remained unchanged. Traditional coolants for automotive radiators inherently have poor thermal conductivity. For example, 60:40 (by mass) ethylene glycol and water mixture (EG/W), which is used in cold climates has a thermal conductivity of 0.36W/m K at room temperature 27°C (300K) whereas aluminum oxide (Al_2O_3) has a thermal conductivity 36.0W/m K, 100 times greater. Thus, mixing these two can bridge the gap of thermal conductivity between fluids and solids. This is fulfilled by nanofluids, which is a new generation of engineered fluid prepared by dispersing nanometer size solid particles like Al_2O_3 of average particle size smaller than 100 nm, into a liquid denoted as the base fluid. Extensive research on nanofluids in recent years has proven that by dispersing small volume of nanoparticles in conventional heat transfer fluids, their thermal conductivity and convective heat transfer can be significantly enhanced [1-4]. Using a better heat transfer fluid in automotive radiators could lead to a reduction in size and pumping power, resulting in more efficient automobiles. With approximately 60 million cars produced yearly[5] in the world, any reduction in the size and weight of the radiator can have substantial benefit due to less metal and energy requirements reducing mining and environmental effect.

Research on automotive radiators with single phase fluids is widely published in the literature. The most comprehensive research done in early years on a variety of heat transfer matrix geometries for radiators and other compact heat exchangers is due to Kays and London[6]. We have adopted from this reference the equations, analytic procedure and heat transfer matrix data in our analysis to study the performance of nanofluids in a radiator. Another authoritative work on heat exchanger design is by Fraas [7], which presents a detailed thermal and hydraulic analysis of a truck radiator. In our analysis herein, we have followed the design

recommendations of coolant and air temperatures, pressure loss, pumping power from this reference. We have also verified the validity of our selected dimensional data for the heat transfer matrix that includes fin size, thickness, spacing and the flat tube dimensions using the information given by Kays and London and Fraas.

Ample research data exist on the thermal and hydraulic studies via experiments and theories on radiators in the publications of the Society of Automotive Engineers (SAE). They are for single phase coolants, such as glycol/water mixtures or with pure water for applications in automobiles in tropical climate. However, very limited research has appeared in the literature thus far, using nanofluids as a coolant in automotive radiators. To the best of our knowledge, the present paper may be the first reported study that considers the thermal and hydraulic performance of three different nanofluids and compares their performance with the base fluid to evaluate their strengths and weaknesses.

We have collected the proper operational parameters, such as liquid and air temperatures, liquid and air Reynolds number, acceptable pressure losses and the heat dissipation rate under which automobile radiators operate from several SAE papers, which are based on single phase coolants. Brief review of those papers follows from which we have selected the real-world values as input for our computation.

Fellague et al. [8]using a 3-dimensional CFD code developed by the Ford Motor company presented a table of face velocities corresponding to three scenarios (idle, 30mph, 60mph), which generated radiator face velocities of 2.14m/s, 3.00m/s, and 4.84m/s, respectively. These results indicate that the car velocity is about 5 times that of the radiator face velocity due blockage effects of the hood. Note that the face velocity is approach air velocity in the wind tunnel and the air velocity through the core of the radiator will be much higher. They adopted an air temperature of about 43°C warming up to about 53°C, a 10°C temperature rise.

Gollin and Bjork [9] tested five radiators in a wind tunnel to compare the performance of pure coolants: water; propylene glycol and mixture coolants: ethylene glycol and water (EG/W); propylene glycol and water (PG/W) with mix ratios of 50:50 and 70:30. The five radiators were for: (1) Chrysler Minivan, (2) Ford Taurus, (3) Ford Pick-up Truck, (4) Jeep Cherokee and (5) Pontiac Bonneville with radiator core area varying from $351in^2$ to $525in^2$. They tested the radiators with four air flow velocities within the range of 2-12m/s (4.5 to 27mph) and the

coolant flow rate of 0.38-2.28kg/s (50-300lbm/min) while maintaining a nominal difference of 60°C between the inlet temperatures of the air and coolant to generate a practical set of experimental data. The most effective coolant was water followed by 50:50 EG/W, 50:50 PG/W, 70:30 EG/W, 70:30 PG/W and finally pure PG.

Beard and Smith [10] summarize analytical and wind tunnel test results for a typical 1.5 liter car engine radiator, with the Reynolds number of coolant not exceeding 5000. They compared experimental and analytical values of heat dissipation. The coolant (water) side Reynolds number varied from 3900 to 9100 for a 3in and 1in core depth, respectively.

Eitet et al. [11] compared experimentally the performance of aluminum versus copper/brass radiator cores for heavy duty trucks. The volumetric flow was about 6000 liter per hour corresponding to 0.42m/s coolant velocity in the radiator tube. A maximum coolant temperature of 95 ±3˚C was adopted in the test. For the same thermodynamic performance/conditions, the difference of inlet temperatures was 63.6˚C. The aluminum radiator with a mass of 9.4kg was shown to be about 10% lighter compared to the copper/brass core radiator.

Liu et al. [12] present theoretical analysis for a heavy duty truck, 6-cyclinder, of 9.73 L displacement, turbocharged diesel engine with rating output of 206W at a rated speed of 2400 RPM with intercooling. They limit the max coolant temperature to 95˚C. Liquid side Reynolds number ranged from 2200 to 10000. Quantity of heat dissipated from the radiator is 116,771kcal/hr, whereas the quantity of heat rejection necessary for the engine is 112,000kcal/hr.

Cozzone [13] presented comparative results for a General Motors 1994 3.8L V6 engine under dynamometer testing with PG/W and EG/W mixtures. They confirmed that the PG based coolant has improved heat transfer coefficient due to nuclear boiling.

Only a handful of publications have appeared in the literature thus far, studying the performance of nanofluids in automobile radiators. Vasu et al. [14] carried out a theoretical study using the ε-NTU method with aluminum oxide at 4% volumetric concentration dispersed in water and concluded a significant improvement in cooling capacity of the nanofluid compared to pure water. This analysis is only applicable to regions of the world, where ambient temperature remains above 0°C throughout the year.

Leong et al. [15] performed a similar theoretical analysis, but considered nanofluids containing copper oxide with a concentration up to 2% dispersed in pure ethylene glycol (EG). However, pure EG is not used in radiators. For cold regions, a 50:50 ethylene glycol and water (EG/W) mixture is used and for extreme cold regions, such as the interior Alaska a 60:40 EG/W mixture is used to guarantee a freeze protection down to -48.3˚C. The mixture of EG/W is a better fluid from thermodynamics view point than pure EG. Leong et al. found 3.8% heat transfer enhancement over the base fluid at a 2% concentration for 6000 and 5000 air and coolant side Reynolds numbers, respectively.

Peyghambarzadeh et al.[16] performed an experimental study on aluminum oxide nanofluids with concentration ranging from 0% to 1.2% in pure ethylene glycol, pure water and ethylene glycol & water mixtures (5,10,20 vol.% EG) base fluids. They presented an impressive 40% increase in Nusselt Number at optimal conditions with nanofluids.

Vajjha et al. [17] carried out a computational study on flat tubes of a radiator of a Chrysler Minivan using two different nanoparticles Al_2O_3 and CuO within a concentration range of 0-6% in 60:40 EG/W by mass, suitable for cold climates. From their analysis in the laminar flow regime, they showed as much as 82.5% and 77.7% reduction in pumping power for a constant heat transfer coefficient with 10% Al_2O_3 and 6% CuO, respectively.

Observing the lack of data on the application of nanofluids in automotive radiators, we undertook the present research project. The automotive radiator modeled was for a Subaru vehicle. The reason for selecting this radiator is its ease in availability and low cost. We could dismantle part of it easily to make accurate measurements of fins and flat tubes. The radiator geometry is displayed in Figure 2.2 under Section 2.4. It operates as a mixed (air side)/unmixed (liquid side) cross-flow compact heat exchanger, which uses a louvered serpentine fin design. It has selective cuts on the fins to influence mixing and turbulence in the boundary layer and promotes heat transfer. This type of radiator is used for engine sizes of 2.2 to 2.5 liter 4-cylinder (137-165hp), which is commonly used in compact cars.

2.2 Project Objective

A detailed computational study using Matlab code was conducted to compare the fluid dynamic and thermal performance of three nanofluids as heat transfer mediums in an automotive radiator operating in the turbulent regime. The three nanofluids were considered: aluminum

oxide (Al_2O_3), copper oxide (CuO) and silicon dioxide (SiO_2) nanoparticles dispersed in the base fluid, EG/W 60:40 by mass. This base fluid is commonly used in cold climates experienced in Alaska and other circumpolar regions for its low freezing temperature around -48.3˚C [18]. Using theoretical and empirical correlations developed for nanofluid properties from the recent literature, we investigated the effects of particle volumetric concentration, coolant and air inlet temperatures and Reynolds number of air and coolant (EG/W & nanofluids) on the thermal performance of the radiator. The objective is to compare pumping power and surface area reduction on the basis of equal heat dissipation with the base fluid and different nanofluids to conclusively evaluate the benefit of nanofluids in automotive radiators.

2.3 Thermodynamic Properties

Correlations for density, specific heat, dynamic viscosity and thermal conductivity of the base fluid, air and nanofluids are required for the computational analysis. Accurate data for properties of the base fluid and air are available in books. Correlations were developed from this data, by curve-fitting within a temperature range suitable for automobiles. These correlations were subsequently substituted in the computation scheme.

2.3.1 Conventional Coolant – 60:40 EG/W

Traditional automotive coolant in cold regions is usually a 50:50 ethylene glycol and water mixture, but in sub-arctic and arctic regions such as Alaska, additional freezing protection is needed, therefore a 60:40 mixture by mass is used. The base fluid properties data was obtained from the ASHRAE Fundamentals Handbook[18] and curve fitted as a function of temperature, over a range of 238K (-35˚C) ≤ T ≤ 398K (125˚C) that will be encountered by an automobile from starting to the fully operating condition. The thermophysical property correlations presented in Table 2.1 , except viscosity was modeled after Yaws [19], with the improvement that we expressed them in the nondimensional form. The viscosity correlation follows the log-quadratic empirical fit recommend by White [20] for liquids. The subscript “0” refers to the fluid property at the standard reference temperature of 273K (T_0). All the thermophysical correlations show a coefficient of determination $R^2 \approx 1$ and an absolute error of less than 0.1%, except for viscosity. To improve the accuracy of the viscosity correlation, the temperature range was split into two segments $238K \le T \le 273K$ and $273K \le T \le 398K$, achieving an error of less than 0.9%.

Table 2.1: EG/W 60:40 properties correlation for $238K \le T \le 398K$ $(-35°C \le T \le 125°C)$				
Property	Correlation	Constants	R^2	Error
Density (kg/m^3)	$\frac{\rho}{\rho_0} = A + B\left(\frac{T}{T_0}\right) + C\left(\frac{T}{T_0}\right)^2$	$\rho_0 = 1091.66 \frac{kg}{m^3}$ $A = 0.9247 \;\; B = 0.2414$ $C = -0.1661$	1	0.01%
Viscosity $(Pa{\cdot}s)$	$ln\left(\frac{\mu}{\mu_0}\right) = A + B\left(\frac{T_0}{T}\right) + C\left(\frac{T_0}{T}\right)^2$	$\mu_0 = 1.1 \times 10^{-2} \frac{kg}{m{\cdot}s}$		
	$238K \le T \le 273K$	$A = 0.3707$ $B = -12.882$ $C = 12.513$	1	0.19%
	$273K \le T \le 398K$	$A = -4.976 \;\; B = -1.942$ $C = 6.9088$	1	0.91%
Specific Heat $(J/kg{\cdot}K)$	$\frac{c_p}{c_{p0}} = A + B\left(\frac{T}{T_0}\right)$	$c_{p,0} = 3042.02 \frac{J}{kg{\cdot}K}$ $A = 0.6185 \;\; B = 0.3814$	1	0.01%
Thermal Conductivity $(W/m{\cdot}K)$	$\frac{k}{k_0} = A + B\left(\frac{T}{T_0}\right) + C\left(\frac{T}{T_0}\right)^2$	$k_0 = 0.342 \frac{W}{m{\cdot}K}$ $A = -0.2939 \;\; B = 1.981$ $C = -0.6868$	0.999	0.11%

2.3.2 Air Properties

The thermophysical properties of air as presented in Table 2.2 were curve-fitted using data from Cengel [21], which presents a broader temperature range $223K \le T \le 373K$ than necessary for automotive radiator application. The density correlation was derived from the ideal gas law. The correlations for specific heat, viscosity and thermal conductivity followed models presented by Yaws [19], but in nondimensional form. As observed for the base fluid correlations, the coefficient of determination is $R^2 \approx 1$ and the absolute error associated with all the correlations are less than or equal to 0.3%.

Table 2.2: Air properties correlations for $223K \le T \le 373K \quad (-40°C \le T \le 100°C)$				
Property	Correlation	Constants	R^2	Error
Density (kg/m^3)	$\frac{\rho}{\rho_0} = A + B\left(\frac{T_0}{T}\right)$	$\rho_0 = 1.292 \frac{kg}{m^3}$ $A = 0 \quad B = 1$	1	0.03 %
Viscosity $(Pa{\cdot}s)$	$\frac{\mu}{\mu_0} = A + B\left(\frac{T}{T_0}\right) + C\left(\frac{T}{T_0}\right)^2$	$\mu_0 = 1.73 \times 10^{-5} \frac{kg}{m{\cdot}s}$ $A = 0.05779$ $B = 1.11$ $C = -0.1681$	0.9998	0.07 %
Specific Heat $(J/kg{\cdot}K)$	$\frac{c_p}{c_{p0}} = A + B\left(\frac{T}{T_0}\right) + C\left(\frac{T}{T_0}\right)^2 + D\left(\frac{T}{T_0}\right)^3$	$c_{p0} = 1006 \frac{J}{kg{\cdot}K}$ $A = 0.5984$ $B = 1.034$ $C = -0.8852$ $D = 0.2526$	0.9793	0.30 %
Thermal Conductivity $(W/m{\cdot}K)$	$\frac{k}{k_0} = A + B\left(\frac{T}{T_0}\right) + C\left(\frac{T}{T_0}\right)^2$	$k_0 = 0.02364 \frac{W}{m{\cdot}K}$ $A = 0.05054$ $B = 1.025$ $C = -0.07624$	1	0.07 %

2.3.3 Nanofluid Properties

For EG/W nanofluid with different nanoparticles suspensions, thermophysical properties data were not available in the literature. Therefore, a comprehensive properties measurement project was undertaken over a period of several years at the University of Alaska Fairbanks to develop general correlations for density, specific heat, thermal conductivity and viscosity of several EG/W based nanofluids.

2.3.3.1 Nanofluids Preparation and Characterization

Several nanofluids were purchased from Alfa Aesar [22] as a concentrated aqueous suspension with average particle size in the range of 15 to 70nm. The nanofluid was subjected to ultrasonication in two stages. In the first stage, the concentrated mother nanofluid (original fluid from manufacturer) was sonicated in a Branson Sonicator under a frequency of 40 kHz and a power of 185W. The mother nanofluid was subjected to three sessions each of 2-hours duration.

Using the density of nanoparticles (e.g. Al_2O_3 particle density of 3600kg/m^3) and that of the EG/W 60:40 at room temperature of 25˚C is 1081kg/m^3, it was calculated, how much mass of the concentrated mother fluid will be added to form concentrations of 1 to 6% by volume of nanoparticles in the EG/W base fluid. Next, using a precision electronic mass balance the exact mass of the concentrated mother nanofluid was measured by adding droplets of nanofluids by a pipette. In the second phase, these dilute nanofluids in bottles were sonicated in the ultrasonicator for 3 hours, which has been found to be adequate to break down the agglomerated particles. Then a small sample of the diluted nanofluid is examined under the transmission electron microscope (TEM). Figure 2.1 shows the TEM image of the Al_2O_3 nanofluid as an example. The particles are perfectly spherical and vary in sizes from around 15nm to about 70nm. From the particle size distribution, the average particle size of 45nm specified by the manufacturer seems to be accurate. No agglomeration of nanoparticles was observed. Further details on the preparation of nanofluids, ultrasonication process and characterization can be found from [3, 23, 24]. The sonicated samples of nanofluid were used in the densometer, specific heat and thermal conductivity apparatus and in the Brookfield viscometer for properties measurement. The properties of nanoparticles are summarized in Table 2.3.

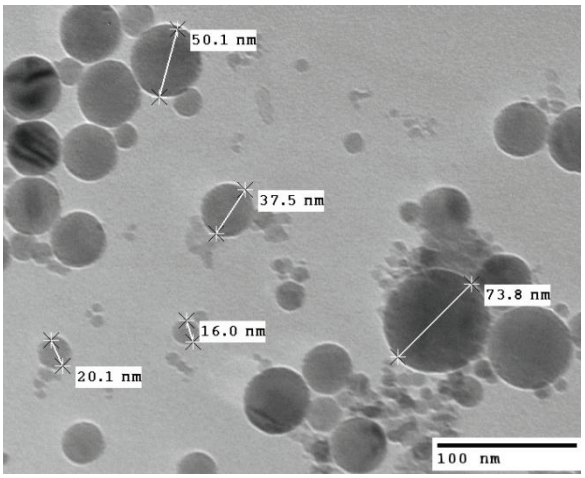

Figure 2.1: A TEM image of Al_2O_3 nanoparticles before properties measurements.

Table 2.3: Nanoparticle Properties

Particle	Diameter (nm)	Density (kg/m^3)	Specific Heat $(J/kg{\cdot}K)$	Thermal Conductivity $(W/m{\cdot}K)$
Al_2O_3	45[3]	3600[3]	765[21]	36.0[3]
CuO[25]	29	6500	533	17.65
SiO_2[21]	20	2220	745	1.38

2.3.3.2 Density

Vajjha et al. [26] used Anton Paar densometer and measured density of three different nanofluids: aluminum oxide, antimony-tin oxide, and zinc oxide. They compared the theoretical density Eq. (2.1) presented by Pak and Cho [2] to their measured values and found the theoretical equation to be in good agreement with the experimental data.

$$\rho_{nf} = \phi\rho_p + (1-\phi)\rho_{bf} \tag{2.1}$$

2.3.3.3 Specific Heat

Vajjha and Das [23] conducted specific heat measurements on three nanofluids (Al_2O_3, ZnO, SiO_2) and developed a correlation given by Eq.(2.2), where the curve-fit coefficients A, B and C are shown in Table 2.4.

$$\frac{c_{p,nf}}{c_{p,bf}} = \frac{(A(T/T_0) + B(c_{p,p}/c_{p,bf}))}{(C+\phi)} \tag{2.2}$$

Table 2.4: Curve-fit coefficients for specific heat of Al_2O_3 nanofluids [23]

Nanofluid	A	B	C	Max. deviation %	Avg. absolute deviation %
Al_2O_3	0.2432703	0.5179	0.4250	5	2.28

The Al_2O_3 and ZnO nanoparticles were dispersed in 60:40 EG/W and the SiO_2 were dispersed in deionized water due to the gelling of the nanofluid. The authors used the Eq. (1.3) presented by Xuan and Roetzel [27] to determine the specific heat for copper oxide and silicon dioxide dispersed in 60:40 ethylene glycol and water mixture.

$$c_{p,nf} = \frac{\phi\rho_p c_{p,p} + (1-\phi)\rho_{bf} c_{p,bf}}{\rho_{nf}} \tag{2.3}$$

2.3.3.4 Thermal Conductivity

Vajjha and Das [3] experimentally determined the thermal conductivity of aluminum oxide, copper oxide and zinc oxide nanofluids using the apparatus by PA Hilton that uses the steady state measurement technique. Koo and Kleinstreuer [1] had presented a thermal conductivity model for nanofluids that added a Brownian motion term to the conventional mixture conductivity model due to Maxwell. This is shown by Eq. (1.5a). Following Koo and Kleinstreuer [1] model Vajjha and Das have developed similar correlations for nanoparticles dispersed in

60:40 EG/W mixture. The equations (1.5a) and (2.5) presented by them have an average deviation of 0.23%, 5.74% and 1.97%, respectively from the experimental data, for three nanofluids shown in Table 2.5. Sahoo [28] developed a correlation for silicon dioxide nanofluid using the same experimental setup. The correlations developed by these authors are given

$$k_{nf} = \frac{k_p + 2k_{bf} - 2(k_{bf} - k_p)\phi}{k_p + 2k_{bf} + (k_{bf} - k_p)\phi} k_{bf} + 5\times10^4 \beta\phi\rho_{bf} c_{p,bf} \times \sqrt{\frac{\kappa T}{\rho_p d_p}} f(T,\phi) \qquad (2.4)$$

Table 2.5: Curve-fit relations proposed by Vajjha and Das[3] and Sahoo[28] valid for $298\,K \le T \le 363\,K$

Type of particles	β	Concentration
Al_2O_3	$8.4407(100\phi)^{-1.07304}$	$1\% \le \phi \le 10\%$
CuO	$9.881(100\phi)^{-0.9446}$	$1\% \le \phi \le 6\%$
SiO_2	$1.9526\ (100\phi)^{-1.4594}$	$1\% \le \phi \le 10\%$

$$f(T,\phi) = (2.8217\times10^{-2}\phi + 3.917\times10^{-3})\left(\frac{T}{T_0}\right) + (-3.0669\times10^{-2}\phi - 3.91123\times10^{-3}) \qquad (2.5)$$

2.3.3.5 Viscosity

Vajjha et al.[25] proposed a nondimensional correlation, Eq. (2.6) for three nanofluids (Al_2O_3,CuO,SiO_2) dispersed in EG/W from 0˚C to 90˚C by combining the experimental data from several researchers, Namburu et al.[29, 30] and Sahoo et al.[31]. The previous researchers used Brookfield viscometer equipped with a computer controlled temperature bath to measure viscosity of nanofluids.

$$\frac{\mu_{nf}}{\mu_{bf}} = A\exp(B\phi) \qquad (2.6)$$

Table 2.6: Curve-fit relations proposed by Vajjha et al. [25] valid for $273\,K \le T \le 363\,K$

Nanoparticle	A	B	Concentration
Al_2O_3	0.983	12.959	$1\% \le \phi \le 10\%$
CuO	0.9197	22.8539	$1\% \le \phi \le 6\%$
SiO_2	1.0249	6.5972	$1\% \le \phi \le 10\%$

2.4 Automotive Radiator

The geometries of the automotive radiator used for computations in this study are those of a 1998 Subaru Forester or Impreza vehicle. The schematic geometry of the radiator is shown in Figure 2.2. This radiator uses a serpentine-louvered fin design with a fin pitch of 24fins/in (9.45fins/cm). Table 2.7 lists the parameters and their values needed for the analysis of the performance of this radiator.

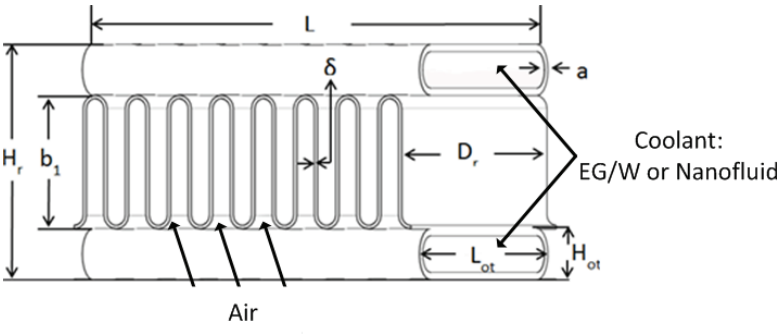

Figure 2.2: A schematic diagram of the radiator geometry of a Subaru Forester/Impreza radiator

Table 2.7: Radiator design parameters			
Parameter	Symbol	Unit	Value
Core Matrix	Inline louvered fin		
Core Geometry	L_r, H_r, D_r	m	0.673 x 0.406 x 0.0163
Number of Tubes	N	----	52
Tube Wall Thickness	a	mm	0.3302
Outside Tube Geometry	L_{ot}, H_{ot}	mm	14.427 x 2.413
Inside Tube Geometry	L_{it}, H_{it}	mm	13.767 x 1.753
Tube – Plate Spacing	b_c	mm	1.753
Tube and Fin Material	Aluminum (Alloy 2024-T6)		
Fin Pitch	P	Fin/cm	10.64
Fin – Plate Spacing	b_a	mm	6.35
Fin Thickness	δ	mm	0.152
Tube and Fin Thermal Conductivity[21]	k_f	$W/(m{\cdot}K)$	177
Fin Length	L_f	mm	3.175
Total Transfer Area/ Volume Between Plates*	β	m^2/m^3	2466
Fin Area/Total Area*	A_{ft}	----	0.887
Air Flow Passage Hydraulic Diameter*	$4r_{h,a}$	mm	1.423

*For simplicity, these surface geometry data ($\beta, A_{ft}, 4r_{h,a}$) were taken from Kays and London [6] for a surface number of 27.03, which is the closest to the number of fins for this radiator.

2.4.1 Surface Geometries

Additional surface geometries are need for both the air and coolant side before performing an analysis. The equations below show how the surface geometries were calculated as presented by Kays and London [6].

Frontal area; $A_{fr}\ (m^2)$

Air Side: $$A_{fr,a} = L_r H_r \tag{2.7}$$

Coolant Side: $$A_{fr,c} = H_r D_r \tag{2.8}$$

Total transfer area/total exchanger volume; $\alpha\ (m^2/m^3)$

Air Side: $$\alpha_a = \frac{\beta b_1}{b_1 + b_2 + 2a} \tag{2.9}$$

Coolant Side: $$\alpha_c = \frac{A_{t,c}}{V_r} \tag{2.10}$$

Total Transfer Area; $A_t\ (m^2)$

Coolant Side: $$A_{t,c} = NL_r\left[2(L_{it} - H_{it}) + \pi(H_{it})\right] \tag{2.11}$$

Free Flow area/Frontal Area; σ

Air Side: $$\sigma_a = \alpha_a r_{h,a} \tag{2.12}$$

Free Flow Area; $A_c\ (m^2)$

Air Side $$A_{c,a} = A_{fr,a}\sigma_a \tag{2.13}$$

Coolant Side $$A_{c,c} = N\left[(L_{it} - H_{it})H_{it} + \frac{\pi}{4}H_{it}^2\right] \tag{2.14}$$

2.5 Thermal and Fluid Dynamic Calculations

The $\varepsilon - NTU$ method was incorporated in Matlab coding to determine thermal and fluid dynamic performance of the radiator. The method is outlined by Kays and London [6] and Figure 2.3 illustrates our implementation of the method. The $\varepsilon - NTU$ method usually doesn't require an iterative process, but doing so provides better values for thermophysical properties of the fluid, which gives a more accurate result, since nanofluids properties are sensitive to temperature.

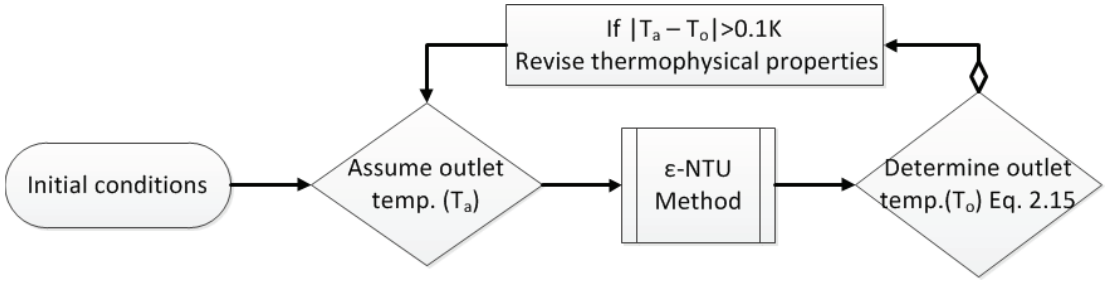

Figure 2.3: Flow chart analysis of the computational approach

$$Q_{NTU} = \varepsilon C_{min}(T_{i,c} - T_{i,a}) = C_a \Delta T_a = C_c \Delta T_c \tag{2.15}$$

2.5.1 Equations for the Air Side of the Radiator

The following equations have been adopted from Kays and London [6]

Mass Flow Rate $$\dot{m}_a = \rho_a A_{c,a} V_a \tag{2.16}$$

Heat Capacity Rate $$C_a = \dot{m}_a c_{p,a} \tag{2.17}$$

A correlation was developed for the Colburn factor by curve-fitting the data from Kays and London [6] on inline louvered fins and is presented as Eq. (2.18).

Colburn Factor $$j_a = \frac{0.1459}{Re^{0.3588}} \qquad 500 \le Re_a \le 8000 \qquad R^2 = 0.9961 \tag{2.18}$$

Convective Heat Transfer Coefficient $$h_a = \frac{j_a \rho_a V_a c_{p,a}}{Pr_a^{2/3}} \tag{2.19}$$

Fin Efficiency $$\eta = \frac{\tanh(mL_f)}{mL_f} \tag{2.20a}$$

where,

$$m = \sqrt{\frac{2h_a}{k_f \delta}} \tag{2.20b}$$

Surface Effectiveness

$$\eta_0 = 1.0 - (1.0 - \eta) \times A_{ft} \tag{2.21}$$

2.5.2 Equations for the Coolant Side of the Radiator

Mass Flow Rate

$$\dot{m}_c = \rho_c A_{c,c} V_c \tag{2.22}$$

Heat Capacity Rate

$$C_c = \dot{m}_c c_{p,c} \tag{2.23}$$

Nusselt Number

Correlation for base fluid, Gnielinski [32]

$$Nu_{bf} = 0.012(Re_{bf}^{0.87} - 280)Pr_{bf}^{0.4} \qquad 1.5 \le Pr \le 500 \quad 3\times10^3 \le Re \le 10^6 \tag{2.24}$$

Correlation for nanofluid, improved Vajjha et al. [25]

$$Nu_{nf} = 0.0222(Re_{nf}^{0.8} - 60)Pr_{nf}^{0.4}(1 + 0.32178\phi^{0.64788}) \qquad 3000 \le Re \le 16000 \tag{2.25}$$

Convective Heat Transfer Coefficient

$$h_c = \frac{Nuk}{D_{h,c}} \tag{2.26}$$

The thermal resistance of the tube wall $(R_t = (t/kA) = 1.80E-6K/W)$ was not included in the calculation. It is 100th of the mean values of either air $(R_a = 1/(\eta_0 h_a A_{t,a}) = 6.37E-4K/W)$ or coolant $(R_c = 1/(h_c A_{t_c}) = 1.84E-4K/W)$ thermal resistance.

Overall Heat Transfer Coefficient (air side) [6]

$$\frac{1}{U_a} = \frac{1}{\eta_0 h_a} + \frac{1}{\left(\frac{\alpha_c}{\alpha_a}\right) h_c} \tag{2.27}$$

Number of Transfer Units

$$NTU = \frac{U_a \alpha_a V_r}{C_{min}} \tag{2.28}$$

Capacity Ratio

$$C^* = \frac{C_{min}}{C_{max}} \tag{2.29}$$

Effectiveness Cross-flow, mixed (air)/unmixed (liquid) [21]

$$\varepsilon = 1 - \exp\left\{-\frac{1}{C^*}\left[1 - \exp(-C^* NTU)\right]\right\} \quad (2.30)$$

Heat Absorbed

$$Q = \varepsilon C_{min}(T_{h,1} - T_{c,1}) \quad (2.31)$$

Friction Factor

Base Fluid[18]

$$f_{bf} = 8\left[\left(\frac{8}{Re_{bf}}\right)^{12} + \frac{1}{(A+B)^{1.5}}\right]^{1/12}$$

$$A = \left[2.457 \ln\left(\frac{1}{\left(7/\mathrm{Re}_{bf}\right)^{0.9} + \left(0.27\varepsilon / D_{h,c}\right)}\right)\right]^{16} \quad (2.32)$$

$$B = \left(37{,}530/\mathrm{Re}_{bf}\right)^{16}$$

Nanofluid [25]

$$f_{nf} = 0.3164 Re_{nf}^{-0.25}\left(\frac{\rho_{nf}}{\rho_{bf}}\right)^{0.797}\left(\frac{\mu_{nf}}{\mu_{bf}}\right)^{0.108} \quad (2.33)$$

$$4000 \le Re \le 16000 \quad 0 \le \phi \le 0.06$$

Pressure Drop

$$\Delta P = \frac{f L_r \rho V^2}{2 D_h} \quad (2.34)$$

Pumping Power

$$\dot{W} = \dot{V}\Delta P \quad (2.35)$$

2.6 Operational Parameters Selected as Inputs

The real-world operational conditions of a radiator, such as inlet and outlet temperatures and flow rates for both coolant and air, must be used to derive meaningful results to compare performance of the radiator using different coolants. The real world operational conditions were collected from past literatures and summarized in Table 2.8 along with the current testing conditions.

Table 2.8: Normal operational conditions for automotive radiators					
Parameters	Sources[7-10, 15, 33-36]		Test Parameters used in computation		
	Min	Max	Min	Max	When held constant
Air inlet temp (K)	289	348	293	313	303
Coolant inlet temp (K)	323	383	323	383	360
Air Reynolds Numbers	500	4000	500	2000	1000
Air Mass Flow Rate (kg/s)	0	20	1	4.6	2.3
Air Face Velocity (m/s)	2	19	4	15	7.6
Coolant Reynolds Number	5000	7000	4500	6500	5500
Coolant Mass Flow Rate (kg/s)	0	3	1.8	2.5	2.08
Coolant flow velocity (m/s)	0	3	1.38	1.96	1.6
Air - h_a (W/m^{2}K)	200	267	139	350	221
Overall heat - U (W/m^{2}K)	75	240	109	215	153
Q (kW)	18	165	31	73	50

2.7 Results

2.7.1 Verification of the Computational Scheme

For verifying the accuracy of the Matlab script developed following the $\varepsilon - NTU$ scheme described under Section 2.5, analyses of several test cases were performed. The examples presented for truck radiator by Fraas [7] and an intercooler and regenerator by Kays and London [6] were computed using our code. A comparison of important parameters such as pumping power, convective and overall heat transfer coefficient, heat transfer rate, NTU and effectiveness obtained from our computations agreed with the values presented by Fraas and Kays and London within 1%. Additional verifications were performed using single phase base fluid (EG/W 60:40) as coolant to prove that the computational scheme is predicting results presented by other researchers for automotive radiators.

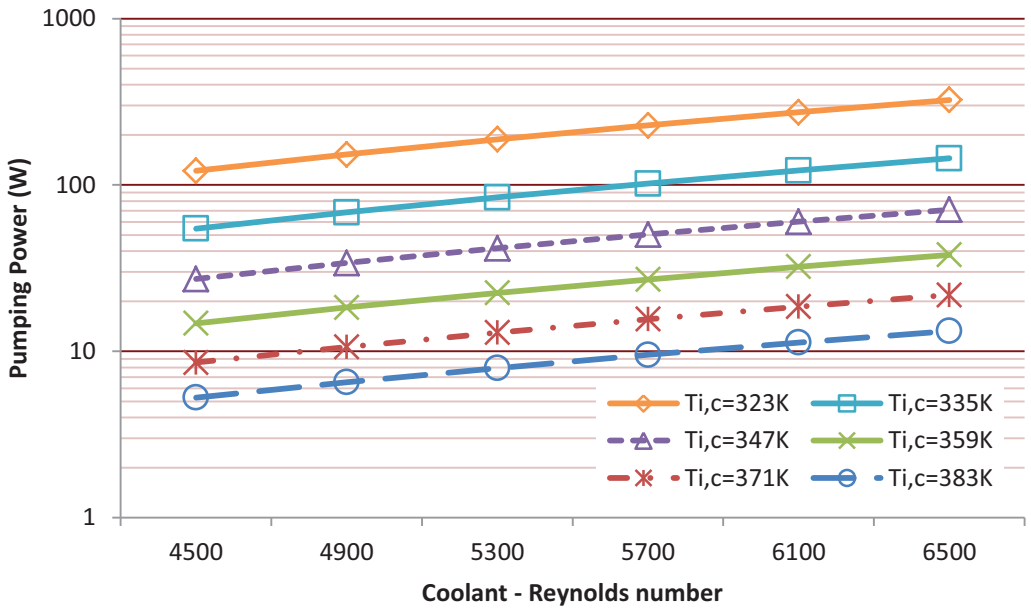

Figure 2.4: Pumping power variation with coolant Reynolds number and coolant inlet temperatures for air Reynolds number $Re_a = 1000$ and air inlet temperature $T_{i,a} = 303\,K$

Shah and Sekulic [37] have presented that the maximum pumping power requirement of an automotive water pump for a midsize car should be around 300W. Our calculations using the typical automobile input data for a Subaru radiator considered here are illustrated in Figure 2.4, which shows a similar maximum pumping power requirement of 323 W at 323 K with a Reynolds number of 6500 agreement.

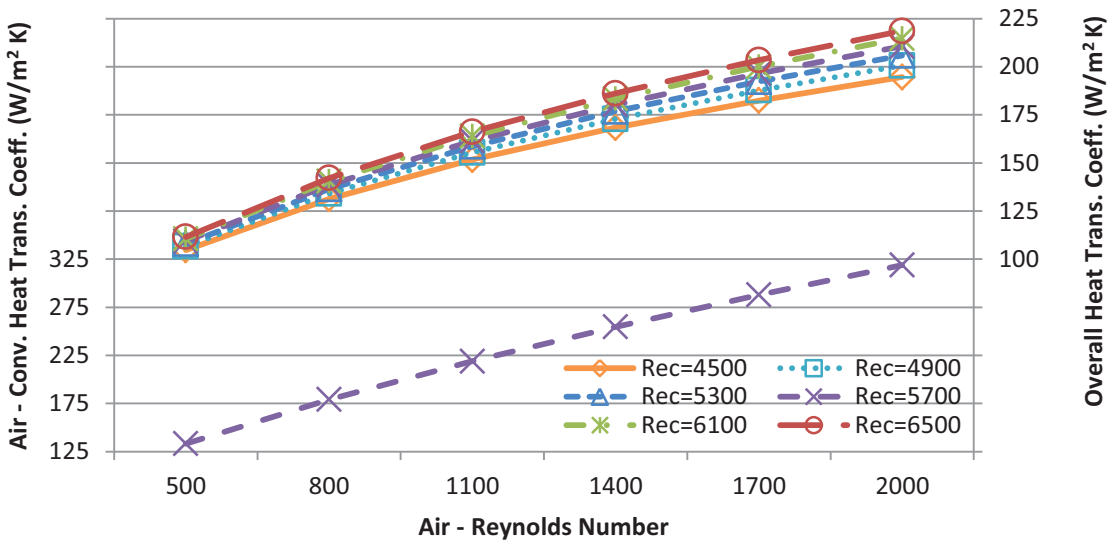

Figure 2.5: Air convective and overall heat transfer coefficients variation for a range of air and coolant Reynolds number.

Leong et al. [15] presented the air side convective heat transfer coefficient to fall in the range of 200-260 W/m^{2}K for $Re_a = 4000 - 6000$. The results of our computation are shown in Figure 2.5, which predicts the air side convection of similar order of magnitude. The difference is due to different fin designs; Leong et al. had continuous plate fins, while we are using louvered-serpentine fins with a wide range of air Reynolds number. The coolant Reynolds number has practically no effect on the air convective heat transfer coefficient expect by the slight change in thermophysical properties, therefore only one coolant Reynolds number of $Re_c = 5300$ has been plotted for the air heat transfer coefficient. On overall heat transfer coefficient the air Reynolds number plays a more significant role than that of the coolant. This is due to the dominance of the air side thermal resistance. Oliet et al. [35] stated an upper bound of 240W/m^{2}K and lower bound 110W/m^{2}K, for the overall heat transfer coefficient. Our computational results displayed in Figure 2.5 show a close agreement within the bounds of 225-100W/m^{2}K.

In Figure 2.6, we verify the ability of our computational scheme to predict the heat transfer rate properly. The effects of the coolant and air Reynolds numbers and the inlet temperature difference (ITD) have been examined on the heat transfer rate. As seen in the figure, the coolant Reynolds number has little effect on the heat transfer rate, while air Reynolds number show significant effect on the heat transfer rate, while the ITD plays an important role as

expected, being the driving force for heat transfer. Our method predicts a maximum heat transfer rate of about 110kW and a minimum of 12KW. As a confirmation of these results, this range encompasses the values presented by other researchers. Computations by Maplesoft [38] for a radiator predicts 70.7kW and Ecer et al. [33] predicted a range of 18-32kW. Kreul [34] presented an approximation that the maximum heat transfer rate for our Subaru with an engine power of 135hp, a heat dissipation of 95kW. Our computation predicts a close value of 100kW as the maximum heat dissipation for our modeled Subaru radiator.

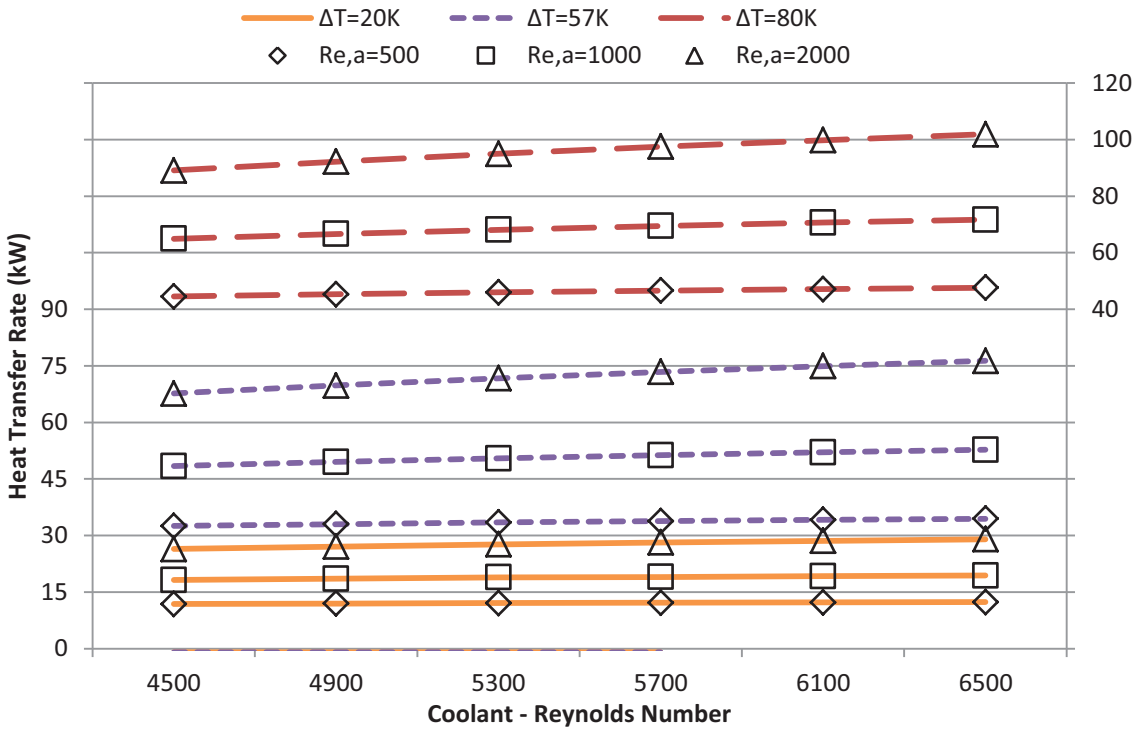

Figure 2.6: A comparison of heat transfer rate due to Reynolds number and inlet temperature difference of fluids.

In Figure 2.7, we present the NTU and effectiveness values for comparison with those reported by Shah and Sekulic [37] and Maplesoft [38]. Shah and Sekulic stated the NTU and effectiveness for automotive radiators were approximately, 0.5 and 40% respectively, which fall in the middle of our computed results shown in Figure 2.7. Maplesoft's values of 0.9 and 50% for NTU and effectiveness respectively are at the upper region of our calculations. This may be due to the fact that their analysis is based on 50:50 EG/W, whereas our analysis is based on 60:40 EG/W. It

is well-known that the thermophysical properties of 50:50 mixture is superior to those of 60:40 mixture as water has superior thermal properties than the EG.

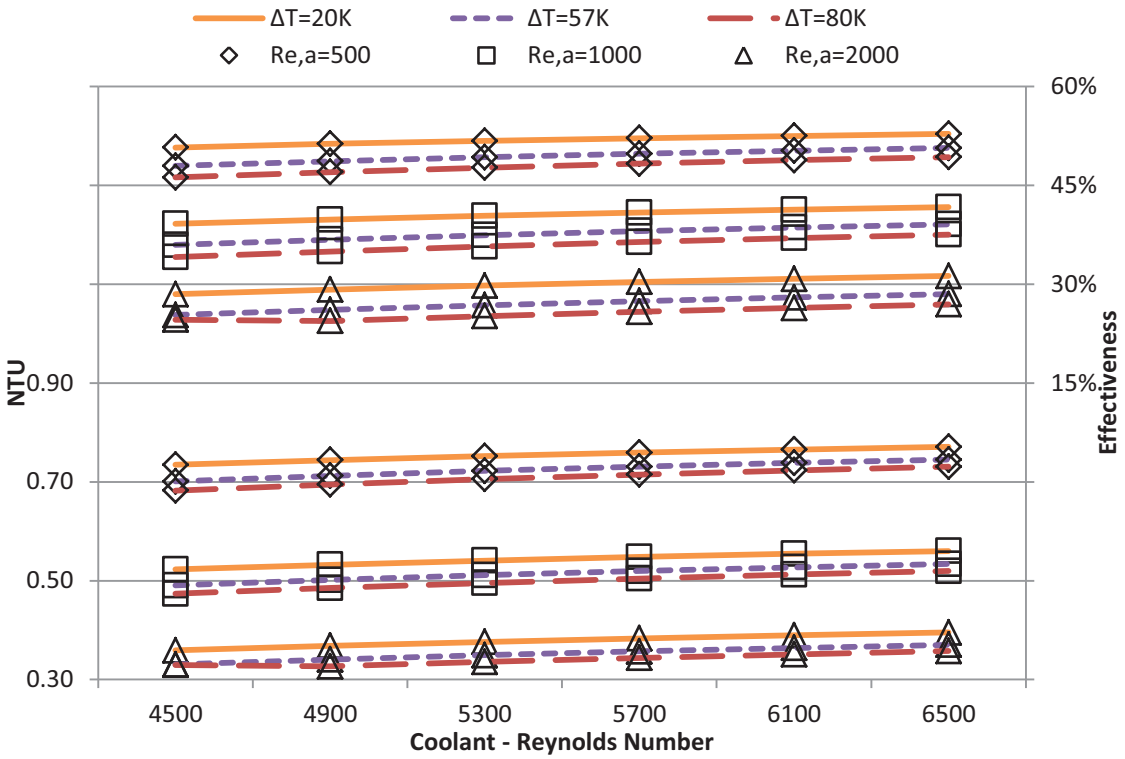

Figure 2.7: The NTU and effectiveness of an automotive radiator as a function of Reynolds number and ITD.

Table 2.9 summarizes the thermal and fluid dynamic performance of the base fluid EG/W (60:40) in an automotive radiator for three operational scenarios: idling, city and highway, which correspond to the lowest, medium and highest performance cases. The idle scenario operates at the lowest ITD of 20K and Reynolds number for air (500) and coolant (4500), which shows the lowest heat dissipation of 11.8kW with the highest value of pumping power 120W. The city or medium performance case shows an ITD of 57K with reasonable Reynolds number of 1000 and 5500 for air and coolant respectively. Here we attain mid-level performance with dissipating 50.9kW with a pumping power cost of 23.5W. The highest or highway performance case shows the highest ITD of 80K with the probably the upper range Reynolds numbers for air (2000) and the coolant (6500). At this case the heat transfer rate is at its maximum dissipation of 102kW with the pumping power at the lowest value of 14.7W. The three cases illustrated here prove

the computational scheme's ability to predict the correct trend of the thermal and fluid dynamic performance of a radiator.

Table 2.9: Performance analysis of automotive radiator for (a) idle, (b) city and (c) highway conditions

Parameter	(a)		(b)		(c)	
Fluid	Air	EG/W	Air	EG/W	Air	EG/W
Inlet temperature (K)	303.0	323.0	303.0	360.0	303.0	383.0
Outlet temperature (K)	313.2	322.0	324.5	353.0	324.6	367.0
Average Temperature (K)	308.1	322.5	313.8	356.5	313.8	375.0
Reynolds number	500	4500	1000	5500	2000	6500
Velocity (m/s)	5.82	2.79	12.02	1.67	24.04	1.46
Volumetric flow rate (m^3/s)	1.01	3.41E-03	2.09	2.04E-03	4.18	1.78E-03
Mass flow rate (kg/s)	1.16	3.64	2.35	2.13	4.69	1.83
Heat transfer coefficient ($W/m^2 K$)	130	5527	206	5266	321	5575
Thermal Resistance (K/W)	9.93E-4	1.75E-4	6.37E-4	1.84E-4	4.18E-4	1.74E-4
Thermal Resistance Ratio (R_a/R_c)	5.7		3.5		2.4	
Overall heat trans. coef. (W/m^2K)	108		153		212	
Effectiveness	0.51		0.38		0.27	
NTU	0.73		0.52		0.36	
Heat dissipated (kW)	11.8		50.9		101.9	
Pressure Loss (kPa) - Coolant	34.97		11.54		8.25	
Pumping power (W) - Coolant	119.17		23.51		14.66	

2.7.2 Nanofluids Performance Evaluation

After verifying the successful prediction of the developed computation scheme for base fluid, it was applied to evaluate performance of different nanofluids. The objective was to determine the optimal conditions for nanofluids to obtain the best performance. Four parameters can be varied to evaluate the performance of nanofluids:

- Volumetric concentration: $T_{i,a} = 303\ K;\ T_{i,c} = 360\ K;\ Re_a = 1000;\ Re_c = 5500;\ \phi = 1-6\%$
- Coolant inlet temperature: $T_{i,a} = 303\ K;\ T_{i,c} = 323-383\ K;\ Re_a = 1000;\ Re_c = 5500;\ \phi = 1\%$
- Coolant Reynolds number: $T_{i,a} = 303\ K;\ T_{i,c} = 360\ K;\ Re_a = 1000;\ Re_c = 4500-6500;\ \phi = 1\%$
- Air Reynolds numbers: : $T_{i,a} = 303\ K;\ T_{i,c} = 360\ K;\ Re_a = 500-2000;\ Re_c = 5500;\ \phi = 1\%$

The performance of nanofluids is then compared on two bases: constant surface area and constant pumping power, while maintaining equal heat dissipation. Using nanofluids in a heat exchanger can either decrease the pumping power (pumping power analysis) of the current system or decrease the required surface area (surface area analysis) of the heat exchanger for a future system, for equal heat transfer rate of the base fluid. The pumping power analysis uses the following numerical scheme, which will determine the amount nanofluids can reduce the pumping power by:

1. Assume initial mass flow rate ($\dot{m}_{bf} = \dot{m}_{nf}$) for nanofluid.
2. Use the $\varepsilon - NTU$ analysis scheme outline in section 2.5.
3. Determine mass flow rate of nanofluid for equal heat transfer: $Q_{bf} = (\dot{m} c_p \Delta T)_{nf}$
4. Repeat process (1-4) with new mass flow rate until no noticeable change in mass flow rate is observed.

The surface area analysis using constant pumping power determines how much we can reduce the required surface area. This was accomplished using the following numerical scheme:

1. Assume same heat transfer area (tube length) for nanofluids as base fluids
2. Use the analysis scheme outline in section 2.5.
3. Determine heat transfer area required for same heat transfer rate as base fluid: $NTU_{bf} = \left(UA / C_{min}\right)_{nf}$
4. With new heat transfer area, calculate the required tube length of the heat exchanger
5. Determine the maximum flow rate at which the nanofluid can perform with equal pumping power: $\dot{W}_{bf} = \left(\dot{V} \cdot \Delta P\right)_{nf}$
6. Repeat analysis (1-5) until no noticeable changes in tube length and flow rate are observed.

The performance comparison of nanofluids is reported following Eq. (2.36).

$$Performance^{*} = (nf - bf) / bf \tag{2.36}$$

2.7.2.1 Performance Analysis on the Effects of Volumetric Concentration

Parameters: $T_{i,a} = 303\ K;\ T_{i,c} = 360\ K;\ Re_a = 1000;\ Re_c = 5500;\ \phi = 1 - 6\%$

The effects of volumetric concentration of nanoparticles on the performance of nanofluids are examined in Figure 2.8 and Figure 2.9. It is noted in nanofluid literature that increasing the

particle concentration increases viscosity and thermal conductivity. An increase in viscosity will increase the Prandtl number but decrease the Reynolds number influencing heat transfer and pumping power. While an increase in thermal conductivity will increase the convection coefficient if the Nusselt number is maintained the same. These two properties are what make nanofluids thermal performance better than base fluid but can also hinder the performance.

2.7.2.1.1 Pumping Power Analysis

Under equal heat dissipation, nanofluids will perform at a much lower Reynolds as shown in Figure 2.8. With a 1% concentration we see the Reynolds number drop as much as 25% compared to the base fluid. Increasing the particle concentration will continue to lower the nanofluids Reynolds number due to the increase in viscosity of the fluid. SiO_2 nanofluid, which has the least increase on viscosity of the three nanofluids, shows the least amount of change but reduces the Reynolds number by as much as 20%. The CuO Reynolds number is much more affected by the particle concentration due to CuO having a stronger effect on viscosity than Al_2O_3.

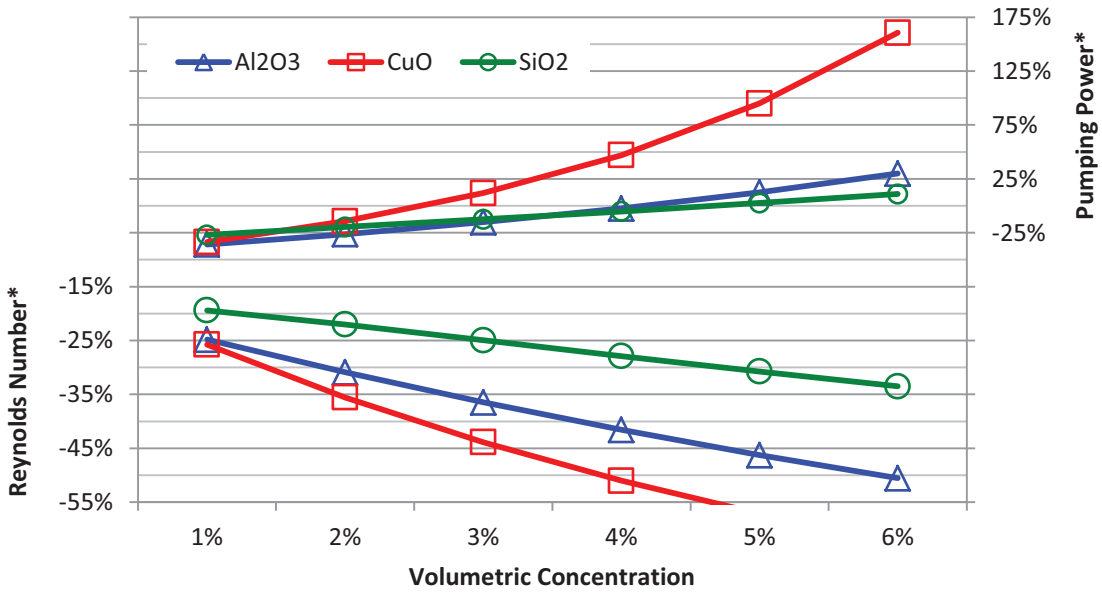

Figure 2.8: The effect of volumetric concentration of nanoparticle on the Reynolds number and pumping power compared to the base fluid

We can also observe in Figure 2.8 that increasing the concentration above 1% shows diminishing performance and above 3% even Al_2O_3 and SiO_2 nanofluids do not show a reduction in pumping

power over the base fluid. This analysis agrees with the earlier published results of Vajjha and Das [24] that the particle volumetric concentration is 1%, may be the optimal concentration for nanofluids. The 1% concentration seems to increase the thermal conductivity sufficiently, without increasing the viscosity much.

Kays and London [6] had presented a performance evaluation criterion for compact heat exchangers by plotting the heat transfer coefficient versus the friction-power characteristic. They represented the friction-power characteristics by Eq. (2.37). The factor E is the friction power expended per unit of surface area, and for a given E value, higher the heat transfer coefficient (h), better thermal performance of the heat exchanger.

$$E = \frac{f}{2\rho^2}\left(\frac{\mu Re}{D_h}\right)^3 \tag{2.37}$$

We have generated a similar plot following Kays and London, shown in Figure 2.9 to compare the performance between three nanofluids with a concentration of 1-3% and the base fluid. The convective heat transfer coefficients were calculated from Eq. (2.24)-(2.26) and friction factor from Eq.(2.32) and (2.33). From Figure 2.9 we notice the 1% Al_2O_3 and CuO concentration provide the highest heat transfer coefficients for a given E value, but as we increase the concentration the performance diminishes. The Al_2O_3 nanofluid shows mild change with increasing the concentration, while CuO nanofluid is greatly affected by particle concentration, with losing about half of its performance gain from 1% to 2% concentration. The SiO_2 nanofluid is the least influenced with increasing concentration, only diminishing the performance minutely. From this analysis, we also reconfirm the thermal performance gain of these three nanofluids lays within the concentration range of 1-3%, with the exception of CuO which showed a diminished performance, below the base fluid, at 3%.

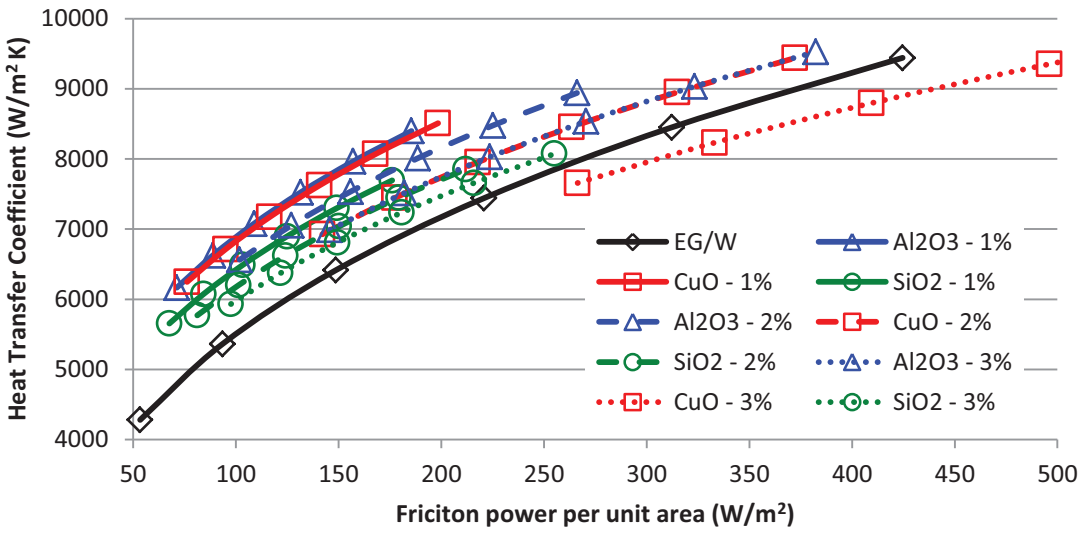

Figure 2.9: A comparison of the heat transfer coefficient and friction power per unit area with three nanofluids of 1-3% concentration and the base fluid.

2.7.2.2 Performance Analysis on the Effects of Coolant Inlet Temperatures

Parameters: $T_{i,a} = 303\ K;\ T_{i,c} = 323 - 383\ K;\ Re_a = 1000;\ Re_c = 5500;\ \phi = 1\%$

The next parameter analysis examines the effects of the coolant inlet temperature on the performance of nanofluid. Nanofluids' viscosity like base fluid is greatly affected by temperature, but unlike base fluid nanofluid thermal conductivity is significantly enhanced by temperature due to the Brownian motion of nanoparticles. Due to this significant change in thermophysical properties, exploring the performance of nanofluid in heat exchangers at various temperatures is necessary.

2.7.2.2.1 Pumping Power Analysis

In Figure 2.10, the reduction in pumping power and volumetric flow rate for 1% concentration of nanoparticles under the same surface area and heat transfer rate are shown. The nanofluids exhibit better thermal performance at higher temperatures. Lowering the volumetric flow by as much as 18% in comparison to the base fluid achieve the same objective. In Figure 2.10, Al_2O_3 shows the best performance with a significant pumping power reduction of about 36%. For Al_2O_3 nanofluid, changing the inlet temperature from 323K to 383K reduces the pumping power 33% and 36% respectively. Even, the SiO_2 nanofluid observed to be the lowest performer among

the three nanofluids, promises a volumetric flow reduction of 12% and pumping power reduction of about 27%. This nanofluid maintains nearly constant characteristic over the coolant inlet temperature range, because it has the least variation of viscosity and thermal conductivity among the three nanofluids.

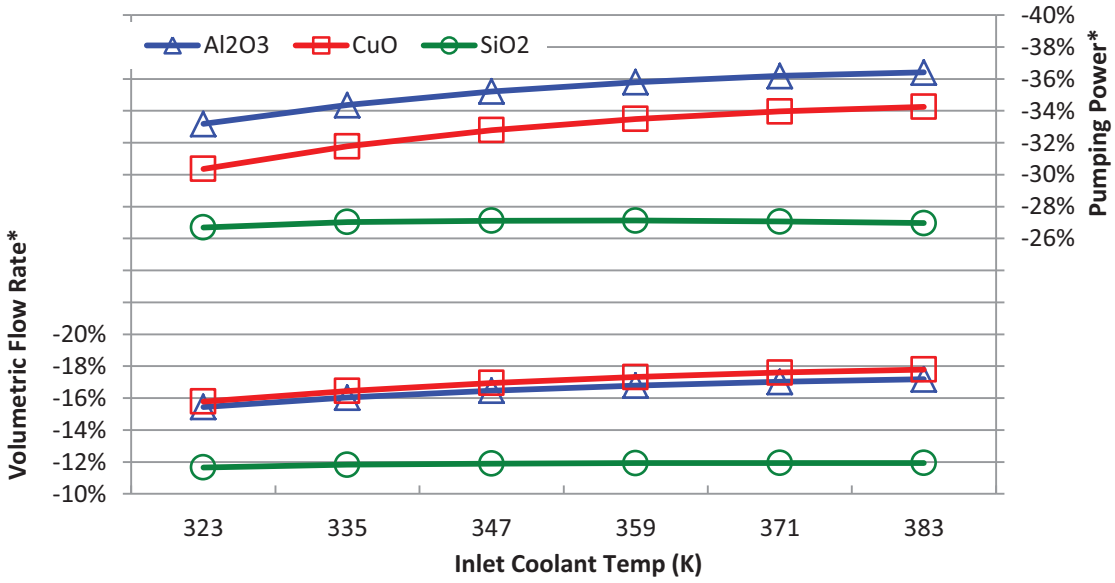

Figure 2.10: Performance comparison on the effects of coolant inlet temperature on volumetric flow rate and pumping power for 1% concentration nanofluids.

2.7.2.2.2 Surface Area Analysis

Next, we examine how temperature affects the heat transfer performance of nanofluid under a constant pumping power condition. From Figure 2.11, we see the heat transfer coefficient of nanofluids increase dramatically from about 19% to 30%, 18% to 29% and 14% to 19% for Al_2O_3, CuO and SiO_2 respectively. This is due to the increase in thermal conductivity from the Brownian motion with increase in coolant inlet temperature. Furthermore, the viscosity decreases with an increase in temperature causing the Reynolds number to rise, which leads to an increase in Nusselt number from Eq. (2.25). The thermal performance of Al_2O_3 and CuO nanofluids are close. The SiO_2 nanofluid lags behind the other two, however, still showing a significant performance 20% more than the base fluid.

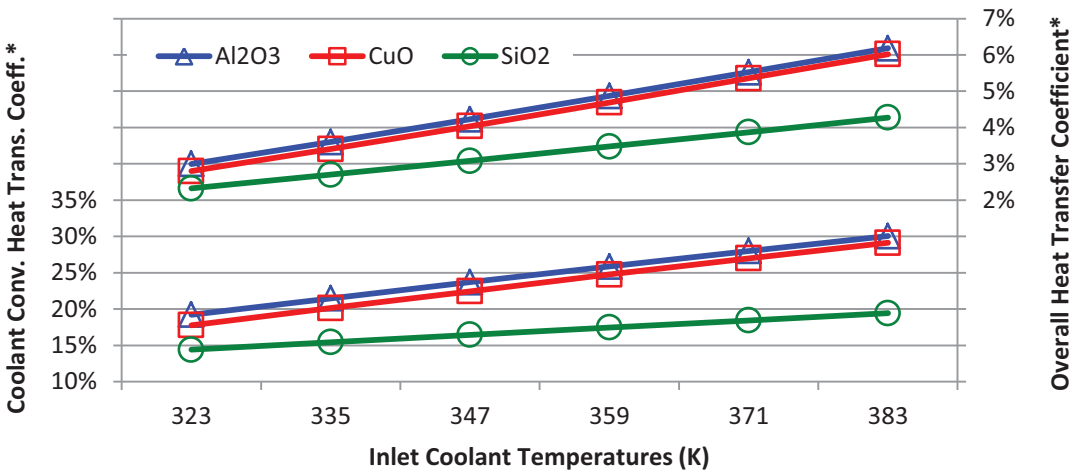

Figure 2.11: The effects of inlet temperature on the performance of nanofluids- heat transfer coefficient and overall heat transfer coefficient

With such high increases in the convective heat transfer coefficient, we see a moderate increase in the overall heat transfer coefficient in Figure 2.11. This is due to the fact that the air side thermal resistance of the convective film is found to be about 3.5 times greater than that on the coolant side. The overall heat transfer coefficient increases by as much as 6% for either Al_2O_3 or CuO. This gain in the overall heat transfer, translates to about 5.5% reduction in surface area of the radiator at the higher coolant temperature for same heat transfer rate and pumping power as the base fluid.

2.7.2.3 Performance Analysis on the Effects of Coolant Reynolds Number

Parameters: $T_{i,a} = 303\ K;\ T_{i,c} = 360\ K;\ Re_a = 1000;\ Re_c = 4500 - 6500;\ \phi = 1\%$

The following analysis finds a specific flow regime where the performance gain using nanofluids is the highest by studying the effects of the coolant Reynolds number.

2.7.2.3.1 Pumping Power Analysis

Computations carried out in the practical coolant Reynolds number range for the automotive radiator are shown in Figure 2.12 to evaluate the effect on the volumetric flow rate and pumping power performance for three nanofluids. We observe as the Reynolds number is increased the performance gain of nanofluid diminishes from 40% reduction in pumping power to 32%. The diminishing effect influences all three nanofluids in the same proportion. The higher

velocity associated with higher Reynolds number causes the pumping power to raise, because it is proportional to the cubic power of the velocity, thereby reducing the pumping power savings. Hence, the lower range of turbulent flow regime is desirable to gain the maximum benefit from using nanofluids.

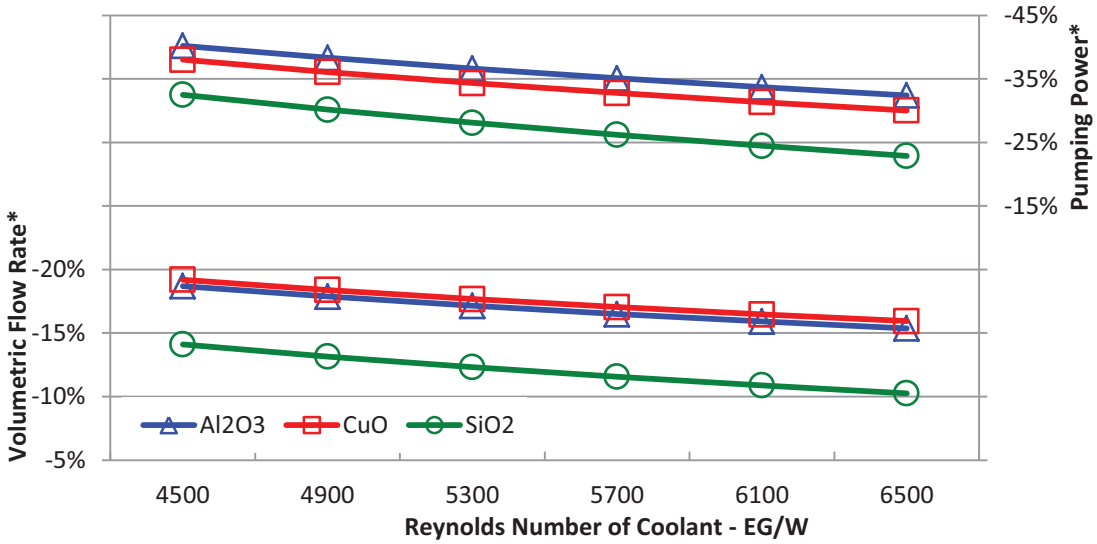

Figure 2.12: Performance comparison on the effects of coolant Reynolds number on volumetric flow rate and pumping power for three different nanofluids.

2.7.2.3.2 Surface Area Analysis

The effects of the coolant Reynolds number on convective heat transfer coefficient, overall heat transfer coefficient and subsequently determining the surface area reduction are studied next. From the Figure 2.12, we noticed that nanofluids performance diminished with increasing Reynolds number. We observe a similar trend in Figure 2.13 for heat transfer coefficient gain. For Al_2O_3 nanofluid, the heat transfer enhancement is 31% at 4500 Reynolds number and 23% at 6500 Reynolds number, which is a significant enhancement in performance.

Now, looking at the overall heat transfer coefficient performance in Figure 2.13, one observes a reduction in performance from 6.5% to 4%. This is due to two factors: diminishing performance in heat transfer coefficient and the increasing difference of thermal resistance between the air and the coolant side. The thermal resistance ratio (R_a / R_c) starts at 2.8 for coolant Reynolds number of 4500 and increases to about 4.1 at Reynolds number of 6500. The higher the thermal resistance ratio the lower the impact of increasing the coolant heat transfer coefficient will have

on the overall heat transfer coefficient. From this analysis, we conclude that nanofluids could save up to 6.2%, 6% or 4.7% using Al_2O_3, CuO or SiO_2 respectively in surface area reduction for the radiator.

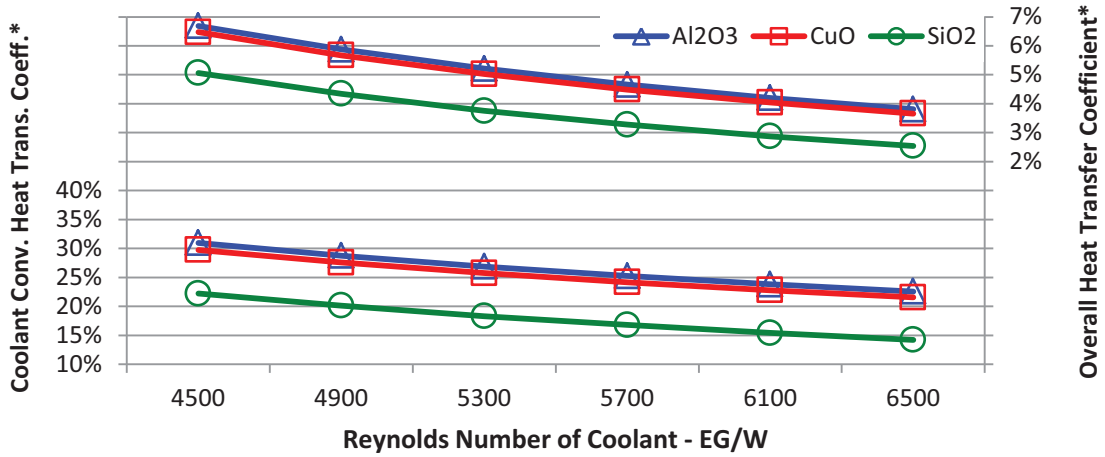

Figure 2.13: Performance comparison on the effects of coolant Reynolds number on convective and overall heat transfer coefficient for three different nanofluids.

2.7.2.4 Performance Analysis on the Effects of Air Reynolds Number

Parameters: $T_{i,a} = 303\ K;\ T_{i,c} = 360\ K;\ Re_a = 500 - 2000;\ Re_c = 5500;\ \phi = 1\%$

2.7.2.4.1 Pumping Power Analysis

As expected no appreciable change in the performance of nanofluids with varying the air Reynolds number from 500-2000 was noticed. Only a slight change in the performance $\leq 1\%$ occurred due to the change in the average temperature of the nanofluid.

2.7.2.4.2 Surface Area Analysis

The air Reynolds number plays a more vital role when looking at overall heat transfer coefficient as shown in Figure 2.14. We present how the coolant side heat transfer coefficient and overall heat transfer coefficient are affected by the air Reynolds number. The coolant heat transfer coefficient stays relatively constant over the range of air Reynolds number with only very marginal change, which is due to slight temperature change for the coolant, but the overall heat transfer coefficient shows considerable change. This is due to the change in the thermal

resistance ratio (R_a / R_c) which decreases from 5.2 at $Re_a = 500$ to 2.3 at $Re_a = 2000$, due to the increase in the air side convective heat transfer coefficient.

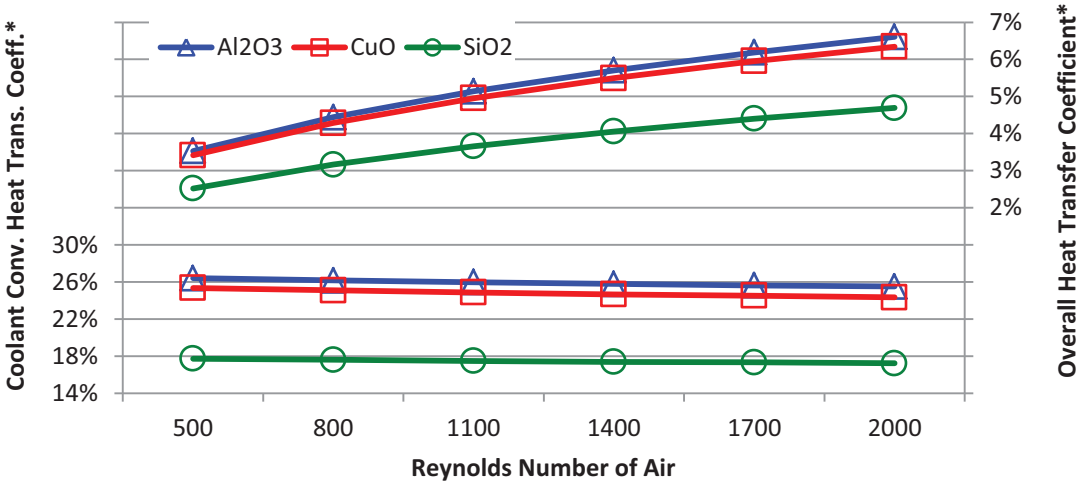

Figure 2.14: The effects of air Reynolds number on the performance of nanofluids- heat transfer coefficient and overall heat transfer coefficient

As explained in Section 2.7.2.3.2, the higher the resistance ratio the smaller the change in overall heat transfer coefficient will be obtained from nanofluids. The reverse is also true, the lower the thermal resistance ratio the greater the impact of nanofluids on the overall heat transfer coefficient. The overall heat transfer coefficient gain increased from 3.5% to 6.6% for Al_2O_3. This trend is also true for the area reduction possible with nanofluids, as evidenced in Figure 2.15, where we observe changes from 3.3% to 6%, 3.2% to 5.9% or 2.4% to 4.4% for Al_2O_3, CuO and SiO_2 respectively.

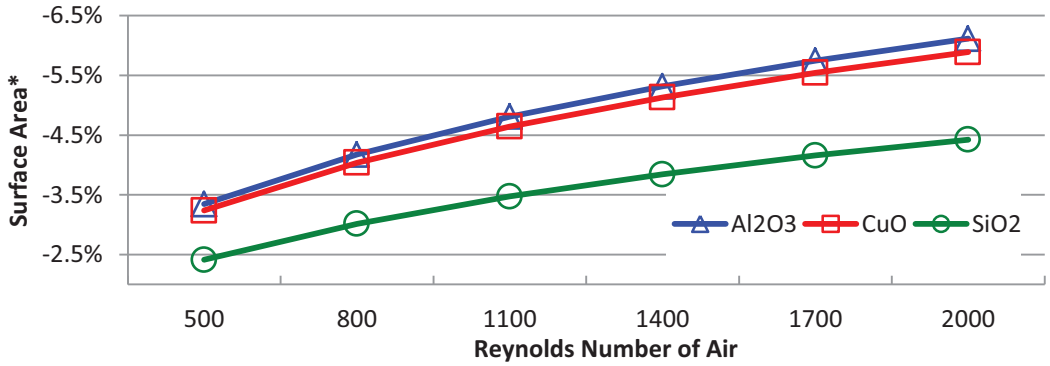

Figure 2.15: The effects of coolant Reynolds number on the surface area reduction with nanofluids.

2.7.3 Performance Summary of Nanofluids

From the knowledge of the analyses performed in preceding sections, we determined the best case scenario for nanofluids performance gain when: $T_{i,c} = 383K$; $Re_a = 2000$; $Re_c = 5500$ and $\phi = 1\%$. Using these parameters we performed the computations and summarized the performance of nanofluids in Figure 2.16 (patterned bars). It is possible to save as much as 35.3% in pumping using Al_2O_3 nanoparticles at a concentration of 1% or reduce the surface area/weight of the radiator by as much as 7.4%. As evidenced in earlier sections, and illustrated in Figure 2.16 once again, Al_2O_3 nanofluid out-performs the other nanofluids, but is closely matched by CuO nanofluid, which achieves savings in pumping power and area of 33.1% or 7.2% respectively. Although not as spectacular, even SiO_2 nanofluid promises reduction in pumping power and surface area on the basis of equal heat transfer in comparison to the base fluid.

Furthermore, to achieve a comprehensive comparison, we analyzed a worst case scenario for nanofluids using the following parameters: $T_{i,c} = 323K$; $Re_a = 500$; $Re_c = 6500$ and $\phi = 1\%$ presented the results in Figure 2.16 (solid bars). It was found that, even for the worst case operational parameters, nanofluids prove their superior performance over the base fluid with reduction in the pumping power by 28.7%, 25.7%, or 21.6% for Al_2O_3, CuO and SiO_2 respectively. The percentage reduction in surface area is now a modest amount in the range of 1.1 to 1.5% for Al_2O_3. This is due to the dominance of the air side thermal resistance; the thermal resistance ratio (R_a / R_c) changes from 2.0 for the best case scenario to 8.5 for the worst case scenario.

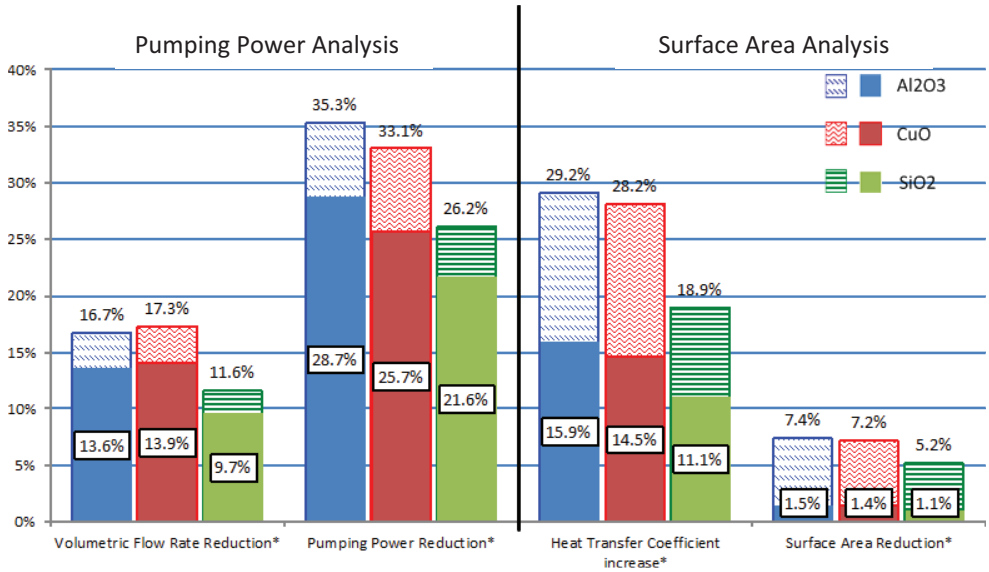

Figure 2.16: Nanofluids performance for best and worst case scenarios for reduction in pumping power or surface area of a radiator

2.7.4 Material and Financial Reductions Estimation

Consider aluminum oxide nanofluid of 1% volumetric concentration and use a conservative value of reducing the surface area of the radiator by 4%.The reduction in surface area is proportional to the reduction in radiator length and weight. The typical weight of the aluminum Subaru radiator examined in this study is approximately 15 pounds (6.8kg). According to International Organization of Motor Vehicle Manufactures [5], approximately 60 million cars are produced worldwide yearly with the average cost of aluminum in 2012 $0.98 per pound [39]. We can then calculate the amount of material and cost saved by reducing the surface area of the radiator by 4%. This does not include lowering mining cost and lowering the impact on the environment.

$$\text{Amount of aluminum saved each year} = (60 \times 10^6)(15)(0.04) = 36 \text{ million pounds}$$
$$\text{Money saved} = (3.6 \times 10^7)(0.98) \approx \$35.3 \text{ million per year}$$

2.8 Conclusions

A detailed computational study was performed for an automotive radiator with three different nanoparticles, Al_2O_3, CuO and SiO_2, dispersed in the base fluid, EG/W 60:40 by mass. Realistic operational parameter ranges were selected and used in computations for the inlet temperatures, air and coolant Reynolds number, from real world data presented by past

researchers. The computational scheme is based on the well-known $\varepsilon - NTU$ method encoded in Matlab.

Several validation studies were performed with the computational scheme with the base fluid and the following parameters: pumping power, convective and overall heat transfer coefficients, heat dissipation, effectiveness and NTU agreed with the results of previous researchers.

After the code validation, nanofluids performance comparisons were conducted examining the effects of different parameters (volumetric concentration, coolant inlet temperature and air and coolant Reynolds numbers) to determine the most optimal condition for nanofluids. From the analysis, it was determined that the nanofluids have a superior performance gain at 1% volumetric concentration, higher coolant inlet temperature, low turbulent flow regime in the tube preferably around $Re_c \leq 5500$ and air side Reynolds number around $Re_a \geq 1000$. At the most optimal conditions of operation it is possible to reduce 35.3% in pumping power or increase the convective heat transfer coefficient by 29%, which in turn reduces the surface area by 7.4% using Al_2O_3 nanofluid. The CuO nanofluid showed slightly lower magnitudes than the Al_2O_3 nanofluid, with 33.1% and 7.2% reduction for pumping power or surface area respectively. The SiO_2 nanofluid had the least performance gain of the three nanofluids, but still could reduce the pumping power and surface area by 26.2% or 5.2%.

2.9 Acknowledgement

Financial support from Alaska NASA and NSF EPSCoR and the Mechanical Engineering Department of University of Alaska Fairbanks is gratefully acknowledged.

2.10 Nomenclature

a	Tube Wall Thickness, m	T_0	Reference temp., 273 K
$A, B, C, \ldots$	Dimensionless curve-fit constants, ()	U	Overall heat transfer coefficient, $W / m^2 \cdot K$
A_c	Free flow area, m^2	V	Velocity, m/s
A_{ft}	Fin area/total area, ()	$\dot{V}$	Volumetric flow rate, m^3/s
A_{fr}	Frontal area, m^2	V_r	Volume of radiator, m^3
A_t	Heat transfer area, m^2	$\dot{W}$	Pumping power, W
b	Plate spacing, m	**Greek Letters**	
C	Heat capacity rate, W/K	α	Total transfer area/total exchanger volume, m^2/m^3
C*	Capacity ratio, ()	β	Total transfer area/volume between plates, m^2 / m^3
c_p	Specific heat, $J / kg \cdot K$	δ	Fin thickness, m
D	Depth, m	ΔP	Pressure drop, Pa
D_h	Hydraulic diameter, $4r_h$, m	ε	Heat exchanger effectiveness, ()
d_p	Particle diameter, m	η	Fin efficiency, ()
f	Friction factor, ()	η_0	Surface effectiveness, ()
H	Height, m	κ	Boltzmann constant, $1.38 \times 10^{-23} J / K$
h	Heat transfer coefficient, $W / m^2 \cdot K$	μ	Viscosity, $Pa \cdot s$
j_a	Colburn factor, ()	ρ	Density, kg / m^3
k	Thermal conductivity, $W / m \cdot K$	σ	Free flow area/frontal area
L	Length, m	ϕ	Volumetric concentration, ()
$\dot{m}$	Mass flow rate, kg/s	**Subscripts**	
N	Number of tubes, ()	0	Properties at reference temp. 273 K
Nu	Nusselt number, ()	a	Air side
NTU	Number Transfer Units, ()	bf	Base fluid
P	Fin pitch, fins/m	c	Coolant side
Pr	Prandtl number, ()	f	Fin
Q	Heat dissipation, W	ot	Outside tube
R^2	Coefficient of determination	nf	Nanofluid
Re	Reynolds number ()	it	Inside tube
r_h	Hydraulic radius	p	Nanoparticle
T	Temperature, K	r	Radiator

2.11 References

[1] Koo, J., and Kleinstreuer, C., 2005, "A new thermal conductivity model for nanofluids," Journal of Nanoparticle Research, 7(2-3), pp. 324-324.

[2] Pak, B. C., and Cho, Y. I., 1998, "Hydrodynamic and heat transfer study of dispersed fluids with submicron metallic oxide particles," Exp Heat Transfer, 11(2), pp. 151-170.

[3] Vajjha, R. S., and Das, D. K., 2009, "Experimental determination of thermal conductivity of three nanofluids and development of new correlations," International Journal of Heat and Mass Transfer, 52(21-22), pp. 4675-4682.

[4] Minkowycz, W. J., Sparrow, E. M., and Abraham, J. P., 2013, Nanoparticle Heat Transfer and Fluid Flow, CRC Press/Taylor & Francis Group.

[5] 2011, "International Organization of Motor Vehicle Manufacturers," http://www.oica.net/category/production-statistics/.

[6] Kays, W. M., and London, A. L., 1984, Compact Heat Exchangers, Krieger Pub. Co.

[7] Fraas, A. P., 1989, Heat Exchanger Design, Wiley.

[8] Fellague, K. A., Hu, S. H., and Willoughby, D. A., 1994, "Determination of the effects of inlet air velocity and temperature distributions on the performance of an automotive radiator," International Congress and Exposition, SAE International, Detroit, Michigan.

[9] Gollin, M., and Bjork, D., 1996, "Comparative performance of ethylene glycol/water and propylene glycol/water coolants in automobile radiators," International Congress and Exposition, SAE International, Detroit, Michigan.

[10] Beard, R. A., and Smith, G. J., 1971, "A method of calculating the heat dissipation from radiators to cool vehicle engines," Automotive Engineering Congress, SAE International, Detroit, Mich.

[11] Eitel, J., Woerner, G. T., Horoho, S., and Mamber, O., 1999, "The aluminum radiator for heavy duty trucks," International Truck and Bus Metting Exposition, SAE International, Detroit, Michigan.

[12] Liu, D., Hou, J., and Xu, X., 1993, "Analysis and computation of characteristic of the water cooling and radiating system for a heavy duty truck diesel engine," Seventh International Pacific Conferences and Exposition on Automotive Engineering, SAE International, Phoenix, Arizona.

[13] Cozzone, G. E., 1999, "Effect of coolant type on engine operating temperatures," International Congress and Exposition, SAE International, Detroit, Michigan.

[14] Vasu, V., Rama Krishna, K., and Kumar, A. C. S., 2008, "Thermal design analysis of compact heat exchanger using nanofluids," International Journal of Nanomanufacturing, 2(3), pp. 271-288.

[15] Leong, K. Y., Saidur, R., Kazi, S. N., and Mamun, A. H., 2010, "Performance investigation of an automotive car radiator operated with nanofluid-based coolants (nanofluid as a coolant in a radiator)," Applied Thermal Engineering, 30(17-18), pp. 2685-2692.

[16] Peyghambarzadeh, S. M., Hashemabadi, S. H., Hoseini, S. M., and Seifi Jamnani, M., 2011, "Experimental study of heat transfer enhancement using water/ethylene glycol based nanofluids as a new coolant for car radiators," International Communications in Heat and Mass Transfer, 38(9), pp. 1283-1290.

[17] Vajjha, R. S., Das, D. K., and Namburu, P. K., 2010, "Numerical study of fluid dynamic and heat transfer performance of Al2O3 and CuO nanofluids in the flat tubes of a radiator," International Journal of Heat and Fluid Flow, 31(4), pp. 613-621.

[18] American Society of Heating, R., and Engineers, A.-C., 2005, ASHRAE Handbook: Fundamentals, American Society of Heating, Refrigerating and Air-Conditioning Engineers, Atlanta, GA.

[19] Yaws, C. L., 1977, Physical Properties: A Guide to the Physical, Thermodynamic, and Transport Property Data of Industrially Important Chemical Compounds, McGraw-Hill, New York, NY.

[20] White, F. M., 2003, Fluid Mechanics, McGraw-Hill, New York, NY.

[21] Çengel, Y. A., 2007, Heat and Mass Transfer: A Practical Approach, McGraw-Hill, New York, NY.

[22] "Alfa Aesar," http://www.alfaaesar.com/.

[23] Vajjha, R. S., and Das, D. K., 2009, "Specific heat measurement of three nanofluids and development of new correlations," Journal of Heat Transfer, 131(7), pp. 1-10.

[24] Vajjha, R. S., and Das, D. K., 2012, "A review and analysis on influence of temperature and concentration of nanofluids on thermophysical properties, heat transfer and pumping power," International Journal of Heat and Mass Transfer, 55(15–16), pp. 4063-4078.

[25] Vajjha, R. S., Das, D. K., and Kulkarni, D. P., 2010, "Development of new correlations for convective heat transfer and friction factor in turbulent regime for nanofluids," International Journal of Heat and Mass Transfer, 53(21-22), pp. 4607-4618.

[26] Vajjha, R. S., Das, D. K., and Mahagaonkar, B. M., 2009, "Density measurement of different nanofluids and their comparison with theory," Petroleum Science & Technology, 27(6), pp. 612-624.

[27] Xuan, Y., and Roetzel, W., 2000, "Conceptions for heat transfer correlation of nanofluids," International Journal of Heat and Mass Transfer, 43(19), pp. 3701-3707.

[28] Sahoo, B. C., 2008, "Measurement of rheological and thermal properties and the freeze-thaw characteristics of nanofluids," Master's, University of Alaska Fairbanks.

[29] Namburu, P. K., Kulkarni, D. P., Dandekar, A., and Das, D. K., 2007, "Experimental investigation of viscosity and specific heat of silicon dioxide nanofluids," Micro & Nano Letters, 2(3), p. 67.

[30] Namburu, P. K., Kulkarni, D. P., Misra, D., and Das, D. K., 2007, "Viscosity of copper oxide nanoparticles dispersed in ethylene glycol and water mixture," Experimental Thermal and Fluid Science, 32(2), pp. 397-402.

[31] Sahoo, B. C., Vajjha, R. S., Ganguli, R., Chukwu, G. A., and Das, D. K., 2009, "Determination of rheological behavior of aluminum oxide nanofluid and development of new viscosity correlations," Petroleum Science and Technology, 27(15), pp. 1757-1770.

[32] Bejan, A., 1993, Heat Transfer, John Wiley & Sons, Inc.

[33] Ecer, A., Toksoy, C., Rubek, V., Hall, R., Gezmisoglu, G., Pagliarulo, V., Caruso, S., and Azzali, J., 1995, "Air flow and heat transfer analysis of an automotive engine radiator to calculate air-to-boil temperature," International Congress and Exposition, SAE International, Detroit, Michigan.

[34] Kreul, A. L., 1954, "Desing of radiators for automotive and industrial engines," SAE International.

[35] Oliet, C., Oliva, A., Castro, J., and Pérez-Segarra, C. D., 2007, "Parametric studies on automotive radiators," Applied Thermal Engineering, 27(11-12), pp. 2033-2043.

[36] Chiou, J. P., 1981, "Study of the arrangement of automobile air-conditioning condenser and engine radiator in the cooling air circuit," International Congress and Exposition, SAE International, Detroit, Michigan.

[37] Shah, R. K., and Sekulić, D. P., 2003, Fundamentals of Heat Exchanger Design, John Wiley & Sons, Hoboken, NJ.

[38] Maplesoft, 2008, "Designing a more effective car radiator," http://www.maplesoft.com/applications/view.aspx?SID=6403.

[39] 2012, "United States Geological Survey," http://minerals.usgs.gov/minerals/pubs/commodity/aluminum/index.html#mcs.

Chapter 3: Experimental and Numerical Investigations of Nanofluids Performance in a Compact Minichannel Plate Heat Exchanger[3]

ABSTRACT: Three nanofluids comprising of aluminum oxide, copper oxide and silicon dioxide nanoparticles in ethylene glycol and water mixture have been studied theoretically to compare their performance in a compact minichannel plate heat exchanger (PHE). The study shows that for a dilute particle volumetric concentration of 1%, all the nanofluids show improvements in their performance over the base fluid. Comparisons have been made on the basis of three important parameters; equal mass flow rate, equal heat transfer rate and equal pumping power in the PHE. For each of these cases, all three nanofluids exhibit increase in convective heat transfer coefficient, reduction in the volumetric flow rate and reduction in the pumping power requirement for the same amount of heat transfer in the PHE. On the cold fluid side of the heat exchanger, a coolant, HFE-7000, has been studied, which has the potential for application in extremely low temperatures, but has not been investigated widely in the literature. Experimental data measured from a minichannel PHE in a test loop using water as the base fluid have validated the test apparatus with excellent agreement of predicted heat transfer rate and the overall heat transfer coefficient with the experimental values. From experiments on a 0.5% aluminum oxide nanofluid, preliminary correlations for the Nusselt number and the friction factor for nanofluid flow in a PHE has been derived. This apparatus will be useful to test different kinds of nanofluids to ultimately determine the effects of parameters such as: volumetric concentration, particle size and base fluid properties on thermal and fluid dynamic performance of nanofluids in compact heat exchangers.

KEY WORDS: Compact heat exchanger, Convective heat transfer, Friction factor, Nanofluids, Nusselt number, Plate heat exchanger, Prandtl number, Reynolds number, Thermophysical properties.

---

[3]Ray, Dustin R., Debendra K. Das and Ravikanth S. Vajjha. 2013. Experimental and Numerical Investigations of Nanofluids Performance in a Compact Minichannel Plate Heat Exchanger. Prepared for submission to International Journal of Heat and Mass Transfer

3.1 Introduction

Nanofluids are stable suspensions of nanometer-sized particles, less than 100 nm, in conventional base fluids such as water, ethylene glycol, propylene glycol, oil and other liquids. Addition of high thermal conductivity metallic nanoparticles such as copper or aluminum increases the thermal conductivity of such colloidal solutions, thus enhancing their overall heat transfer capability. Starting with the initial research of Choi and Eastman [1] in 1995, the past decade and half has witnessed an abundant amount of experimental as well as numerical studies to explore the advantages of nanofluids as a heat transfer medium over the conventional liquids. Das et al. [2] have compiled a comprehensive volume on various aspects of research on the science and technology of nanofluids in their book covering the progress up to 2006. A new book edited by Minkowycz et al. [3] presents ten chapters contributed by experts in the field summarizing the latest developments of nanoparticle heat transfer and fluid flow up to 2013. At present nanofluids research occurs worldwide, showing a general conclusion that nanofluids can be a superior heat transfer fluid. This objective can be achieved provided the design conditions of nanofluids flowing in heat exchanges are carefully optimized by parametric runs to take advantage of the proper combination of the thermophysical properties of nanofluids. In this paper we have addressed how the effect of these properties yields superior performance.

Since nanofluids are a new class of engineered fluids, a great deal of research efforts has been devoted thus far to determining their thermophysical properties accurately, because they are essential to determine the convective heat transfer and the pumping power. However, until now, a limited amount of research has been presented on the theoretical analysis and actual testing of nanofluids in heat exchangers to compare their thermal and fluid dynamic performances with conventional fluids. To augment this lack of data, we have begun experimental and theoretical investigations of nanofluids and base fluids in plate heat exchangers (PHEs). The approach presented in this paper can be easily adapted to any type of compact heat exchanger.

The motivation for this research comes from exploring the application of nanofluids as the coolant in the active thermal control (ATC) loop to dissipate heat from NASA's future spacecrafts. The ATC loop presented by Ungar and Erickson [4] is shown in Figure 3.1. The

amount of heat generated in the crew module is about 2.5 kW which has to be dissipated through a compact liquid to liquid heat exchanger [4, 5]. In the present study, we have examined a compact PHE of this thermal rating due to its ease of availability to compare nanofluids performance. According to the classification described by Kandlikar et al. [6], this is a minichannel heat exchanger, because the smallest channel dimension necessary to meet this classification is 3 mm and our heat exchanger has a channel dimension of 2 mm. Compact heat exchangers have heat transfer area to volume ratio starting around 700 m^2/m^3 as described by Shah[7]. This PHE has a compactness factor of about 1000 m^2/m^3, placing it well into the realm of compact heat exchangers. Although this paper covers a PHE, from the knowledge of the described methodology it will be a straightforward extension to substitute in the experiment or analysis, characteristics of other types of compact heat exchangers and evaluate their performance under nanofluids flows. The test loop described in this paper under the Experimental Study section can be adapted to testing different types of compact heat exchangers, microchannel devices, heat sinks and cold plates, which find wide applications in the thermal management. Due to the continuous miniaturization of electronic devices and micro electromechanical systems, the heat density has increased significantly over the years. Therefore, the investigation on nanofluids, which are shown in this paper to have superior thermal performance than the corresponding base fluids shows, be capable of removing high heat flux in compact heat exchangers. The information presented here should be beneficial in optimizing thermal management systems. For NASA ,the reduction in size, weight and pumping power for heat exchangers would translate to substantial cost savings, since it costs about $12, 000 [8] to lift 1 lb. of payload into orbit.

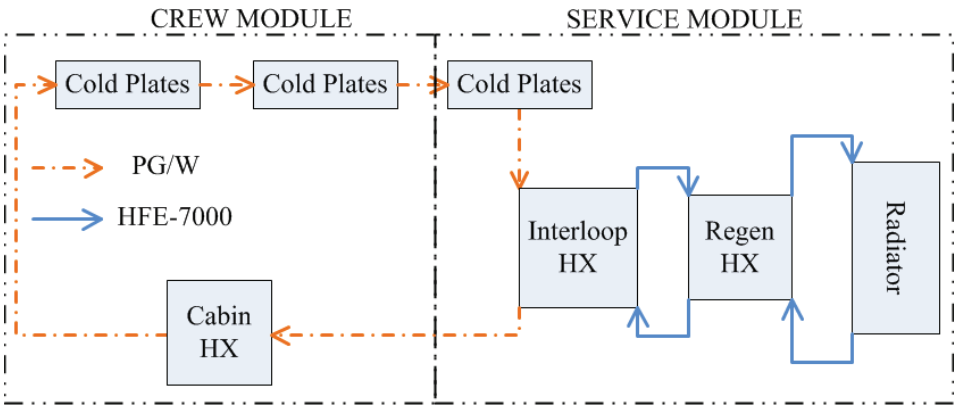

Figure 3.1: A simplified two-loop schematic diagram of the proposed ATCS loop [4]

Plate heat exchangers have been widely studied for single phase fluids and subsequently have found applications in two-phase vapor-liquid flows occurring in condensers and evaporators. A recent comprehensive book by Wang et al. [9] covers all aspects of PHE applicable for base fluids, but not for nanofluids. The research on nanofluids flow in plate heat exchanger is quite limited and we cite some of them here. Mare et al. [10] experimentally studied two nanofluids, Al_2O_3 and carbon nanotubes dispersion in pure water under laminar flow conditions. They measured a 42% and 50% improvement in heat transfer coefficient for Al_2O_3 and carbon nanotube suspensions respectively, when compared with pure water. They described a parameter to compare the heat transfer gain versus the pumping power loss due to the use of nanofluids and reported a gain of 22% and 150% for Al_2O_3 and carbon nanotube respectively, while comparing thermal-hydraulic performance with pure water. Jokar and O'Halloran [11] conducted computational fluid dynamic (CFD) analysis on Al_2O_3-water nanofluid with volumetric concentrations of 1 to 4% in the laminar flow regime. Their results showed that as the nanofluids volumetric concentration increased the total heat transfer in the PHE decreased slightly. They attributed this unusual behavior to the complex flow regimes in the three dimensional geometries of PHEs. Many researchers have shown that the heat transfer rate increases with an increase in the concentration in simple flow geometries as in circular pipes. Another reason for their under prediction of the heat transfer rate may be due to the thermal conductivity correlation they used in their computation. Their thermal conductivity plot shows a very low enhancement of about 2% at a fixed temperature even for an appreciable particle volumetric concentration of 4%. This unusually low value of thermal conductivity enhancement could be easily nullified by the standard l error in a CFD computational.

Pantzali et al. [12] performed experimental investigation of a 4% copper oxide (CuO) suspension in water in a PHE transferring heat up to 3.5 kW. Their experimental data showed a nearly similar Nusselt number for both base fluid and the nanofluid operating under similar Reynolds and Prandtl numbers. They concluded that nanofluids can be beneficial under laminar flow conditions. However, to be beneficial under turbulent flow condition, the increase in thermal conductivity must be accompanied by only a marginal increase in viscosity.

Fard et al. [13] conducted numerical and experimental studies in concentric tube and plate heat exchangers using zinc oxide (ZnO) nanofluid in water of 0.5% volumetric concentration.

Corresponding to equal mass flow rates of 10 g/s on the hot as well as the cold side of the PHE, they measured an overall heat transfer coefficient of 20% higher for the ZnO nanofluid in comparison with the distilled water. They also performed a three dimensional CFD analysis of the fluid flow in the PHE using the commercial CFD code, CFX. They reported an average error between the numerical prediction and experimental data to be around 7.5% for the PHE.

Tiwari et al. [14] experimentally studied four nanofluids: cerium oxide (CeO_2), Al_2O_3, titanium dioxide (TiO_2) and silicon dioxide (SiO_2) made from the base fluid water with volumetric concentration up to 3%. The experimental results showed that a maximum enhancement of 35.9% in the overall heat transfer coefficient in the PHE occurred with the CeO_2 nanofluid at an optimum volumetric concentration of 0.75%.At this condition the optimum performance index, defined as the ratio of heat transfer to pumping power, turned out to yield an enhancement of 16% over the base fluid.

Pandey and Nema [15] performed an experimental investigation on a PHE with pure water and Al_2O_3 nanoparticles in water up to 4% volumetric concentration. From their experimental data they presented correlations for Nusselt number and friction factor as a function of particle volumetric concentration and Peclet number ($Re \cdot Pr$). They also calculated the exergy loss in the PHE and found that the lowest exergy loss occurred at a volumetric concentration of 2%.

We have presented experimental and theoretical analysis, which prove through parametric runs that in optimized applications, the use of nanofluids in place of the conventional fluids can reduce the pumping power requirement and the size of the heat exchanger, while achieving the same amount of heat transfer. Therefore, nanofluids can be an attractive candidate for many applications in the thermal systems. Another valuable attribute of this study is that it evaluates the performance of an extremely low temperature coolant, HFE-7000 [16], which is under consideration by NASA for use in the surface radiators in the space Figure 3.1. For some location and orientation of the spacecraft, when it is obstructed from the solar rays, it may experience the effective sky temperature to be as low as -100° C, [5]. Therefore, this heat transfer fluid, whose freezing point is - 122.5° C is selected, so that it does not freeze in the radiator coil. The study of this kind of fluid is also important for heat transfer applications in cold regions of the world, such as the circumpolar nations, where the ambient temperature may reach -60° C. The equipment of oil and gas fields of Alaska is subjected to such temperatures during every winter.

3.2 Objectives

- **Experimental:** An experimental investigation of Al_2O_3 nanofluid with 0.5% particle volumetric concentration dispersed in an EG/W 60:40 base fluid was conducted in a brazed plate heat exchanger in a test loop. From experimental data preliminary correlations of Nusselt number (*Nu*) and a friction factor (*f*) were developed. These experimental results allowed us to compare quantitatively, the thermal and fluid dynamic performance of a nanofluid and abase fluid.
- **Theoretical:** A detailed theoretical study using the well-established single-phase fluid correlation of Focke et al. [17] for PHE was conducted by means of Matlab scripts to compare the fluid dynamic and thermal performance of four heat transfer mediums on the hot side. The mediums are: EG/W 60:40 pure liquid and three nanofluids of Al_2O_3, CuO and SiO_2 nanofluids of 1% volumetric concentration in the same base fluid. For all four cases, the coolant on the cold side of the PHE was considered to be the HFE 7000, absorbing about 2.5 kW of heat as proposed in the ATC system of NASA.

3.3 Correlations for Thermophysical Properties

Three types on nanoparticles, Al_2O_3, CuO and SiO_2, were selected because they have been widely studied by nanofluids researches in recent years as promising additives. Accurate formulas for the thermophysical properties: density, viscosity, specific heat and thermal conductivity are necessary for these nanofluids to perform the thermal and fluid dynamic analysis.

3.3.1 Ethylene Glycol and Water Mixture (EG/W) 60:40 by Mass

From curve-fitting the data presented in the ASHRAE [18] handbook for the EG/W 60:40 by mass, the following correlations, with a very low degree of error less than 1%, for density, viscosity, specific heat and thermal conductivity of the base fluid were determined. The reason for selecting the proportion of 60 to 40 is due to the lowest freezing point (- 48 $^\circ$ C) attained by this ratio, which is very important for applications in extreme cold regions. This fluid is adopted on the hot side for the PHE and is considered in the primary loop of the NASA ATC system. The choice of NASA is propylene glycol/water (PG/W due to its low toxicity. However, properties correlations for PG/W based nanofluids are not yet available. So, EG/W was used to obtain a

general trend. All the properties correlations for the EG/W base fluid is presented in Table 3.1. The log-quadratic equation for viscosity follows the curve-fit recommended by White [19], while deriving the viscosity correlation for water. All other properties correlations follow the guidelines of Yaws [20] with the refinement that they are derived in the nondimensional form.

Table 3.1: EG/W 60:40 properties correlation for 238 K ≤ T ≤398 K (-35 ° C ≤ T ≤ 125 ° C)

Property	Correlation	Constants	R^2	Error
Density (kg/m^3)	$\frac{\rho}{\rho_0} = A + B\left(\frac{T}{T_0}\right) + C\left(\frac{T}{T_0}\right)^2$	$\rho_0 = 1091.66 \frac{kg}{m^3}$ $A = 0.9247$; $B = 0.2414$; $C = -0.1661$	1	0.01%
Viscosity ($Pa{\cdot}s$)	$ln\left(\frac{\mu}{\mu_0}\right) = A + B\left(\frac{T_0}{T}\right) + C\left(\frac{T_0}{T}\right)^2$	$\mu_0 = 1.1\times10^{-2} \frac{kg}{m{\cdot}s}$		
	238 K ≤ T ≤ 273 K	$A = 0.3707$; $B = -12.882$; $C = 12.513$	1	0.19%
	273 K ≤ T ≤ 398 K	$A = -4.976$; $B = -1.942$; $C = 6.9088$	1	0.91%
Specific Heat ($J/kg{\cdot}K$)	$\frac{c_p}{c_{p,0}} = A + B\left(\frac{T}{T_0}\right)$	$c_{p,0} = 3042.02 \frac{J}{kg{\cdot}K}$ $A = 0.6185$; $B = 0.3814$	1	0.01%
Thermal Conductivity ($W/m{\cdot}K$)	$\frac{k}{k_0} = A + B\left(\frac{T}{T_0}\right) + C\left(\frac{T}{T_0}\right)^2$	$k_0 = 0.342 \frac{W}{m{\cdot}K}$ $A = -0.2939$; $B = 1.981$; $C = -0.6868$	0.999	0.11%

3.3.2 HFE-7000 for Cold Side

From the data presented in the 3M literature [16] the following correlations in Table 3.2 for the base fluid HFE-7000 were adopted. The equations for density, specific heat and thermal conductivity were given in the 3M literature [16]. The equation for viscosity was derived by curve-fitting the data given in the 3M literature following the log-quadratic correlation of White [19]. This fluid has been selected for the cold side of the PHE and will circulate in the secondary loop of NASA's ATC system.

Table 3.2: Correlations for HFE-7000 base fluid properties.	
Property	Correlation
Density (kg/m^3)	$\rho = 1472.6 - 2.880 \cdot T(°C)$ $-120°C \le T \le 30°C$
Viscosity* ($Pa \cdot s$)	$ln\left(\frac{\mu}{\mu_0}\right) = A + B\left(\frac{T_0}{T}\right) + C\left(\frac{T_0}{T}\right)^2$ $153\,K \le T \le 303\,K$; $R^2 = 0.9978$ Max. error 2.41%
	$\mu_0 = 5.45 \times 10^{-4}\ kg/m.s$ $A = 11.78$; $B = -19.742$; $C = 7.9785$
Specific Heat ($J/kg \cdot K$)	$c_p = 1223.2 + 3.0803 \cdot T(°C)$ $-120°C \le T \le 30°C$
Thermal Conductivity ($W/m \cdot K$)	$k = 0.0798 - 0.000196 \cdot T(°C)$ $-120°C \le T \le 30°C$

The advantages of the HFE-7000 as a coolant are its low freezing point of -122.5 ° C at 1 atmosphere and low viscosity. Compared to the EG/W, the viscosity ratio ($\mu_{EG/W} / \mu_{HFE}$) is about 11.64 at room temperature 20 ° C and 95 at -40 ° C**.** The disadvantage of HFE-7000 is its low thermal conductivity compared to other coolants; $k_{EG/W} / k_{HFE} \approx 4.69$ at 20 ° C and 3.50 at -40 ° C. Therefore, HFE-7000 can be enriched by doping with nanoparticles, as the particles would enhance the inherently low thermal conductivity but would not be over-penalizing in increasing viscosity, as it is very low to begin with.

3.3.3 Nanofluids Properties

Vajjha et al. [21] compared the theoretical density Eq. (3.1) presented by Pak and Cho[22] based on conservation of mass to measured density values of three different nanofluids; aluminum oxide, antimony-tin oxide, and zinc oxide(ZnO) and found the theoretical equation to be in good agreement of the data. Therefore, the equation was adopted for the density calculation.

$$\rho_{nf} = \rho_p \phi + \rho_{bf}(1 - \phi) \tag{3.1}$$

Vajjha and Das [23] conducted specific heat measurements on three nanofluids: Al_2O_3, SiO_2 and ZnO and developed a correlation given by Eq. (3.2), where A, B and C are curve-fit coefficients for each nanoparticle.

$$\frac{c_{p,nf}}{c_{p,bf}} = \frac{A\left(T/T_0\right) + B\left(c_{p,p}/c_{p,bf}\right)}{\left(C+\phi\right)} \tag{3.2}$$

The specific heat of CuO and other nanofluids can be calculated using Eq. (3.3), developed by Xuan and Roetzel [24], which is based on thermal equilibrium between the particles and the base fluid.

$$c_{p,nf} = \frac{\rho_p c_{p,p}\phi + \rho_{bf} c_{p,bf}\left(1-\phi\right)}{\rho_{nf}} \tag{3.3}$$

Koo and Kleinstreuer [25] developed a thermal conductivity model for nanofluids that added a Brownian motion term to the classical Maxwell model, shown in Eq. (3.4a). Following Koo and Kleinstreuer model, Vajjha and Das [26] and Sahoo et al. [27] developed similar correlations for nanoparticles dispersed in EG/W 60:40 base fluid. They experimentally determined the thermal conductivity of aluminum oxide, copper oxide, zinc oxide and silicon dioxide using a thermal conductivity apparatus that uses the a steady state technique. They derived Eq. (3.4b) and the curve fit relation $\beta = f(\phi)$ for each nanofluid.

$$k_{nf} = \frac{k_p + 2k_{bf} - 2\left(k_{bf} - k_p\right)\phi}{k_p + 2k_{bf} + \left(k_{bf} - k_p\right)\phi} k_{bf} + 5\times10^4 \beta\phi\rho_{bf} c_{pbf} \times \sqrt{\frac{\kappa T}{\rho_p d_p}} f\left(T,\phi,etc.\right) \tag{3.4a}$$

$$f\left(T,\phi\right) = \left(2.8217\times10^{-2}\phi + 3.917\times10^{-3}\right)\left(\frac{T}{T_0}\right) + \left(-3.0669\times10^{-2}\phi - 3.91123\times10^{-3}\right) \tag{3.4b}$$

Vajjha et al. [28] proposed a nondimensional correlation Eq. (3.5) for three nanofluids(Al_2O_3,CuO,SiO_2) prepared from EG/W base fluid, where A and B are curve-fit constants for each nanoparticle by combining the data sets from Namburu et al. [29, 30] and Sahoo et al.[31].

$$\frac{\mu_{nf}}{\mu_{bf}} = Aexp\left(B\phi\right) \tag{3.5}$$

3.4 Plate Heat Exchanger

We used a SWEP B5H PHE [32] for experimentation and analysis. Some geometrical data was not available from the manufacturer due to the proprietary nature of their design. Therefore, some geometry listed in Table 3.3 was derived from computational runs. We assumed certain realistic dimensions and made several run with manufacturer software (SSP G7) runs, until our performance predictions agreed with those of SWEP. To get a clear explanation of the geometry

and different parameters of a PHE listed in Table 3.3, the book by Wang et al. [9] is an excellent source. The book also provides flow configurations, Nusselt number, friction factor correlations and thermal/fluid dynamic performance equations needed for rating or designing a plate heat exchanger.

Table 3.3: SWEP B5H plate heat exchanger geometry [32]	
Plate width, W (m)	0.071
Plate length, L (m)	0.154
Channel spacing, b (m)	0.002
Thickness of plate, t (m)	4.12E-04
Thermal conductivity of plate material (AISI 316)@ 300 K [33], k_{phe} (W/m K)	13.4
Chevron angle, β_{phe} (Degrees)	45
Total number of channels, $N_h = 1, N_c = 2$	3
Enlargement factor, ϕ_{phe}	1.10
Equivalent diameter, $D_e \approx 2b$ (m)	0.004
Projected area per plate, $A_p = W \times L$ (m^2)	9.80E-03
Fluid flow area per channel, $A_f = W \times b$ (m^2)	1.42E-04
Surface area on one fluid side of PHE, $A_t = A_p \times \phi_{phe}$ (m^2)	2.41E-02

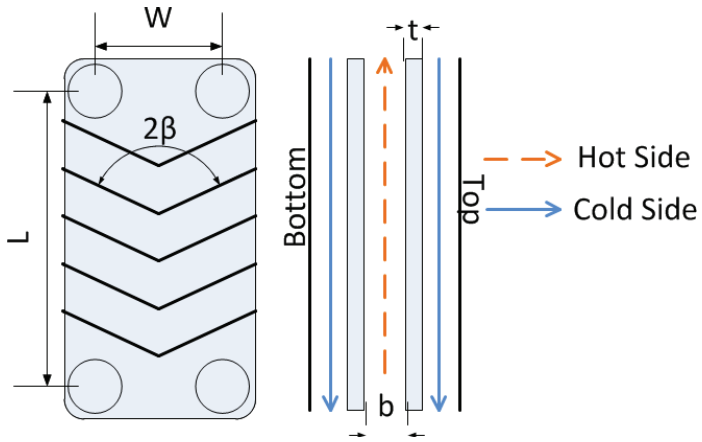

Figure 3.2: Plate heat exchanger internal view

3.5 Experimental Study

3.5.1 Experimental Setup

The experimental setup is shown in Figure 3.3. In the loop, shown on the left side of the figure, the hot fluid is circulated in the heat exchanger. Nanofluids and EG/W mixture are circulated in

this loop. There are four electrical heaters of 2 kW capacities each, installed on inlet and outlet sides of the tank. The outlet temperature of the fluid from the tank is controlled by a solid state control, so that the tank delivers a desired high temperature fluid to the heat exchanger. Presently the heat exchanger is set to be cooled by the cooling water supply in the laboratory. The present goal is to test various nanofluids on the hot fluid loop while they are being cooled by water. From the experimental data we aim to develop correlations for the Nusselt number and friction factor for several nanofluids as a function of Reynolds number, Prandtl number, chevron angle, nanoparticles volumetric concentration, particle size and particle properties. In place of the PHE, other types of compact liquid to liquid heat exchangers and cold plates can also be tested in this loop. In the future the cooling side can be made into a closed loop and different coolants other than water can be circulated as necessary.

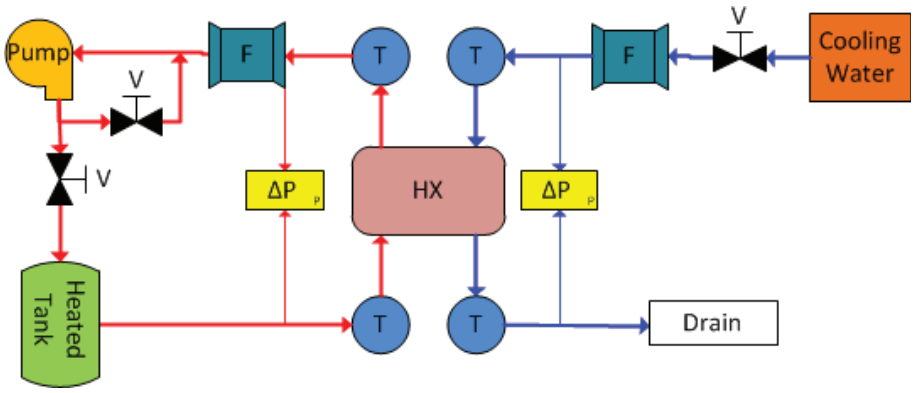

Figure 3.3: Schematic diagram of the apparatus to test the performance of different nanofluids in compact heat exchangers. F: flow meter, T: thermistors, ΔP: differential pressure sensor, HX: heat exchanger, V: flow control valve

The data collected was taken once steady-state was achieved meaning temperatures, flow rates and differential pressure readings were relatively constant and the energy balance between hot and cold sides was within ±5%. For each trial run, three measurements were taken over nine minutes once steady state was achieved. The parameters measured in this experimental setup are: inlet and outlet temperatures, volumetric flow rates and differential pressure across the heat exchanger for both the hot and cold fluid.

3.5.2 Equations to Derive Data from Experiments

From the measured data the required performance results were calculated using the following equations. The thermophysical properties of the fluids were calculated using the average bulk temperature as described by Eq. (3.6).

$$T_{avg} = \frac{T_i + T_o}{2} \tag{3.6}$$

The heat transfer rates were determined by using the energy balance equations for both the hot and cold side.

$$Q_h = \dot{m}_h c_{p,h} \left(T_{h,i} - T_{h,o} \right) \tag{3.7a}$$

$$Q_c = \dot{m}_c c_{p,c} \left(T_{h,i} - T_{h,o} \right) \tag{3.7b}$$

The log mean temperature difference was calculated using the temperatures for a counter-flow configuration.

$$LMTD = \frac{\left(T_{h,i} - T_{c,o} \right) - \left(T_{h,o} - T_{c,i} \right)}{\ln \left[\frac{T_{h,i} - T_{c,o}}{T_{h,o} - T_{c,i}} \right]} \tag{3.8}$$

Overall heat transfer coefficient Eq. (3.9) was calculated using the average heat transfer rate Eq. (3.10)

$$U = \frac{Q_{avg}}{A_t \, LMTD} \tag{3.9}$$

$$Q_{avg} = \frac{Q_h + Q_c}{2} \tag{3.10}$$

The Reynolds number (3.11a) and Prandtl number (3.11b) were calculated based on the average bulk temperatures of the fluids on the hot and cold side of the plate heat exchanger.

$$Re = \frac{\rho V D_e}{\mu} \tag{3.11a}$$

$$Pr = \frac{c_p \mu}{k} \tag{3.11b}$$

A fanning friction factor was also calculated using Eq. (3.12).

$$f = \frac{\Delta P D_e}{2 V^2 L \rho} \tag{3.12}$$

3.5.3 Experimental Results

3.5.3.1 Benchmark Test Case with Water

A benchmark test was performed on the PHE using water as the test fluid on both hot and cold side. This fluid was selected for benchmark test case because the heat exchanger supplier had provided test results with water flow. On the hot side the flow rate and temperatures were varied to achieve a range of Reynolds number from 700 to 2700. On the cold side the flow conditions were maintained nearly the same to generate a relatively constant convective heat transfer coefficient. This helps subsequently in determining the convective heat transfer coefficient on the hot side by the Wilson plot method.

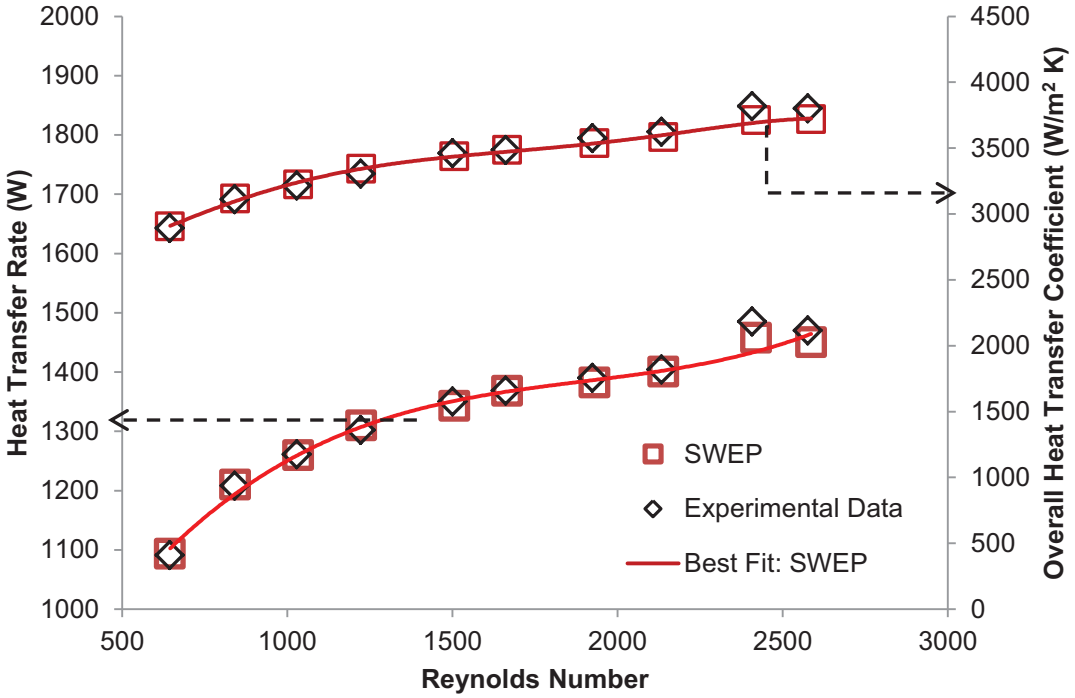

Figure 3.4: A benchmark test case with water comparing the experimental heat transfer rate and overall heat transfer coefficient with the predicted values by SWEP model as a function of Reynolds number.

Results of the benchmark test are shown in Figure 3.4 as the variation of the heat transfer rate and overall heat transfer coefficient with the Reynolds number in the PHE. The experimental

data agree very closely with the prediction obtained by using the modeling software that is available from the manufacturer SWEP [32]. The differences between the SWEP model prediction and the experimental data are: minimum -0.57%, maximum 1.9% and average 0.40% for heat transfer rate. The overall heat transfer coefficient deviation between SWEP model prediction and the experimental data are: minimum -1.09%, maximum 2.82% and average: 0.61%.

3.5.3.2 Test with Nanofluid

As found during our literature review, no well-established correlations exist thus far, which are valid for several nanofluids in predicting Nusselt number and the friction factor, in plate heat exchangers. It is well-known in the nanofluids research that a very dilute concentration of nanoparticles may perform the best by enhancing the thermal conductivity while not increasing the viscosity to a high value. Furthermore, the narrow passages of compact heat exchangers may increase agglomeration of nanoparticles and be prone to clogging. Therefore, the authors started with a very dilute concentration (0.5%) of Al_2O_3 particles by volume dispersed in the EG/W mixture. Al_2O_3 was selected as it gives a good enhancement of thermal conductivity while not increasing the viscosity prohibitively.

3.5.3.3 Nanofluids Preparation an Characterization

The Al_2O_3 nanofluid was purchased from Alfa Aesar [34] as a 50% (by mass) aqueous suspension with average particle size of 45 nm. The nanofluid was subjected to ultrasonication in two stages. In the first stage, the concentrated mother nanofluid (original fluid from manufacture) was sonicated in a Branson Sonicator under a frequency of 40 kHz and a power of 185 W. The mother nanofluid was subjected to three sessions each of 2-hours duration. This process breaks down the particles that have agglomerated due to long term storage.

The volume of fluid in the primary loop of the test set up is about 2.5 liters. Using the density of Al_2O_3 particle at 3600 kg/m^3 and that of the EG/W 60: 40 at room temperature of 25˚C is 1081 kg/m^3, it was calculated, how much mass of the concentrated mother fluid will be added to form a concentration of 0.5% by volume of Al_2O_3 in the EG/W base fluid of 2.5 liter. Next, using a precision electronic mass balance the exact mass of the concentrated mother nanofluid is

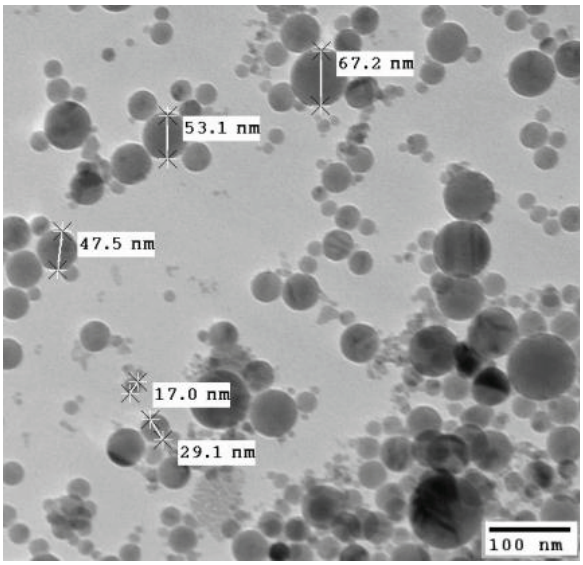

Figure 3.5: TEM image of Al_2O_3 nanoparticles taken before nanofluid was charged into the test loop.

measured by adding droplets of nanofluids by a pipette to a test tube. This precise amount of concentrated nanofluid was carefully added to the EG/W 60:40 base fluid. In the second phase, these dilute nanofluids in bottles were sonicated in the ultrasonicator for three hours, which has been found to be adequate to break down the agglomerated particles. Then a small sample of this diluted nanofluid is examined under the transmission electron microscope (TEM). Figure 3.5 shows the TEM image of the nanofluid. The particles are perfectly spherical and vary in sizes from around 10 nm to about 90 nm. From the particle size distribution, the average particle size of 45 nm specified by the manufacturer seems to be correct. No agglomeration of nanoparticles is observed. Further details on the preparation of our nanofluids, ultrasonication process and characterization can be found from [23, 26, 35].

The hot side of the loop was charged with the nanoparticles and circulated over a range of Reynolds number from 150 to 750. Heat transfer rates and overall heat transfer coefficients were measured and plotted at different Reynolds numbers in Figure 3.6. Next, using the SWEP software and the thermophysical properties of nanofluids, we computed the heat transfer rate and overall heat transfer coefficients. Although the SWEP software was developed for single phase liquids, significant research in recent years have shown that for low concentration nanofluids can also be modeled with single phase theory. In Figure 3.6, the results show there is an excellent agreement between the heat transfer rates and overall heat transfer coefficient between our experimental data and the predictions obtained by the SWEP model. The differences between the experimental data and the SWEP predictions for heat transfer rates are: minimum -0.70%, maximum -0.26% and average: -0.47%, and the differences for the overall heat transfer coefficients are: minimum -0.34%, maximum 0.91% and average: 0.68%.

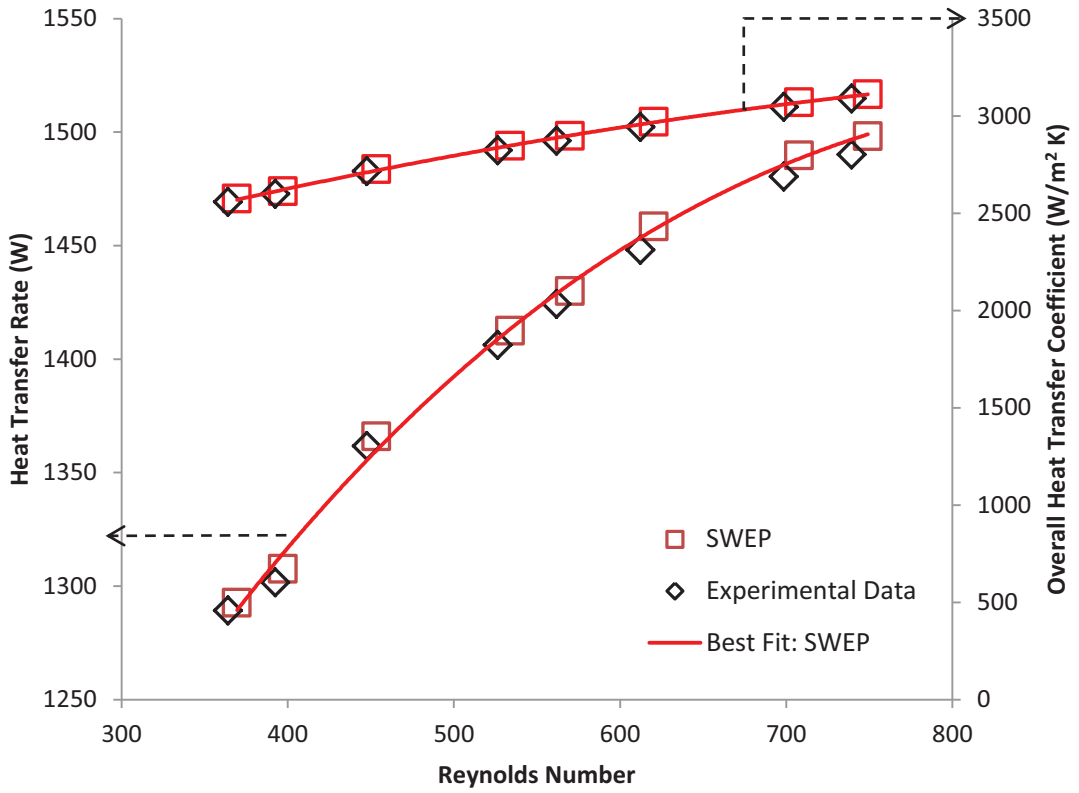

Figure 3.6: Comparison of heat transfer rate and overall heat transfer coefficient measurements with SWEP prediction for nanofluid, Al_2O_3 dispersed in EG/W with a concentration of 0.5%

3.5.3.4 Development of Nusselt Number Correlation

From the agreement in Figure 3.6 of the previous section, between experimental and the prediction by SWEP model, it appears that one correlation may be suitable for both single phase fluids as well as the low concentration nanofluid. Therefore, we used the data collected from the water and Al_2O_3 experiments to develop a single preliminary correlation for the given plate heat exchanger. The Nusselt number correlation was achieved using the Wilson plot method. The Wilson plot method is explained by Shah [36] and Muley and Manglik [37] have applied the method to PHE. The overall heat transfer coefficient for plate heat exchanger is related with the heat transfer coefficient without considering fouling resistance Eq. (3.13).

$$\frac{1}{U} = \left(\frac{t}{k_{phe}}\right) + \left(\frac{1}{h_h}\right) + \left(\frac{1}{h_c}\right) \tag{3.13}$$

Most correlation defines the Nusselt number as a power-law relationship between Reynolds and Prandtl numbers, is expressed in Eq. (3.14).

$$Nu = C_1 Re^{C_2} Pr^{C_3} \tag{3.14}$$

Using the definition of Nusselt number Eq. (3.15), we eliminate the Nusselt number from Eq. (3.14) and Eq. (3.16) is obtained.

$$Nu = \frac{h \cdot D_h}{k} \tag{3.15}$$

$$h = \left[C_1 \left(\frac{k}{D_e} \right) \cdot Re^{C_2} Pr^{C_3} \right] \tag{3.16}$$

Now, combining Eq. (3.13) and (3.16), Eq. (3.17) is derived. We used the nonlinear curve fitting function of MATLAB, *nlinfit,* to determine curve fit constants, C_1, C_2, C_3.

$$\frac{1}{U} = \left(\frac{t}{k_{phe}} \right) + \left[C_1 \left(\frac{D_e}{k} \cdot Re^{C_2} Pr^{C_3} \right) \right]_h^{-1} + \left[C_1 \left(\frac{D_e}{k} \cdot Re^{C_2} Pr^{C_3} \right) \right]_c^{-1} \tag{3.17}$$

From historical *Nu* correlations for internal flows, it has been noted that the exponent of Reynolds number C_2 varies between 0.6 and 0.8 and the exponent of Prandtl number, C_3 varies between 0.3 and 0.5. With these suggested constraints, sweeps of the coefficients were performed and all coefficients determined for the best coefficient of determination $R^2 = 0.9924$ for the data shown in Figure 3.7. The correlation, Eq. (3.18), is in good agreement with the experimental data. Also by comparison, our proposed correlation is similar in form to the well-established correlation Focke et al. [17] developed for plate heat exchanger from extensive experimental data, which is listed in the later section as Eq. (3.31). The chevron angle of PHE was proprietary information of manufacturer and this number can vary between 30 to 60 degrees in plate heat exchangers. The good agreement between our experimental data and the Focke et al. correlation Figure 3.7 with a chevron angle of 45 degrees, leads us to believe that the chevron angle of our PHE is possibly 45 degree and we have used that value in Table 3.3.

$$\begin{gathered} Nu = 0.3053 Re^{0.75} Pr^{0.3} \qquad 150 \le Re \le 1500 \\ R^2 = 0.9924 \end{gathered} \tag{3.18}$$

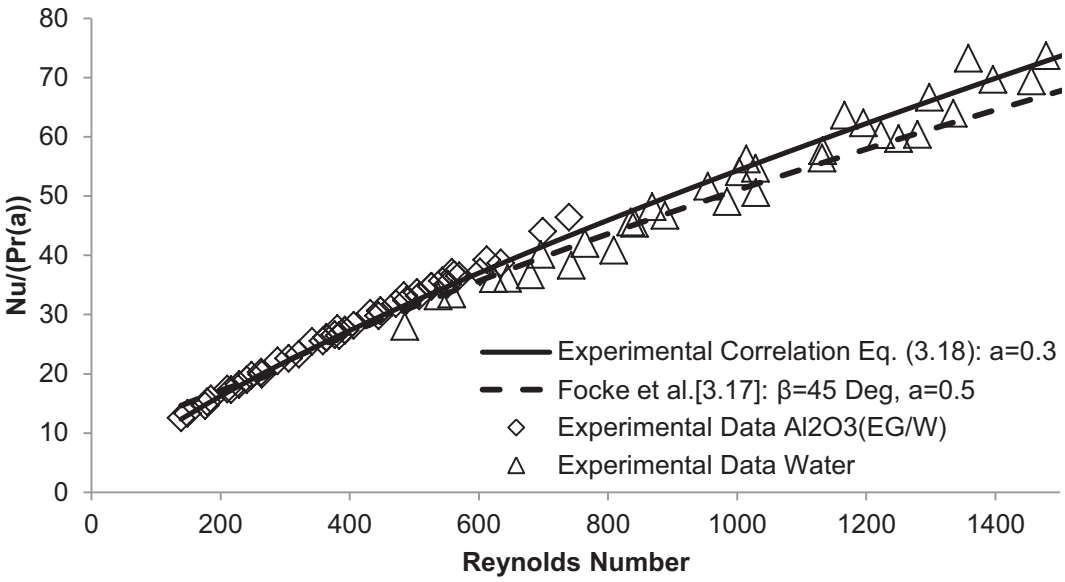

Figure 3.7: A heat transfer correlation for the Nusselt number as a function of Reynolds and Prandtl numbers for a low concentration nanofluid.

3.5.3.5 Development of Friction Factor Correlation

Using the differential pressure measurements a friction factor correlation was developed. The two ends of the differential pressure transducer connected to the inlet and outlet pipes of the PHE, also contained quick connect fittings for ease of dismantling, and the inlet and outlet ports. Therefore, the measurement included pressure losses from the plate heat exchanger, ports and the quick-connect fittings. The pressure losses at inlet and outlet ports were easily accounted for by subtracting out the pressure losses as presented in (3.19a-b). However, the loss characteristics of the quick-connect fittings were estimated approximately, resulting our measured pressure loss showing higher than that occurring solely in the PHE.

$$\Delta P_{phe} = \Delta P_{measured} - \Delta P_{port} \tag{3.19a}$$

$$\Delta P_{port} = \frac{1.5\rho V_{port}^2}{2} \tag{3.19b}$$

A fanning friction factor was calculated using Eq. (3.12). The friction factor correlation, Eq. (3.20), shown in Figure 3.8 shows higher value than those predicted by SWEP model at lower Reynolds number but conforms to their prediction as the Reynolds number increase. We believe this is due to inaccuracy of loss estimates in the connection fittings. The form of the correlation

matches the traditional Blasius type relation with negative exponent of Reynolds number and its trend is similar to the results from SWEP Model.

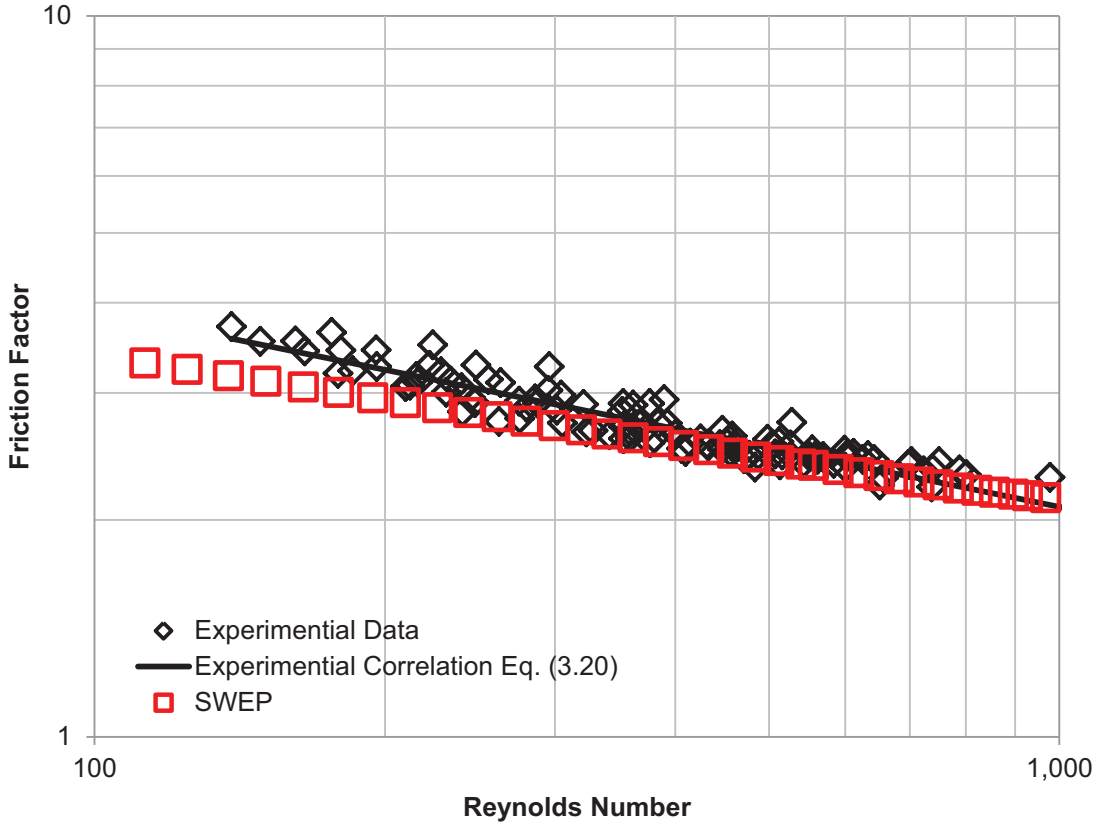

Figure 3.8: Experimental friction factor variation with Reynolds number and comparison with the results predicted by the SWEP Model

$$f = 13.64 Re^{-0.2719} \quad 120 \le Re \le 1000$$
$$R^2 = 0.88 \tag{3.20}$$

3.5.3.6 Heat Transfer Coefficient Enhancement

Using the developed correlation for Nusselt number Eq. (3.18), a comparison between the base fluid (EG/W) and Al_2O_3 nanofluid of 0.5% concentration was made for the convective and overall heat transfer coefficients on basis of constant Reynolds number. Figure 3.9 shows Al_2O_3 nanofluid increases thermal performance of the base fluid for a given Reynolds number. The convective heat transfer coefficient increased by: 9.18% minimum, 11.09% maximum and

10.35% average, while the overall heat transfer coefficient increased by: 3.30% minimum, 4.85% maximum and 3.98% average.

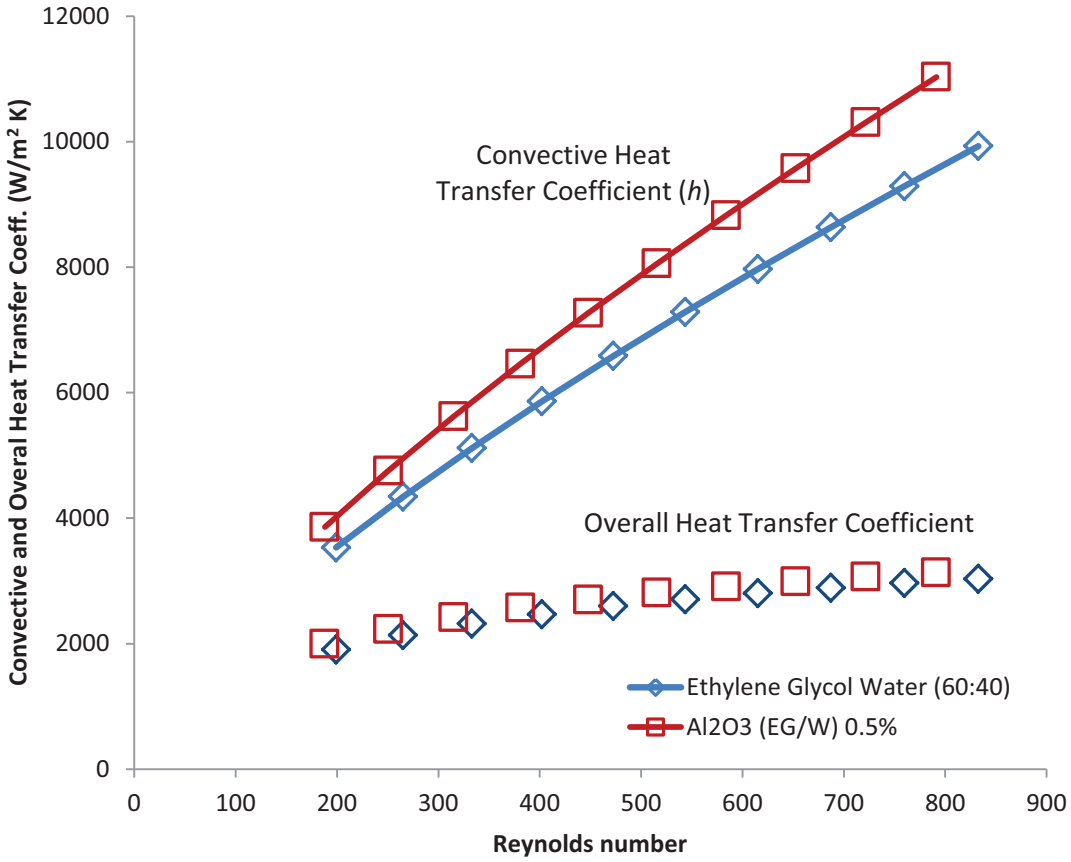

Figure 3.9: Comparison of convective and overall heat transfer coefficients of EG/W base fluid and Al_2O_3 nanofluids on the basis of constant Reynolds numbers

3.5.3.7 Analysis of Uncertainties in Measurements

Systematic experimental errors for calculated parameters such as: heat transfer Rate (*Q*), Overall heat transfer coefficient (*U*), Reynolds number (*Re*), Prandtl number (*Pr*), Nusselt number (*Nu*), and friction factor (*f*) were estimated using the uncertainties associated with the individual measurements listed in Table 3.4. The uncertainties of measured parameters: volumetric flow rate, temperature and pressure were obtained from the specifications of the sensor manufacturer and those for the PHE dimensions from the specifications of SWEP. The uncertainties in the thermophysical properties of (Al_2O_3, 0.5%) were obtained from the papers cited earlier under the nanofluids properties section. The primes in Table 3.4 denotes ratio

$\delta x' = \delta x / x$. As explained by White [19] for the uncertainty of experimental data, if *P* is a power-law expression with *x* variables, Eq. (3.21a), then the uncertainty of *P* can be calculated as a root-mean-square average of all other uncertainties given by Eq. (3.21b).

$$P = f(x_1^{n_1}, x_2^{n_2}, x_3^{n_3}..) \tag{3.21a}$$

$$\frac{\delta P}{P} = \left[\left(n_1 \frac{\delta x_1}{x_1} \right)^2 + \left(n_2 \frac{\delta x_2}{x_2} \right)^2 + \left(n_3 \frac{\delta x_3}{x_3} \right)^2 + ... \right]^{1/2} \tag{3.21b}$$

Table 3.4: Uncertainty analysis

Measurements	PHE Geometries	Thermophyscial properties
$\delta \dot{V}' = 1\%$	$\delta L' = 0.65\%$	$\delta \rho' = 0.00\%$
$\delta T' = 0.22\%$	$\delta W' = 2.50\%$	$\delta c_p{}' = 3.00\%$
$\delta \Delta P' = 0.08\%$	$\delta b' = 1.50\%$	$\delta \mu' = 4.10\%$
	$\delta A_{port}{}' = 0\%$	$\delta k' = 3.69\%$

Calculated
(The parameters corresponds to equations presented in earlier sections)

Table 3.3	$\delta A_t' = \sqrt{\delta L'^2 + \delta W'^2} = 2.58\%$	(3.9)	$\delta U' = \sqrt{\delta Q'^2 + \delta A_t'^2 + \delta LMTD'^2} = 5.05\%$
	$\delta A_c' = \sqrt{\delta W'^2 + \delta b'^2} = 2.92\%$		$\delta V'^2 = \sqrt{\delta \dot{V}'^2 + \delta A_{port}'^2} = 1.00\%$
	$\delta D_e' = \sqrt{\delta b'^2} = 1.50\%$	(3.19a)	$\delta \Delta P_{port}' = \sqrt{\delta \rho'^2 + (2\delta V')^2} = 2.00\%$
(3.7)	$\delta Q' = \sqrt{\delta \dot{V}'^2 + \delta \rho'^2 + \delta A_c'^2 + \delta c_p'^2 + 2\delta T'^2} = 4.31\%$	(3.19b)	$\delta \Delta P_{phe} = \sqrt{\delta \Delta P'^2 + \delta \Delta P_{port}'^2} = 2.00\%$
(3.11a)	$\delta Re' = \sqrt{\delta \dot{V}'^2 + \delta \rho'^2 + \delta D_e'^2 + \delta A_c'^2 + \delta \mu'^2} = 5.34\%$	(3.12)	$\delta f' = \sqrt{\delta \Delta P_{phe}'^2 + \delta D_e'^2 + (2\delta \dot{V}'^2) + \delta L'^2 + \delta \rho'^2} = 3.27\%$
(3.11b)	$\delta Pr' = \sqrt{\delta \mu'^2 + \delta c_p'^2 + \delta k'^2} = 6.28\%$	(3.17)	$\delta Nu' = \sqrt{\delta U'^2 + \delta k'^2 + \delta D_e'^2} = 6.43\%$
(3.8)	$\delta LMTD' \approx \sqrt{4 \cdot \delta T'^2} = 0.44\%$	(3.15)	$\delta h' = \sqrt{\delta Nu'^2 + \delta k'^2 + \delta D_e'^2} = 7.56\%$

The calculations show the uncertainties for: Reynolds number, Prandtl number, Nusselt number, and friction factor are 5.34%, 6.28%, 6.43% and 3.27%, respectively.

3.6 Active Thermal Control System (ATCS)

In the introduction section, an ATCS for NASA for future spacecraft cooling was presented in Figure 3.1. The heat from the crew cabin, battery and electronics are estimated to be about 2.5

kW. This heat is to be collected by propylene glycol/water (PG/W) coolant and transferred to the HFE-7000 fluid through the inter loop heat exchanger. The HFE-7000 fluid circulating through the radiator, which is located on the surface of the spacecraft, dissipates that heat by radiation to the outer space, which may be as cold as -100 $^{\circ}$ C. Our study has focused on benefits that may be achieved by introducing nanoparticles in both coolant loops through a series of calculations by comparing the performance of the interloop compact heat exchanger for its heat transfer ability and the required pumping power.

The thermophysical properties for PG/W nanofluids are not available in the literature at present. Therefore, we have used the available correlations for EG/W nanofluids in the following analysis. Although PG/W nanofluid will differ in thermophysical properties, the overall trends should be similar as the two base fluids are of glycol origin and similar nature. Furthermore, upon development of correlations for the PG/W nanofluid, which is continuing at present, the computations presented here in can be easily repeated to improve the results.

The specification of the NASA interloop compact heat exchanger is not available, since it is a proprietary design. Therefore, we have used the compact SWEP B5H plate heat exchanger in its place, whose geometry had been presented earlier in Table 3.3. The inlet temperatures and total heat dissipation have been matched to the requirements of NASA's ATCS. The mass flow rates and the number of channels in the PHE have been modified to fulfill the total heat dissipation of 2.5 kW. A summary of the parameters used to meet the thermal load of the ATCS loop is presented in Table 3.5. These values will be used in the preceding analysis to determine thermal and fluid dynamic performance of the base fluids (EG/W, HFE-7000) and three different nanofluids with Al_2O_3, CuO, and SiO_2 nanoparticles.

Table 3.5: Analysis parameters used for the computations of nanofluids performance

	Hot Side	Cold Side
Fluid	EG/W, N.F. (EG/W)	HFE, N.F.(HFE)
Mass Flow Rate (kg/s)	0.2	0.1
Inlet Temp[4] (K)	302.2	277.5
Heat Dissipated[4] (kW)	2.5	
Heat Exchanger	SWEP B5H PHE ($N_h = 5, N_c = 6$)	

3.7 Thermal and Fluid Dynamic Calculations

3.7.1 Numerical Scheme for Rating Analysis

Numerical scheme using the Effectiveness-Number of Transfer Units method outlined by Wang et al. [9] for PHEs was developed using Matlab coding to compare the performance of three nanofluids and the base fluid under three different conditions equal: (i) mass flow rate, (ii) heat transfer rate and (iii) pumping power. One such scheme is illustrated in Figure 3.10. Normally an iterative process isn't necessary with $\varepsilon - NTU$ method, but doing so achieves better values for average fluid properties with using Eq. (2.15) to determine the exit temperatures.

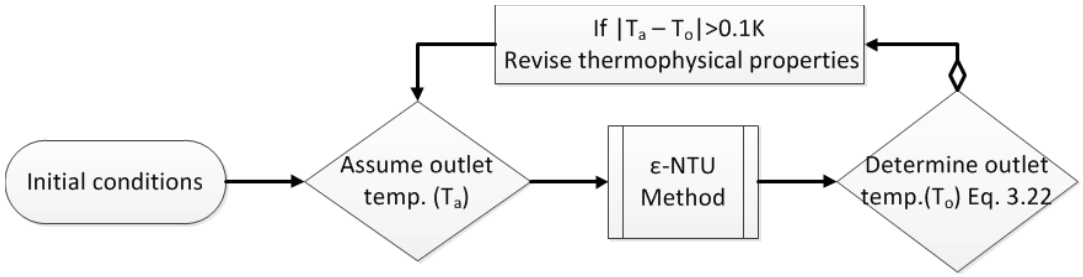

Figure 3.10: A numerical scheme for rating analysis

$$Q_{NTU} = \varepsilon C_{min}(T_{h,i} - T_{c,i}) = C_h \Delta T_h = C_c \Delta T_c \tag{3.22}$$

Vajjha and Das [35] had performed comprehensive theoretical analyses for a number of nanofluids based on experimental correlations of heat transfer and pumping power in a circular tube. Their objective was to determine the influence of particle volumetric concentration. They found adding particles to a base fluid increased thermal conductivity and convective heat transfer coefficient but also increased the viscosity, therefore the pumping power increased. From their tradeoff analysis, they found a dilute nanofluid of volumetric concentration around 1% yielded gain in heat transfer while not increasing the pumping power significantly. Therefore, we have adopted the 1% volumetric concentration in our following analyses to compare the performance of different nanofluids circulating in the hot side of the PHE.

3.7.2 Equations for Plate Heat Exchangers

The following equations have been adopted from Wang et al. [9] to perform the thermal and fluid dynamic analysis of the PHE.

Heat capacity rate

$$C = c_p \dot{m} \tag{3.23}$$

Heat capacity ratio

$$C^* = \frac{C_{min}}{C_{max}} \tag{3.24}$$

Overall heat transfer coefficient

$$\frac{1}{U} = \frac{1}{h_h} + \frac{1}{h_c} + \frac{t}{k} \tag{3.25}$$

Number of transfer units

$$NTU = \frac{UA_t}{C_{min}} \tag{3.26}$$

Effectiveness for counter-flow heat exchanger

$$\varepsilon = \frac{1 - exp\left[-(1-C^*)NTU\right]}{1 - C^* exp\left[-1(1-C^*)NTU\right]} \tag{3.27}$$

Heat transfer rate

$$Q = \varepsilon C_{\min}(T_{h,i} - T_{c,i}) \tag{3.28}$$

Pressure drop

$$\Delta P = \frac{2 f \rho L V^2}{D_e} \tag{3.29}$$

Fanning friction factor is determined using correlation given in Eq. (3.32).

Pumping power

$$\dot{W} = \Delta P \times \dot{V} \tag{3.30}$$

For calculating the convective heat transfer coefficient and the friction factor on the cold and hot side of the PHE, several correlations from Wang et al. [9] were considered, which are based on single phase fluid, as nanofluids data is not available. This book contains correlations by several researchers, including such as Focke et al. [17] and Muley and Manglik [37]. Focke et al. provides continuous correlations for Reynolds number from 150 to 20,000 in comparison to Muley and Manglik correlation valid for Re>1000. During our parametric runs the Reynolds number of different base fluids and nanofluids sometimes fell below 1000 and varied over a wide range. Therefore, the continuous correlations by Focke et al. were adopted in the numerical scheme to cover all the Reynolds numbers. The correlations of Focke et al. [17] for a chevron angle $\beta = 45°$ are presented below.

$$Nu = \begin{cases} 1.67\,\mathrm{Re}^{0.44}\,\mathrm{Pr}^{1/2} & 45 < \mathrm{Re} < 300 \\ 0.405\,\mathrm{Re}^{0.7}\,\mathrm{Pr}^{1/2} & 300 < \mathrm{Re} < 2000 \\ 0.84\,\mathrm{Re}^{0.6}\,\mathrm{Pr}^{1/2} & 2000 < \mathrm{Re} < 20,000 \end{cases} \quad (3.31)$$

$$f = \begin{cases} 0.3025 + 91.75/\mathrm{Re} & 150 < \mathrm{Re} < 1800 \\ 1.46\,\mathrm{Re}^{-0.177} & 1800 < \mathrm{Re} < 30,000 \end{cases} \quad (3.32)$$

3.7.3 Fluid Properties for Performance Analysis

The fluid properties of the base fluids and nanofluids are evaluated at their average bulk temperatures from the correlations presented in the earlier sections. Nanofluids show the correct trend of higher density, lower specific heat, higher viscosity and higher thermal conductivity in comparison to the base fluid shown in Table 3.6.

Table 3.6: Fluid thermo-physical properties

Fluid	60:40 EG/W	HFE-7000	1% Al_2O_3 EG/W	1% CuO EG/W	1% SiO_2 EG/W
Avg. temperature (K)	300.17	287.60	300.11	300.07	300.14
Density (kg/m^3)	1080.00	1430.54	1105.23	1134.25	1091.22
Specific heat (J/kg K)	3157.19	1268.19	3079.04	3006.39	3108.42
Viscosity (Pa s)	3.99E-03	4.70E-04	4.48E-03	4.63E-03	4.38E-03
Thermal conductivity (W/m K)	0.360	0.077	0.400	0.402	0.379
Prandtl number	34.98	7.74	34.46	34.63	35.94

3.7.4 Performance Comparison on the Same Mass Flow Rate Basis

Table 3.7 presents the results of an analysis on the basis of the same mass flow rate of 0.2 kg/s for the hot side considering four different fluids; (i) base fluid EG/W, (ii) 1% Al_2O_3 , (ii) 1% CuO, (iv) 1% SiO_2, all dispersed in EG/W. The mass flow rate of the cold side fluid HFE-7000 is maintained the same at 0.1 kg/s. The inlet temperature of the hot and cold fluid is held the same as seen by the ATCS loop. Approximately 2.5 kW of heat is transferred through the PHE. As observed from Table 3.7, the increase in the convective heat transfer coefficient is 4.75%, 3.98% and 2.25% for Al_2O_3, CuO and SiO_2 nanofluids respectively, over that produced by the base fluid. There is also a reduction in the volumetric flow rates of all the nanofluids in comparison to the base fluid, with copper oxide yielding the maximum reduction of 4.78% while transferring the same amount of heat. Only CuO reduced the pumping power in comparison to the base fluid

with 1.73%. Slight increase (less than 1%) in the overall heat transfer coefficient (*U*) produced by the nanofluids is noticed, although it is not as high as the convective heat transfer coefficient increase. This fact is due to the low value of convective heat transfer coefficient on the cold fluid, HFE -7000, side in comparison to the hot fluid side, nearly 1 to 4, making the cold fluid side thermal resistance become dominant. Further optimization on the cold fluid side to raise the convective heat transfer coefficient will make the performance of nanofluids even better.

Table 3.7: Performance comparison on the same mass flow rate basis

Fluid	60:40 EG/W	HFE-7000	1% Al_2O_3 EG/W	1% CuO EG/W	1% SiO_2 EG/W
Mass flow rate (kg/s)	0.2	0.1	0.2	0.2	0.2
Inlet temperature (K)	302.20	277.50	302.20	302.20	302.20
Outlet temperature (K)	298.14	297.71	298.03	297.94	298.07
Reynolds number	274	972	245	236	250
Nusselt number	116.78	139.01	110.22	108.86	113.68
Heat transfer coefficient (W/m^2 K)	10542.7	2678.9	11043.3	10962.5	10780.0
Heat transfer coefficient increase (%)	**----**		**4.75%**	**3.98%**	**2.25%**
Volumetric flow rate (m^3/s)	1.85E-04	6.99E-05	1.81E-04	1.76E-04	1.83E-04
Volumetric flow rate decrease (%)	**----**		**-2.28%**	**-4.78%**	**-1.03%**
friction factor	0.6372	0.3969	0.6777	0.6906	0.6693
Pumping power (W)	0.568	0.018	0.577	0.558	0.584
Pumping power decrease (%)	**----**		**1.56%**	**-1.73%**	**2.89%**
Overall heat trans. coef. (W/m^2 K)	2008.1		2025.6	2022.8	2016.5
Overall heat trans. coef. increase (%)	**----**		**0.87%**	**0.74%**	**0.42%**
Heat capacity ratio (C_{min}/C_{max})	0.20		0.21	0.21	0.20
Effectiveness	0.82		0.82	0.82	0.82
NTU	1.91		1.93	1.92	1.92
Heat dissipated (kW)	2.56		2.57	2.56	2.56
Heat dissipated increase (%)	**----**		**0.20%**	**0.04%**	**0.08%**

3.7.5 Performance Comparison on Same Heat Dissipation Basis

Numerical Scheme:

1. Assume same mass flow rate for nanofluid as base fluid
2. Use the analysis scheme outline in section 3.7.1.
3. Determine mass flow rate of nanofluid for equal heat transfer: $Q_{bf} = (\dot{m} c_p \Delta T)_{nf}$
4. Repeat process (1-4) until no noticeable change in mass flow rate

Table 3.8 summarizes the results computed for the case when the heat dissipation in the plate heat exchanger was maintained constant at 2.56 kW. The heat transfer coefficient increases by about 3.53% and 3.73% by using the Al_2O_3 and CuO nanofluid. The volumetric flow requirement for the same two nanofluids reduced by 4.84 and 5.30% compared to the base fluid, respectively. For the same amount of heat transfer, Al_2O_3 nanofluid requires 4.72% lower pumping power while the CuO nanofluid requires 3.01% lower pumping power in comparison with the base fluid. This analysis proves that nanofluids shows better performance than the base fluid, while transferring an equal amount of heat with a lower pumping power. Also it is observed that the SiO_2 nanofluid performance is inferior to the other two nanofluids, therefore SiO_2 will not be considered in further analysis.

Table 3.8: Performance comparison on the same heat dissipation basis

Fluid	60:40 EG/W	HFE-700	1% Al_2O_3 EG/W	1% CuO EG/W	1% SiO_2 EG/W
Heat dissipated (kW)	2.56	0.00	2.56	2.56	2.56
Mass flow rate (kg/s)	0.2	0.1	0.195	0.199	0.198
Inlet temperature (K)	302.20	277.50	302.20	302.20	302.20
Outlet temperature (K)	298.14	297.71	297.93	297.91	298.03
Reynolds number	274	972	238	235	247
Nusselt number	116.78	139.01	108.97	108.60	113.15
Heat transfer coefficient (W/m^2 K)	10542.7	2678.9	10914.8	10936.2	10728.2
Heat transfer coefficient increase (%)	**----**		**3.53%**	**3.73%**	**1.76%**
Volumetric flow rate (m^3/s)	1.85E-04	6.99E-05	1.76E-04	1.75E-04	1.81E-04
Volumetric flow rate decrease (%)	**----**		**-4.84%**	**-5.30%**	**-2.10%**
friction factor	0.6372	0.3969	0.6884	0.6928	0.6736
Pumping power (W)	0.568	0.018	0.541	0.551	0.569
Pumping power decrease (%)	**----**		**-4.72%**	**-3.01%**	**0.21%**
Overall heat trans. coef. (W/m^2 K)	2008.1		2021.2	2021.9	2014.7
Overall heat trans. coef. increase (%)	**----**		**0.65%**	**0.69%**	**0.33%**
Heat capacity ratio (C_{min}/C_{max})	0.20		0.21	0.21	0.21
Effectiveness	0.82		0.82	0.82	0.82
NTU	1.91		1.92	1.92	1.91

3.7.6 Performance Comparison on the Same Pumping Power Basis

Numerical Scheme:

1. Assume same heat transfer area/ length for nanofluids as base fluids
2. Use the analysis scheme outline in section 3.7.1.
3. Determine heat transfer area required for same heat transfer rate as base fluid:

$$NTU_{bf} = \left(\frac{UA}{C_{min}} \right)_{nf}$$

4. With new heat transfer area, calculate the required length of the heat exchanger
5. Determine the max flow rate the nanofluid can perform at with equal pumping power by: $\dot{W}_{bf} = \left(\dot{V} \cdot \Delta P \right)_{nf}$
6. Repeat analysis (1-5) until no noticeable change in length and flow rate

The analysis in Table 3.9 was conducted by using the equal pumping power of 0.568 W obtained in Table 3.7 and Table 3.8, while transferring 2.56 kW of heat. Due to the high thermal resistance on the cold side (HFE), increasing the heat transfer coefficient of the hot side by as much as 5% would not show any significant savings in the area reduction (<1%). An increase in heat transfer coefficient of about 4.75% is observed with the Al_2O_3 nanofluid. A volumetric flow rate reduction of 3.74% was found for the CuO nanofluid and a slight increase of overall heat transfer coefficient, less than 1%, and a slight decrease of the required heat transfer surface area, for all three nanofluids was obtained. If the heat transfer coefficient on the cold side (HFE-7000) can be increased, then the overall heat transfer coefficient can be further increased, which will result in a further reduction in the required heat transfer surface area.

Table 3.9: Performance comparison on the same pumping power basis				
Fluids	60:40 EG/W	HFE-7000	1% Al_2O_3 EG/W	1% CuO EG/W
Pumping power (W)	0.568	0.018	0.568	0.568
Mass flow rate (kg/s)	0.2	0.1	0.200	0.202
Inlet temperature (K)	302.20	277.50	302.20	302.20
Outlet temperature (K)	298.14	297.71	298.04	297.99
Reynolds number	274	972	245	239
Nusselt number	116.78	139.01	110.22	109.37
Heat transfer coefficient ($W/m^2 K$)	10542.7	2678.9	11043.3	11015.3
Heat transfer coefficient increase (%)	**----**		**4.75%**	**4.48%**
Volumetric flow rate (m^3/s)	1.85E-04	6.99E-05	1.81E-04	1.78E-04
Volumetric flow rate decrease (%)	**----**		**-2.28%**	**-3.74%**
friction factor	0.6372	0.3969	0.6776	0.6861
Overall heat trans. coef. ($W/m^2 K$)	2008.1		2025.5	2024.5
Overall heat trans. coef. increase (%)	**----**		**0.87%**	**0.82%**
Heat capacity ratio (C_{min}/C_{max})	0.20		0.21	0.21
Effectiveness	0.82		0.82	0.82
NTU	1.91		1.91	1.91
Heat trans. area decrease (%)	**----**		**-0.86%**	**-0.65%**
Heat dissipated (kW)	2.56		2.56	2.56

3.7.7 Performance Comparison with Doping HFE-7000 with Nanoparticles

Since HFE-7000, the fluid on the cold side of the heat exchanger has remained as a base fluid in all our previous calculations; an investigation was conducted with doping it with 1% concentration of Al_2O_3 nanoparticles, which has shown an overall improved performance among the three nanoparticles as seen in previous sections. We have used the thermophysical properties equations presented for the EG/W based nanofluids for HFE-7000 by replacing the properties of EG/W with that of HFE- 7000. This is because nanofluid correlations for HFE-7000 have not been developed yet. It is understood that the computed final results (Table 3.10) may not be precise, but may provide an approximate trend. The last three columns show comparison under same (a) mass flow rate, (b) heat transfer rate and (c) pumping power basis, where the hot side is maintained as EG/W. Under a heat transfer of 2.56 kW, it shows that by doping the HFE-7000 we can reduce the size of the heat exchanger surface by about 3.11%. A side benefit

for reducing the required surface area also reduced the pumping power requirements for the hot side by 3%.

Table 3.10: Performance comparison of doped HFE-7000 on the basis of same: (a) mass flow rate, (b) heat dissipation and (c) pumping power

			a	b	c
Fluid	60:40 EG/W	HFE-7000	1% Al_2O_3 HFE-7000	1% Al_2O_3 HFE-7000	1% Al_2O_3 HFE-7000
Mass flow rate (kg/s)	0.2	0.1	0.100	0.09958	0.10116
Heat dissipated (kW)	2.56		2.57	2.56	0.00
Pumping power (W)	0.568	0.018	0.017	0.017	0.017
Inlet temperature (K)	302.20	277.50	277.50	277.5	277.5
Outlet temperature (K)	298.14	297.71	297.97	298.0	297.7
Density (kg/m^3)	1080.00	1430.54	1451.86	1451.84	1452.24
Specific heat (J/kg K)	3157.19	1268.19	1256.10	1256.13	1255.71
Viscosity (Pa s)	3.99E-03	4.70E-04	5.25E-04	5.25E-04	5.25E-04
Thermal conductivity (W/m K)	0.360	0.077	0.087	0.087	0.087
Prandtl number	34.98	7.74	7.57	7.56	7.58
Reynolds number	274	972	870	866	878
Nusselt number	116.78	139.01	127.17	126.80	128.18
Heat transfer coefficient (W/m^2 K)	10542.7	2678.9	2774.6	2766.7	2795.0
Heat transfer coefficient increase (%)	**----**		**3.57%**	**3.28%**	**4.33%**
Volumetric flow rate (m^3/s)	1.85E-04	6.99E-05	6.89E-05	6.86E-05	6.97E-05
Volumetric flow rate decrease (%)	**----**		**-1.47%**	**-1.88%**	**-0.35%**
Pumping power decrease (%)	**----**		**-0.20%**	**-1.33%**	**-0.06%**
Overall heat trans. coef. (W/m^2 K)	2008.1		2061.4	2057.0	2072.6
Overall heat trans. coef. increase (%)	**----**		**2.65%**	**2.44%**	**3.21%**
Heat capacity ratio (C_{min}/C_{max})	0.20		0.20	0.20	0.20
Effectiveness	0.82		0.83	0.83	0.82
NTU	1.91		1.98	1.98	1.91
Heat trans. area decrease (%)	**----**		**----**	**----**	**-3.11%**
Heat dissipated increase (%)	**----**		**0.33%**	**----**	**----**

3.7.8 Performance Comparison using Present Experimental Correlations

Unlike the earlier tables of performance comparison based on a single phase correlations of Focke et al. [17] a new table, Table 3.11, was prepared based on the newly developed correlations equations (3.18) and (3.20). The computed results show the thermal performance

improvement with aluminum oxide with a volumetric concentration of 0.5%, matching the experimental conditions. The last three columns show comparison under same (a) mass flow rate, (b) heat transfer rate and (c) pumping power basis, where the cold side fluid is water to conform to the experimental conditions. For a given, heat dissipation of 2.73 kW, it shows that 0.5% concentration can reduce pumping powering by as much as 5.65% or reduce the size of the heat exchanger surface by about 2.01%.

Table 3.11: Performance comparison of EG/W on the basis of constant: (a) mass flow, (b) heat dissipation study, (c) pumping power

			a	b	c
Fluid	60:40 EG/W	Water	0.5% Al_2O_3 EG/W	0.5% Al_2O_3 EG/W	0.5% Al_2O_3 EG/W
Mass flow rate (kg/s)	0.0500	0.0350	0.0500	0.0491	0.0505
Heat dissipated (kW)	2.73		2.75	2.73	2.73
Pumping power (W)	0.896	0.094	0.890	0.845	0.896
Inlet temperature (K)	338.00	293.00	338.00	338.00	338.00
Outlet temperature (K)	321.36	311.68	321.02	320.82	321.33
Density (kg/m^3)	1063.26	995.32	1076.06	1076.12	1075.96
Specific heat (J/kg K)	3282.61	4176.23	3240.26	3239.86	3240.91
Viscosity (Pa s)	1.77E-03	8.12E-04	1.88E-03	1.88E-03	1.87E-03
Thermal conductivity (W/m K)	0.375	0.614	0.414	0.414	0.414
Prandtl number	15.45	5.52	14.77	14.80	14.71
Reynolds number	775	590	729	713	739
Velocity (m/s)	0.322	0.121	0.319	0.313	0.322
Nusselt number	101.97	61.04	96.04	94.59	96.94
Heat transfer coefficient (W/m^2 K)	9580.6	9383.8	9952.2	9799.9	10049.5
Heat transfer coefficient increase (%)	**----**		**3.88%**	**2.29%**	**4.89%**
Volumetric flow rate (m^3/s)	4.70E-05	3.52E-05	4.65E-05	4.56E-05	4.69E-05
Volumetric flow rate decrease (%)	**----**		**-1.19%**	**-3.04%**	**-0.16%**
Pumping power decrease (%)	**----**		**-0.71%**	**-5.65%**	**----**
Overall heat trans. coef. (W/m^2 K)	4152.9		4222.8	4193.5	4238.5
Overall heat trans. coef. increase (%)	**----**		**1.68%**	**0.98%**	**2.06%**
Heat trans. area decrease (%)	**----**		**----**	**----**	**-2.01%**
Heat dissipated increase (%)	**----**		**0.77%**	**----**	**----**

3.7.9 Overall Heat Transfer Coefficient Improvement

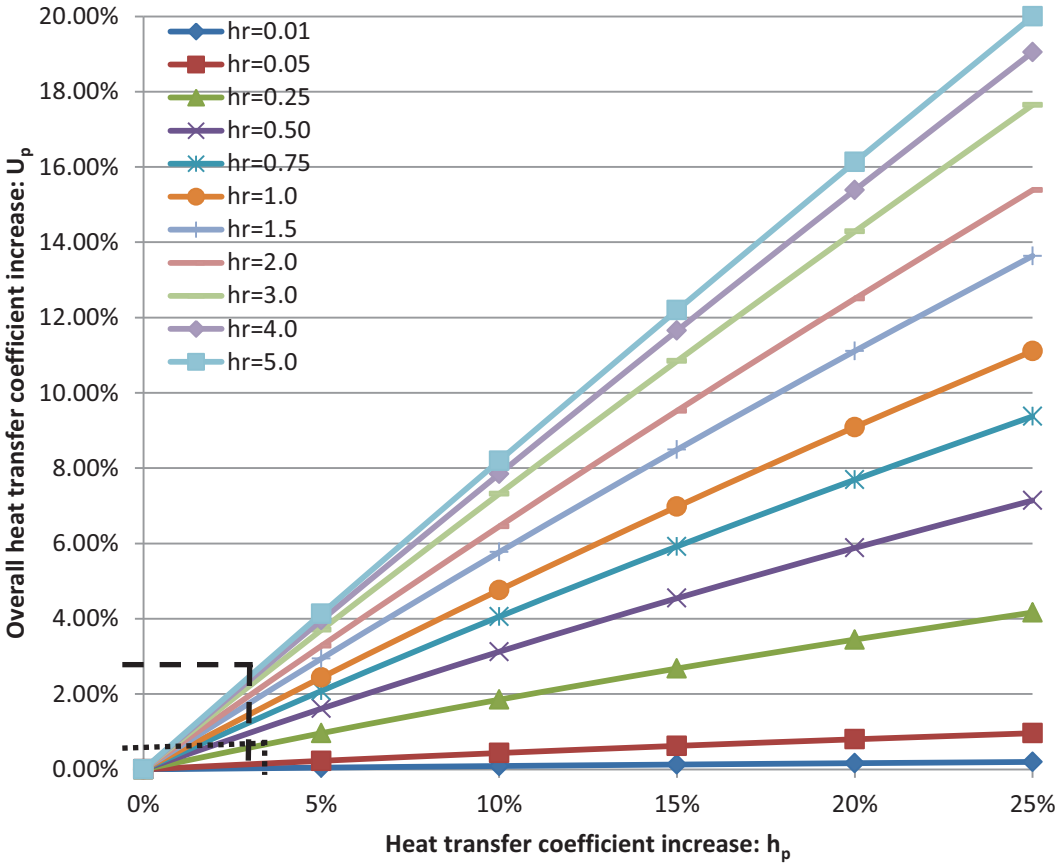

Figure 3.11: A plot of the performance of nanofluids considering the effect of the convective heat transfer coefficient and the overall heat transfer coefficient.

Figure 3.11 created from the analysis shows how much improvement of overall heat transfer coefficient can be attained by increasing the convective heat transfer coefficient by dispersing nanoparticles. The x-axis represents percentage increase of the heat transfer coefficient ($h_p = (h_{nf} - h_{bf}) / h_{bf}$). The y-axis represents the percentage increase in the overall heat transfer coefficient ($U_p = (U_{bf} - U_{nf}) / U_{bf}$). Each line represents a different scenario in a heat exchanger based on the heat transfer coefficient ratio ($h_R = h / h_{bf}$) between the non-doped fluid and the base fluid. Using the example of Table 3.9, the heat transfer coefficient increase is 4.75% and the heat transfer coefficient ratio is about 0.25. From the plot, we see from the dotted line then the overall heat transfer coefficient will improve by about 0.9%. Another

example would be from Table 3.10, where now the heat transfer coefficient increase is 4.33% and the heat transfer coefficient ratio is about 4. From the plot, we can see from the dashed line the overall heat transfer coefficient is about 3%. Both of the examples predicted similar values of overall heat transfer coefficient increase in Table 3.9 and Table 3.10. The plot shows that for nanofluids to have significant impact on the overall heat transfer coefficient (5%), which would be about the same in area reduction. The nanofluids would need to increase the heat transfer coefficient by as much as 15% with a heat transfer coefficient ratio of about 0.5.

3.8 Conclusions

The experimental results show an agreement within 1 to 2% between the test data and the predicted values of the heat transfer rate and the overall heat transfer coefficient for water flow in the PHE by the SWEP modeling software. With this validation of test setup, preliminary experiment with 0.5 % aluminum oxide nanofluid show improvement of the convective and overall heat transfer coefficient as much as 11% and 4.85%, respectively. Preliminary curve-fit correlations have been developed for the Nusselt number and friction factor of nanofluid flow in a compact minichannel PHE. Using these new correlations it was found that a 0.5% Al_2O_3 nanofluid can reduce pumping power by 5.65% or reducing the surface area of the heat exchanger by 2%. Using this apparatus, different nanofluids with varying characteristics can be tested to develop generalized correlations for Nusselt number and friction factor with nanofluids in compact heat exchangers.

Theoretical studies on three different nanofluids of 1 % volumetric concentration in a minichannel PHE transferring about 2.5 kW of heat revealed that all nanofluids have better performance compared to the base fluid. Because of the variations of thermophysical properties of different nanofluids, they exhibited strengths and weaknesses in various areas. On the basis of an equal mass flow rate of 0.2 kg/s on the hot side of the PHE, aluminum oxide gave a 4.75% enhancement in the convective heat transfer coefficient, Copper oxide gave a 4.78% reduction in the volumetric flow rate, and 1.73% reduction in the required pumping power, when compared with the base fluid, which was EG/W. On the basis of same heat dissipation of 2.5 kW the most promising results were the savings in pumping power: 4.72% for Al_2O_3 and 3.01% for CuO. On the basis of equal pumping power of 0.586 W while transferring about 2.5 kW of heat Al_2O_3 nanofluid gave a heat transfer surface area reduction of about 0.86%. Although this area

reduction is small, further optimization with different heat transfer, flow rates and different volumetric concentration may yield improved surface area reduction. Furthermore, in all the above comparisons, the cold side of the PHE carrying HFE-7000 has been maintained as a base fluid. Due to HFE-7000's low value of viscosity it can be doped with nanoparticles to enhance the convective heat transfer coefficient, which has been about 25% (of the order of 2500 versus 10,000 from the above tables) of that on the hot side, providing the dominant thermal resistance. Doping the HFE- 7000 by 1% Al_2O_3 reduces the surface area by about 3.11%, which also reduced the pumping power requirements by the hot side by about 3%. The method outlined in this paper would help applications leading to miniaturization, compactness, and higher heat density.

3.9 Nomenclature

A, B, C	Dimensionless coefficients	U	overall heat transfer coefficient, W/m^2 K
A_f	Fluid flow area per channel, m^2	V	mean velocity, m/s
A_p	Projected area per plate, m^2	$\dot{V}$	volumetric flow rate, m^3/s
A_t	Surface area on one fluid side of PHE, m^2	W	Plate width, m
b	Channel spacing, m	$\dot{W}$	pumping power, W
C	Heat Capacity Rate, W/K		**Greek Letters**
c_p	specific heat, J/kg K	β_{phe}	Chevron Angle, degrees
D_e	Equivalent diameter, (m)	ΔP	differential pressure loss, Pa
d_p	particle diameter, m	μ	coefficient of dynamic viscosity, kg/m s
f	fanning friction coefficient	ϕ	particle volumetric concentration
h	convective heat transfer coefficient, W/m^2 K	ϕ_{phe}	Enlargement factor
k	thermal conductivity, W/m K	ρ	density, kg/m^3
L	Plate length, m	κ	Boltzmann constant, 1.381 x 10^{-23} J/K
$LMTD$	Log mean temperature difference, K	ε	heat exchanger effectiveness
$\dot{m}$	mass flow rate, kg/s		**Subscripts**
N	No. of channels	0	properties at reference temperature, 273K
NTU	number of transfer units	avg	Average
Nu	Nusselt number, $Nu = hd/k$	bf	base fluid
Pr	Prandtl number, $Pr = (\mu C_p)/k$	c	cold fluid stream
Q	heat transfer rate, W	f	Fluid
R^2	coefficient of determination	h	hot fluid stream
Re	Reynolds number, $Re = (\rho V d)/\mu$	i	Inlet
t	Thickness of plate, m	nf	nanofluid
T	temperature, K	o	Outlet
T_0	reference temperature, 273 K	p	Particle

3.10 References

[1] Choi, S. U. S., and Eastman, J. A., 1995, "Enhancing thermal conductivity of fluids with nanoparticles," p. Medium: ED; Size: 8 p.

[2] Das, S. K., Choi, S. U. S., Yu, W., and Pradeep, T., 2008, Nanofluids: Science and Technology, Wiley, Hoboken, NJ.

[3] Minkowycz, W. J., Sparrow, E. M., and Abraham, J. P., 2013, Nanoparticle Heat Transfer and Fluid Flow, CRC Press/Taylor & Francis Group.

[4] Ungar, E. K., and Erickson, L. R., 2011, "Assessment of the use of nanofluids in spacecraft active thermal control systems," SPACE 2011, American Institute of Aeronautics and Astronautics, Long Beach, California, p. 10.

[5] Stephan, R. A., 2009, "Overview of NASA's thermal control system development for exploration project," International Conference On Environmental Systems, SAE Technical Paper, Savannah, Georgia.

[6] Kandlikar, S. G., Garimella, S., Li, D., Colin, S., and King, M., 2006, Heat Transfer and Fluid Flow in Minichannels and Microchannels, Elsevier Science & Technology.

[7] Shah, R. K., 1987, "Classification of heat exchangers," Heat Exchangers: Thermal-Hydraulic Fundamentals and Design, S. Kakaç, A. E. Bergles, and F. Mayinger, eds., McGraw-Hill, Washington,DC.

[8] 2002, "Space Transportation Costs: Trends in Price Per Pound to Orbit 1990-2000," F. Corporation, ed., Futron Corporation, Bethesda, Maryland.

[9] Wang, L., Sundén, B., and Manglik, R. M., 2007, Plate Heat Exchangers: Design, Applications and Performance, WIT Press, MA.

[10] Maré, T., Halelfadl, S., Sow, O., Estellé, P., Duret, S., and Bazantay, F., 2011, "Comparison of the thermal performances of two nanofluids at low temperature in a plate heat exchanger," Experimental Thermal and Fluid Science, 35(8), pp. 1535-1543.

[11] Jokar, A., and O'Halloran, S. P., 2013, "Heat transfer and fluid flow analysis of nanofluids in corrugated plate heat exchangers using computational fluid dynamics simulation," Journal of Thermal Science and Engineering Applications, 5(1), p. 011002.

[12] Pantzali, M. N., Mouza, A. A., and Paras, S. V., 2009, "Investigating the efficacy of nanofluids as coolants in plate heat exchangers (PHE)," Chemical Engineering Science, 64(14), pp. 3290-3300.

[13] Fard, M. H., Talaie, M. R., and Nasr, S., 2011, "Numerical and experimental investigation of heat transfer of ZnO/water nanofluid in the concentric tube and plate heat exchangers," Thermal Science, 15(1), pp. 183-194.

[14] Tiwari, A. K., Ghosh, P., and Sarkar, J., 2013, "Performance comparison of the plate heat exchanger using different nanofluids," Experimental Thermal and Fluid Science, 49, pp. 141-151.

[15] Pandey, S. D., and Nema, V. K., 2012, "Experimental analysis of heat transfer and friction factor of nanofluid as a coolant in a corrugated plate heat exchanger," Experimental Thermal and Fluid Science, 38, pp. 248-256.

[16] 3M, 2010, "3M Novec Engineered Fluid HFE-7000," 3M Electronics Markets Materials Division, p. 6.

[17] Focke, W. W., Zachariades, J., and Olivier, I., 1985, "The effect of the corrugation inclination angle on the thermohydraulic performance of plate heat exchangers," International Journal of Heat and Mass Transfer, 28(8), pp. 1469-1479.

[18] American Society of Heating, R., and Engineers, A.-C., 2005, ASHRAE Handbook: Fundamentals, American Society of Heating, Refrigerating and Air-Conditioning Engineers, Atlanta, GA.

[19] White, F. M., 2003, Fluid Mechanics, McGraw-Hill, New York, NY.

[20] Yaws, C. L., 1977, Physical Properties: A Guide to the Physical, Thermodynamic, and Transport Property Data of Industrially Important Chemical Compounds, McGraw-Hill, New York, NY.

[21] Vajjha, R. S., Das, D. K., and Mahagaonkar, B. M., 2009, "Density measurement of different nanofluids and their comparison with theory," Petroleum Science & Technology, 27(6), pp. 612-624.

[22] Pak, B. C., and Cho, Y. I., 1998, "Hydrodynamic and heat transfer study of dispersed fluids with submicron metallic oxide particles," Exp Heat Transfer, 11(2), pp. 151-170.

[23] Vajjha, R. S., and Das, D. K., 2009, "Specific heat measurement of three nanofluids and development of new correlations," Journal of Heat Transfer, 131(7), pp. 1-10.

[24] Xuan, Y., and Roetzel, W., 2000, "Conceptions for heat transfer correlation of nanofluids," International Journal of Heat and Mass Transfer, 43(19), pp. 3701-3707.

[25] Koo, J., and Kleinstreuer, C., 2005, "A new thermal conductivity model for nanofluids," Journal of Nanoparticle Research, 7(2-3), pp. 324-324.

[26] Vajjha, R. S., and Das, D. K., 2009, "Experimental determination of thermal conductivity of three nanofluids and development of new correlations," International Journal of Heat and Mass Transfer, 52(21-22), pp. 4675-4682.

[27] Sahoo, B. C., Das, D. K., Vajjha, R. S., and Satti, J. R., 2013, "Measurement of the thermal conductivity of silicon dioxide nanofluid and development of correlations," Journal of Nanotechnology in Engineering and Medicine, 3(4), pp. 041006-041006.

[28] Vajjha, R. S., Das, D. K., and Kulkarni, D. P., 2010, "Development of new correlations for convective heat transfer and friction factor in turbulent regime for nanofluids," International Journal of Heat and Mass Transfer, 53(21-22), pp. 4607-4618.

[29] Namburu, P. K., Kulkarni, D. P., Dandekar, A., and Das, D. K., 2007, "Experimental investigation of viscosity and specific heat of silicon dioxide nanofluids," Micro & Nano Letters, 2(3), p. 67.

[30] Namburu, P. K., Kulkarni, D. P., Misra, D., and Das, D. K., 2007, "Viscosity of copper oxide nanoparticles dispersed in ethylene glycol and water mixture," Experimental Thermal and Fluid Science, 32(2), pp. 397-402.

[31] Sahoo, B. C., Vajjha, R. S., Ganguli, R., Chukwu, G. A., and Das, D. K., 2009, "Determination of rheological behavior of aluminum oxide nanofluid and development of new viscosity correlations," Petroleum Science and Technology, 27(15), pp. 1757-1770.

[32] SWEP, "Product Catalogue," http://www.swep.net.

[33] Çengel, Y. A., 2007, Heat and Mass Transfer: A Practical Approach, McGraw-Hill, New York, NY.

[34] "Alfa Aesar," http://www.alfaaesar.com/.

[35] Vajjha, R. S., and Das, D. K., 2012, "A review and analysis on influence of temperature and concentration of nanofluids on thermophysical properties, heat transfer and pumping power," International Journal of Heat and Mass Transfer, 55(15–16), pp. 4063-4078.

[36] Shah, R. K., 1990, "Assessment of modified Wilson plot techniques for obtaining heat exchanger design data," Heat Transfer, p. 6.

[37] Muley, A., and Manglik, R. M., 1999, "Experimental study of turbulent flow heat transfer and pressure drop in a plate heat exchanger with chevron plates," Journal of Heat Transfer, 121(1), pp. 110-117.

Chapter 4: Conclusions and Recommendations

4.1 General Conclusions

Conclusions from Chapter 2: A detailed computational study was performed for an automotive radiator with three different nanoparticles, Al_2O_3, CuO and SiO_2, dispersed in the base fluid, EG/W 60:40 by mass.

- From the analysis, it was determined that the nanofluids have a superior performance gain at 1% volumetric concentration, higher coolant inlet temperature, low turbulent flow regime in the tube preferably around $Re_c \leq 5500$ and air side Reynolds number around $Re_a \geq 1000$.
- At the most optimal conditions of operation, it is possible to reduce the pumping power by 35.3%, 33.1% and 26.2% or the surface area by 7.4%, 7.2% and 5.2% using Al_2O_3, CuO and SiO_2 nanofluids respectively on the basis of equal heat transfer rate.

Conclusions from Chapter 3: Experimental and theoretical studies were performed for a plate heat exchanger (PHE) using nanofluids.

- The experimental benchmark results show a close agreement within 1 to 2% between the experimental data and the predicted values of the heat transfer rate and the overall heat transfer coefficient for water flow in the PHE by the SWEP modeling software.
- Preliminary curve-fit correlations were developed for the Nusselt number and friction factor for 0.5% concentration aluminum oxide nanofluid in a compact minichannel PHE.
- This nanofluid showed improvement for convective and overall heat transfer coefficient as much as 11% and 4.85%, respectively over the base fluid.
- Using the new correlations developed from the experimental study, it was determined that a 0.5% Al_2O_3 nanofluid can reduce pumping power by 5.65% or the surface area of the heat exchanger by 2% for equal heat dissipation in comparison to the base fluid.
- Theoretical studies on three different nanofluids (Al_2O_3, CuO, SiO_2) of 1% volumetric concentration in a minichannel PHE transferring about 2.5 kW of heat, suitable for application in future NASA spacecrafts, revealed that all nanofluids have better performance than the base fluid.

- On the basis of an equal mass flow rate of 0.2 kg/s on the hot side of the PHE, aluminum oxide gave a 4.75% enhancement in the convective heat transfer coefficient.
- On the basis of same heat dissipation of 2.5 kW, the most promising results were the savings in pumping power: 4.72% for Al_2O_3 and 3.01% for CuO.
- On the basis of equal pumping power of 0.586 W while transferring about 2.5 kW of heat, Al_2O_3 nanofluid gave a heat transfer surface area reduction of about 0.86%.
- Doping the low temperature coolant HFE- 7000 with 1% Al_2O_3 nanoparticles can reduce the surface area by about 3.11%. This can also reduce the pumping power requirements on the hot side by about 3%.

4.2 Recommendations for Future Research

Automotive radiator: To validate the theoretical findings of this thesis, experimental work is necessary. An approximate model using Similitude theory can be developed using the radiator from a liquid cooling system for computers. This is currently available and the radiator's size is small enough to allow the use of a currently available wind tunnel for control flow rates of air.

Plate heat exchanger (PHE): The work presented in this paper provides preliminary results for nanofluids in plate heat exchangers. Continuing this study would require a more in-depth benchmark test with a single phase fluid, due to the complex nature of PHE and disagreement among the published correlations available until now. The internal geometries of plate heat exchanger would need to be ascertained accurately from the manufacturer, some are not easily available due to the proprietary nature.

Heat recovery system: Nanofluids could be applied to recover heat from the exhaust of diesel generators. With the heating season of Alaska around 6 months, improving the amount of heat obtained from the exhaust gas could prove to be valuable and cost effective. A system exists in Ruby, Alaska recovering heat with EG/W. The research would consist of an analytical and numerical analysis using real world data obtained from the diesel generator located in Ruby to accurately determine enhanced heat recovery with different nanofluids.

Viscosity: Extension of the viscosity data of nanoparticles dispersed in EG/W to cover the full temperature range $(233K \le T \le 363K)$ for building heating and automobile radiators in cold regions are necessary. The new data would be developed using a Brookfield viscometer. Next,

combine the new data set with existing data to develop a single correlation for the viscosity of EG/W nanofluids.

Microchannel heat exchanger: Microchannel heat exchangers provide the highest surface area to volume ratio than any other heat exchanger. Combining microchannel heat exchangers with thermally efficient nanofluids could prove to be a highly efficient heat exchanger. Analytical, numerical and experimental studies would provide invaluable information to the research community. A starting point would be to begin with a minichannel heat exchanger as they are much more explored. This would serve as an aid in validating the analysis, numerical and experimental results for microchannels.

Nanofluids in turbulent regime: Nanofluids shows great performance gain over the base fluid, but the performance gain diminishes with increasing the Reynolds number. Understanding how and what is causing this diminishing performance would lead to a better understanding about the interactions of the nanoparticles with the base fluid. This will also aid in determining optimal applications for nanofluids.

Nusselt number and friction correlations for turbulent flow: It is necessary to extend the existing turbulent flow correlations for Nusselt number and friction factor for nanoparticles dispersed in EG/W and propylene glycol and water mixture (PG/W) to cover the full temperature range $(233K \le T \le 363K)$ applicable to practical systems. Using the existing data and generating new experimental data, Nusselt number and friction factor correlations for both EG/W and PG/W nanofluids for turbulent flow should be developed for a broader ranges of Reynolds and Prandtl numbers.

Electrical conductivity: The research presented in this paper has been focused on the improvement of thermophysical properties provided by nanofluids over the base fluid, but the dispersed nanoparticles generally increase the electrical conductivity of the base fluid. Exploring the effects of nanoparticle concentration, temperature, pH, zeta-potential or fluid flow on the electrical conductivity could open other applications of nanofluids.

Long term usage of nanofluids: With limited experimental results on nanofluids' applications there is even less or possibly no information on the long term usage of nanofluids and whether they retain their superior performance for an extend period. Several areas could be explored that would be vital to the nanofluids research community. The most important area to

investigate is: does agglomeration occur even with continuous circulation and the benefits of adding an inline sonicator. Another area to explore is the wear and internal erosion using nanofluids on the system (pipe, pump, valves, bends, etc.). The final topic would be looking at the effects of nanofluids and fouling/scaling on the pipes. Do nanofluids prevent or increase the rate of fouling/scaling?

Surface tension: Surface tension is an important parameter when the heat transfer fluid is used in boiling applications (e.g. steam generators or refrigerants-evaporators). Examining how nanoparticles affect the bubble formation and either increases or decreases the surface tension of the base fluid would be valuable, if nanofluids are applied to cases of nucleate boiling.

Contact angle: Contact angle of a fluid plays an important role in petroleum engineering applications and in the filtration process. Studies of contact angle of nanofluids as a function of volumetric concentration and particle size would be valuable in the design of nano-filters.